INFORMATION TO USERS

This manuscript has been reproduced from the microfilm master. UMI films the text directly from the original or copy submitted. Thus, some thesis and dissertation copies are in typewriter face, while others may be from any type of computer printer.

The quality of this reproduction is dependent upon the quality of the copy submitted. Broken or indistinct print, colored or poor quality illustrations and photographs, print bleedthrough, substandard margins, and improper alignment can adversely affect reproduction.

In the unlikely event that the author did not send UMI a complete manuscript and there are missing pages, these will be noted. Also, if unauthorized copyright material had to be removed, a note will indicate the deletion.

Oversize materials (e.g., maps, drawings, charts) are reproduced by sectioning the original, beginning at the upper left-hand corner and continuing from left to right in equal sections with small overlaps. Each original is also photographed in one exposure and is included in reduced form at the back of the book.

Photographs included in the original manuscript have been reproduced xerographically in this copy. Higher quality 6" x 9" black and white photographic prints are available for any photographs or illustrations appearing in this copy for an additional charge. Contact UMI directly to order.

UMI

A Bell & Howell Information Company
300 North Zeeb Road, Ann Arbor MI 48106-1346 USA
313/761-4700 800/521-0600

Université d'Ottawa · University of Ottawa

Smart Structure Integrity Monitoring Using Transient Response

By

Kuoc-Vai Iong

A thesis submitted to the School of Graduate Studies and Research in partial fulfillment of the requirements for the degree of Master of Applied Science in Mechanical Engineering.

Ottawa-Carleton Institute for Mechanical and Aerospace Engineering

Ottawa, Ontario, Canada

Abstract

Applications of smart structures equipped with real time monitoring of structural integrity are expanding rapidly. In the present thesis, a non-destructive testing method was used to detect damage in a simple beam-like smart structure. In this study, two continuous beams perfectly connected, one of them equipped with a piezoceramic sensor and two piezoceramic actuators, were used to identify the changes in the boundary conditions. A non-destructive damage detection method for this simple smart structure was applied to two extreme cases. These cases were: two beams with a perfect connection and the original beams completely disconnected. Transient responses for the two cases were compared and the differences were analyzed for detecting the presence of damage. To illustrate the approach, the classic Euler-Bernoulli beam model for vibration analysis was used. Computer simulations based on the analytical modeling were performed. A quantitative measure of the safety of the beam and an index of safety were introduced. Experimental verification of the concept of the method was successfully carried out. The results confirm the feasibility of the proposed structural integrity monitoring method.

ACKNOWLEDGEMENTS

The author is deeply indebted to Prof. Firooz Bakhtiari-Nejad for his generous encouragement, knowledge advise, invaluable guidance, and numerous hours of discussion throughout this work, without which this thesis would not have been possible. In addition, I was very fortunate to have received a great deal of help and innovative ideas from him.

The author wishes to express his deep appreciation to Prof. D.J. Gorman [6], Prof. D. Redekop, Prof. N.U. Ahmed and Dr. Yousefi-Koma Aghil [59] for their helpful discussions and long suggestions.

The author also wishes to express his thanks to The Sensor Technology Company which supported the work by providing the sensor and actuator used in this research.

I would like to acknowledge the members of my defence committee, Prof. D.A. Staley, Prof. D.J. Gorman and Prof. W. Hallett for taking their time to examine my thesis.

Special thanks are due to Dr. Aria Alasty, Mr. J. de Carufel, Mr. Mohammad Eghtesad, Mr. Bumsoo Kim and Mr. Rahim Jassemi for their suggestions, encouragement and moral support. The author is also very thankful to Prof. Li-Gao Zhou (Vice-rector of University of Macau), Mr. C.L. Lei (Director of studies, Escola Superior Das Forças De Segurança De Macau), Prof. Rui Martins (Dean of FST, UM), Prof. V.P. Iu (Associate Dean of FST, UM), Prof. S.H. Chuang (Department Head of ME, NCHU, R.O.C.), Prof. Y.M. Zhu, Prof D. Xue, Prof. L. Zhang, Prof. Z. Wang, Prof. Charles Csaba Szilvassy, Dr. G.K. Er, Prof. L.C. Lin (NCHU, R.O.C.), Dr. K.M. Mok, and Mr. V.K. Sin (UM) for their encouragement.

Very special thanks are due to the author's mother, Ms. Tim Kok(郭添), for her loving support, enormous patience and constant encouragement.

Finally, the most important person that the author wishes to express his deep sense of gratitude is to his thesis academic advisor, Prof. D. Necsulescu, not only for the guidance and critical suggestion but also for teaching of the art of carrying out a research project.

TABLE OF CONTENTS

List of Figures

List of Tables

Nomenclature

$a_N^+ \& a_N^-$ positive and negative attenuating waves respectively

$a_F^+ \& a_F^-$ positive traveling and negative traveling waves respectively

A cross section area of the beam

c velocity of longitudinal wave propagation

D_i dielectric displacement

d_{kij} the piezoelectric constant at zero stress

E Young's modulus

E_k electric field

$F(x,t)$ applied force

$f(x,t)$ force per unit length

G shear modulus of elasticity

I moment of inertia

IS index of safety

k Timoshenko shear coefficient (which is equal to 5/6)

k wavenumber

l length of each beam

L total length of the two beam system

l_p actuator location

l_s sensor location

M total mass of the beam

S_{ij}	strain tensor
S_{ijkl}^{E}	the complex mechanical compliance at zero electric field
t	time in seconds
t_b	thickness of the beam
T_{kl}	stress in PZT along the y-axis
u	axial displacement
w_b	width of the beam
x	position along the length of the beam
y	lateral vibration displacement
y_{cant}	lateral vibration displacement of cantilever beam
$y_{cl\text{-}cl}$	lateral vibration displacement of clamped-clamped beam
ϱ	density of the beam
ϖ_c	Euler and Timoshenko cutoff frequency
Ω	frequency of excitation force
α	magnitude of acceleration due to excitation force
ε_{ik}^{T}	permittivity
Φ	sensor diameter
ψ	total angle change due to bending

Introduction

All load-carrying members of a structure suffer degradation even when not in service, and such degradation might be due to corrosion, crack or fatigue. Inspection and maintenance on such systems need to be carried out at specific times in their life cycle. Many of the methods, used so far to detect the damage, were based on samples and used destructive testing. However, damage that is not detected continuously and not corrected immediately may potentially cause more damage and eventually catastrophic failures. In order to ensure safe operating conditions, it is necessary to monitor the damage in real-time. The advantage of using smart structures with regard to non-destructive testing is that the condition of the structure can be continuously monitored and therefore it is possible to determine the life duration left. In this thesis, a new non-destructive testing method is verified for a simple smart structure to detect damage. The simple structure chosen is a beam-like structure consisting of two continuous beams perfectly joined and equipped with a piezoceramic sensor and two piezoceramic actuators for a smart structure analysis. This nondestructive damage detection approach was applied to the two extreme cases to verify that the method may be applied to a larger variety of cases. These two cases are a) jointed beams with a perfect connection and b) the original beams completely disconnected. Transient responses for the two cases were compared and the differences were analyzed for detecting the presence of damage.

To illustrate the approach, the classic Euler-Bernoulli beam model for vibration analysis was used. Computer simulation, based on analytical modeling, was performed. Also, experimental verification was conducted. In this study, beam response to various excitations was assumed to remain in the elastic domain. This preliminary verification permitted the performance of the approach to be tested, and to justify further steps in its development for more complex structures. For example, the above approach can be extended to the plate case as a generalization of the beam case. A two-dimensional analog of Euler-Bernoulli beam model gives the thin plate model, while the two-dimensional analog of Timoshenko beam model gives Mindlin-Timoshenko plate model.

Chapter 1

Literature Review on Smart Structures

1.1 An Introduction to Intelligent Material Systems and Structures

It is expected that in the 21st century, materials will contain embedded or attached actuators and/or sensors. They will also contain miniaturized support electronics including power electronics and a computer processor with a communication network along with the intelligent structure to respond to the environment. The key innovation is the introduction of sensors and actuators into these materials. During service, these materials will be able to adapt to changes in mission requirements. These materials will be capable of self diagnosis and self repair. The materials and structures constructed from these materials are referred to as metamorphic materials, intelligent materials, smart structures, intelligent structures, etc.

Research and development on smart structures has been identified as an interdisciplinary area of activity in its own right where smart or intelligent here implies the ability to sense. The topic of smart structures and materials is extremely broad. Not only the qualifiers of intelligent, smart or sensible but also

adaptive are suitable to be used to describe and/or classify materials and structures which contain their own sensors, actuators and computational/control capabilities and/or hardware.

The early 'Smart Materials' contained, for the most part, embedded and/or distributed sensors for strain and temperature. Now, many approaches are being tried from various starting points in many scientific fields. For example, in the field relating to artificial intelligence and neuro-computers, intelligent functions, which have traditionally relied upon using software, and electronic circuits could be partly substituted by intelligent materials. Recently some of the applications for hypersonic vehicles by using Smart structures were also mentioned by August, James A. (1996) [61]. The science relating to intelligent materials will play an important role for technology innovation.

Intelligent structures can be categorized into two general classifications as mechanically intelligent structures and optically intelligent structures. A mechanically intelligent structure is *capable* of altering its mechanical states (position or velocity) or its mechanical characteristics (Stiffness or damping). An optically intelligent structure could change color to match its background.

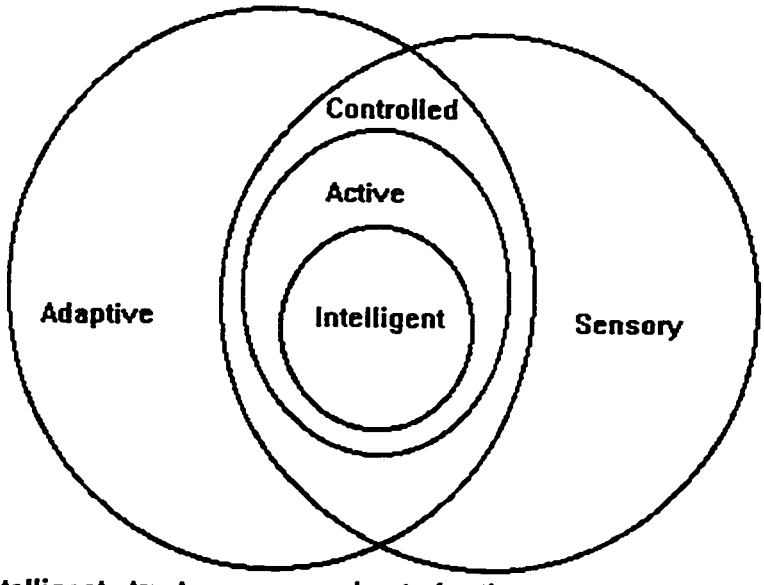

Fig 1. Intelligent structures as a subset of active structures on which as a subset of controlled structures.

As show in Fig 1 [2], structures which have sensors distributed throughout are a subset referred to as sensory structures. These structures have sensors which might detect displacements, strains, mechanical states or properties, electromagnetic states or properties, temperature or heat flow, or the presence of damage. Smart structures with actuators distributed throughout are defined as adaptive or alternatively, actuated. The overlap structures which contain both adaptive structures and sensory structures linked by closed-loop control are referred to as controlled structures. *Intelligent structures* are a subset of the active structures that have highly distributed actuator and sensor systems with structural functionality and, in addition, distributed control functions and computing architecture [1].

1.2 Definitions of Smart Structures.

Several different definitions are given for the Smart structures by different authors in different fields.

The Japanese concept of a smart structure is given [1] as :

"materials which manifest their own functions intelligently depending on environment changes."

Their definition of 'environment' was never particularly clear. The concept was explained by classifying the 'intelligence' of materials into 3 categories.

(1) *Primitive Functions*- this level constitutes essentially adaptive (which were referred to as 'primitive') functions related to sensor, effector, and processor capabilities.

(2) *Macroscopic Functions*- this level contains the intelligence inherent in materials.

(3) *Social Utility*- this level considers the intelligence of materials from the viewpoint of human beings and refers to material 'properties' that are to be classified as 'friendly', 'rational or irrational', and are 'harmonious'.

Vincent in 1989, as quoted in Ref. [1], described intelligent materials as being "materials which can feel the equivalent of pain (i.e., overloading) and which can be used to make a self-designing structure." Another definition and concept by Nakatani in 1989 [1] stated that: "Materials possessed of *intelligence* are such

materials that can make the suitable responses by processing the various types of signals, environmental conditions and its objectives. Intelligent materials have a characteristic autonomy, flexible versatility and high adaptability to mankind and nature". Spillman in 1996 has given a formal definition of a smart structure in his paper [45] where sensing requirements and potential sensing alternatives are discussed.

A very good question arrives as to whether smart materials can be considered a subset of smart structures, whether a smart structure and an intelligent structures are the same thing, etc. This discussion is confused by the technical community due to the truly multidisciplinary nature of this new field. In June 1996 Spillman [54] has given an interesting discussion on this subject : " Smart materials and structures: What are they ?" In his paper the results of the survey are presented and discussed and a formal definition of the field of smart materials and structures is also proposed.

1.3 Materials for Sensors and Actuators used in Smart Structures

Materials which are commonly used as sensors or actuators in Smart Structures are Shape Memory Alloys, Electrorheological Fluids, Shape Memory Polymers, and Piezoelectric Sensors and Actuators. In this section only piezoelectric sensors and actuators will be discussed in detail.

In developing intelligent structures in which actuation, sensing, and processing elements are physically integrated within the structure, the use of piezoelectric actuators places certain requirements on the electronic components which drive them. Piezoelectric materials, characterized by their ability to deform under the application of an electric field, have found numerous applications in the field of structural control. Much work has been performed in characterizing piezoelectric elements, developing sensors and controllers, and addressing the requirements for embedding piezoelectric elements and electronic processing components. Piezoelectric sensors are built of materials that generate an electrical response to an applied force. Piezoelectric materials can be crystals and ceramics, but because they have a brittle nature, the piezoelectric sensors are generally made of one of the family of polymers, polyvinyldene fluoride, also known as PVDF or PVF_2. The polymer is made piezoelectric by polarizing it in either a uniaxial or biaxial film. The uniaxial film indicates stress in one direction by producing a voltage. Biaxial films indicate stress in one or two directions [1].

1.4 Technology Development Overview for Intelligent Structures

Several research trends have been combined to establish the research in intelligent structures. One is a transition to laminated materials. In the past, structures were manufactured form large pieces of monolithic material which were machined, forged or formed to a final structural shape, making it difficult to

imagine the incorporation of active elements. Present day laminated materials, which are built up from smaller constitutive elements, allow for the easy incorporation of active elements within the structure. One can now envision the incorporation of an intelligent structure carrying actuators, sensors, processors, and interconnections within the laminated material. The development of microelectronics, bus architectures, switching circuitry, fiber optic technology and the development of information processing, artificial intelligence, and control disciplines are also essential to the development of intelligent structures.

The sum of these evolving technologies are the transition to laminated materials, the exploitation of the off-diagonal terms in material constitutive relations, and the advances in microelectronics [2].

In order to present the critical components, a review of features of common smart material and structures will be presented as follows :[1]

Sensors: embedded (or bonded) or intrinsic sensor(s) which recognize and measure the intensity of the stimulus which could be stress, strain, thermal, electric, magnetic, chemical, radiation, etc.

Actuators: embedded or intrinsic actuator(s) to respond to the stimulus.

Control Mechanism: for controlling the response to the stimulus according to a predetermined relationship. Also capable of selecting response if more than one option is available.

Time and Nature of Response: fast response to stimulus. The system returns to its original state as soon as the stimulus is removed.

There are four critical components to the evolution and application of intelligent structures [2].

(1) Actuators for intelligent structures.

(2) Sensory elements.

(3) Control methodologies and algorithms

(4) Controller architecture and implementation hardware.

Actuators for Intelligent Structures

Actuators for intelligent structures must be capable of being highly distributed and influencing the mechanical states of the structure. The ideal mechanical actuator would directly convert electrical inputs in strain or displacement into the host structure. The principal actuating mechanism of strain actuators is referred to as actuation strain, which is the controllable strain not due to stress. Actuation strains are produced by a variety of phenomena, with the most common being temperature and moisture absorption. Other examples include piezoelectricity, electrostriction, magnetostriction, and the shape memory effect.

Sensory elements

The sensors which can be utilized in intelligent structures are those that do not require an external reference, for example acceleration and strain sensors.

Sensory elements of intelligent structures must be sensitive to the mechanical states of the structure and capable of being highly distributed. The ideal sensor for an intelligent structure converts strain or displacement directly into electrical

outputs. The primary functional requirement for such sensors are their sensitivity to the strain or displacement, spatial resolution, and bandwidth. Secondary requirements include the transverse and temperature sensitivity, linearity and limited hysteresis, electromagnetic compatibility, and small size of sensor packaging. Although actuators are often large size they must be accommodated in the built-up laminates, and it is desirable also to make sensors small enough to be placed in interlaminar or otherwise unobtrusive positions.

Control Methodologies and Algorithms.

Three levels of control methodology and algorithm design are local control, global algorithmic control and high cognitive functions.

The objectives of control are to add damping and/or absorb energy and minimize residual displacements.

Controller Architecture and Implementation Hardware.

The presence of actuators, sensors, and highly distributed control functionality throughout the structure implies that there must be a distributed computing architecture. The functional requirements for such a computing architecture include a bus architecture, an interconnection scheme, and distributed processing. The bus architecture should be chosen to yield a high transmission rate of data in convenient (often digital) form throughout the structure. The interconnections must be suitable for connecting a (potentially) large number of

devices, actuators, sensors, and processors with the least degradation of structural integrity.

1.5 Health Performance Monitoring

Smart structures have arrived as tools to allow health monitoring of equipment containing a network of sensors, such as strain gauges and thermocouples, connected to a data collection and analysis system. An automated Health Monitoring System (HMS) is used for measuring and monitoring how a structure is behaving under various loading conditions.

Sensors and actuators are classified as analog or digital, contacting or non-contacting, active or passive, distributed or discrete. Point sensors and actuators or conventional devices are generally discrete in nature. The advantages of applying point sensors or actuators is that little about the system requirements has to be known beforehand. On the other hand, this is also a drawback, since knowledge about the system cannot be integrated into the sensor/actuator design process. Moreover, in some applications, some information may be lost when such sensors are used, e.g., some natural frequencies and mode shapes could be missed if the sensors are placed at nodal points or flexure lines. Distributed sensors assume two generic morphologies. In the first, it is necessary to make measurements only at discrete, pre-determined points (or along specific limited lengths) of a distributed sensor. The measurement system has the character of a series-distributed array of discrete transducers, which is called in

the literature a quasi-distributed sensor system. In the second, the measurement may be made continuously over the entire sensor length as a function of position at any point along the sensor. These are called fully distributed, intrinsically-distributed, or more often, simply distributed sensors.

Similarly, there are two types of distributed actuators. In the first, the actuating force is induced at discrete locations or on small areas of the structure. In the second, the actuator is spatially distributed along or embedded in the structure in such a way that the force is induced at each point along the actuator's domain.

The analysis algorithms can be divided into two categories:

(a) algorithms that translate raw signals into meaningful information about strain values and other parameters.

(b) algorithms that use strain and other required parameters to assess shape and integrity of the structure and make decisions for changes in the shape of structure.

The first type of algorithms are sensor-specific and are closely tied to the sensor pre-processor if applicable. The sensors measure the response and feed this information to the controller. The controller determines what actuators forces are required to keep the disturbances from degrading the performance of the structure. The actuators provide the required forces at specific locations.

Optical fibres are typically 30 to 50 times larger than the structural fibres and can cause stress and strain concentrations and significantly degrade the strength and fatigue properties of the host composite structure. Optical fibres are also

susceptible to breakage during manufacturing, due to fatigue and impact damage.

Outputs from most sensors are electrical signals that need to be processed and interpreted. Physically meaningful information can be obtained only after the sensors are calibrated. Therefore, it is important that a micro-mechanics analysis be performed to accurately characterize the sensor-host interaction and the local perturbation of the elastic fields due to the presence of the sensor.

1.6 Specific applications using Smart Structure

In this section, two specific applications of smart structures will be given. These applications are mainly concerned about health monitoring system of aircraft and truss structures.

1.6.1 Aircraft Health Monitoring Systems (HMS) Applications

Aircraft are highly complex systems, composed of a variety of electronic, hydraulic and propulsion systems and a light weight/high stiffness structure, and have to withstand severe loading conditions. In addition the whole system is highly safety critical and suffers degradation even when not in service. Such complex systems require extended maintenance.

Automatic monitoring of an aircraft's health and integrity would reduce the enormous amounts of time and money spent on structural maintenance and inspections [47].

In the airline industry most of the maintenance effort is related to monitoring. Only a smaller amount of maintenance effort should be related to repair.

Ideally the aircraft of the future will monitor its own health and provide alternative control autonomously. Recent developments in new materials, innovate sensor technology, and computer hardware and software make this possible. This future aircraft will have more than just smart structures, it will be a "smart airplane" [29]. All systems will be monitored including propulsion, flight control, avionics and structures. Also, subsystems such as landing gear, hydraulics, pneumatics and environmental control will be monitored individually and as a complete operating system.

HMS for an aircraft will be capable of performing pre and post flight inspections autonomously. The inspection check list will be displayed via CRT to the pilot. Any discrepancies will be brought to the pilot's attention along with recommended actions. Maintenance personnel will be able to obtain the status of any system or subsystem. The on board computer will contain diagnostic procedures and recommend methods of repair. The maintenance manuals, flight manuals, and illustrated parts breakdown manuals will be in the aircraft's computer memory. The diagnostic software will be menu driven and will lead the person, level by level, to the action required. Illustrations will be displayed on a

CRT. Shape memory alloys designed to reroute structural load paths could provide the means to maintain the airplane integrity, allowing it to land safely.

Future aircraft health and usage monitoring systems will be designed as built-in systems and must be able to monitor damage on-condition. Major damage to be detected includes fatigue and corrosion in metallic structures and delaminations in composite structures resulting either from material degradation (aging) or mishandling, including mis-repair.

Inspection and maintenance on a military aircraft occur at specific times in its life cycle. The longevity of an aircraft is determined by the number of flight hours and the severity of those hours. One major contribution of smart structures is the potential to monitor the structural loads accurately and enable precise determination of the life duration.

1.6. 2 Truss structure integrity Identification using PZT Sensor-Actuator

The signature pattern of a truss can be monitored using a PZT patch bonded to a truss node, based on the measurement of its electric admittance, which is coupled with the mechanical impedance of the truss. The admittance of a truss can then be compared with the admittance for the original healthy truss. Statistical algorithms can then be applied to determine a damage index of the truss based on the signature pattern difference. Experimental proof that the

detection range of a bonded PZT sensor on a truss is highly constrained to its immediate neighborhood. This allows accurate determination of the damage location in a complex real-world structure with a minimum mathematical modeling and numerical computation [3].

Examination of the mechanical impedance of a structure at the location of interest has proven to be an effective way to assess the structure integrity, or the health condition of the structure. With conventional transducers such as accelerometer and force gauge, or impedance head, it is economically and technically impractical to implement real time monitoring of a large truss with hundreds of nodes. When a piezoceramic patch serves as a collocated actuator/sensor bonded to a structure, its electric admittance is modulated by the mechanical impedance of the structure. This provides a simple way of acquiring the signature pattern of the structure as the electric admittance is much easier to measure than the mechanical impedance. In addition, weight and geometry of this sensor/actuator are negligible so that its attachment to the structure will essentially introduce no impact on both static and dynamic characteristics of the structure.

Due to the tiny size and negligible weight, it is feasible to attach large quantity of PZT sensors/actuators to the nodes of a large scale truss as a permanent monitoring network without introducing noticeable changes in its structural characteristics.

1.7 General Applications of Using Smart structure.

In this section three general applications of smart structures related to composite structures and active control of structures will be presented.

1.7.1 Embedded Sensors in Composite Structures

Embedded sensors are critical to structural health monitoring in high performance applications, e.g. "Smart" skins and structures. Optical fibre sensors have been the principal sensing technique for these applications.

Microelectromechanical systems, (MEMS) include useful mechanical structures, sensors, actuators and signal processing electronics fabricated on a common semiconductor substrate such as silicon.

Two critical issues in applying microdevice technology to structural composite monitoring are their ability to :

(1) be manufactured at a scale compatible with the composite fiber architecture

(2) survive the temperatures and pressures present during composite fabrication.

Embedded sensors are considered defects in a composite structure. The effects of embedding small discrete sensors on mechanical properties is minimal. Embedded microsensors can be developed which will not have significant adverse effects on the mechanical properties of composite materials, such that

the use of such sensors need not impact the service performance of composite structures containing them.

1.7.2 Active Damage Mitigation in Composite Structure by Actuation of Piezoceramic Patches

Damage in the form of local cracks or distributed microcracks causes a reduction of natural frequencies and increase in vibration damping. Natural frequency measurements are a very attractive form of damage detection tests since they can be made at a single point on the component and are independent of position chosen, since this change in natural frequencies is caused by a localized reduction of stiffness due to damage anywhere in the structure [41].

The consequences of all damage in composite structures are changes in stiffness, strength, and fatigue properties. Measurement of strength or fatigue properties during damage development is not feasible because both of them require destructive testing. However stiffness can be measured frequently during damage development because it directly effects the dynamic response of the structure. The widely used method is to identify the occurrence, location, and extent of the damage from measured structural dynamic characteristics such as frequencies and mode shapes.

Using a piezoelectric actuator it is possible to excite the member at different sinusoidal frequencies and with a piezoelectric sensor the response of the member can be measured and the dynamic parameters of the structure can be

evaluated. The advantage of using active materials for the system identification is that the condition of the structure can be continuously monitored by using an onboard microprocessor and, the sensor output can be continuously evaluated [41].

Once the presence of a defect has been detected, the next step is to locate the damage. No analytical model is available to locate the position of damage from system identification data. An alternate method is to train a neural network with dynamic responses that result from structures with known locations and types of defects. After sufficient training the network may be able to find the position and type of defect in a damaged structural member. The last step consists of mitigation of the damage. The structure is embedded with piezoelectric patches at the time of manufacturing to change the stiffness and damping of the structure so that the loading on the damaged structure can redistributed to minimize the effect of such damage. These kinds of damage detection and mitigation schemes are most suitable for military applications like tanks, helicopters, small jet fighters operating from aircraft carriers, etc. [41]. Damage that is not detected continuously and not corrected may potentially cause more damage and eventually catastrophic structural failure. Since these vehicles during their wartime service go through very little maintenance, this kind of detection scheme can permit real time corrective action or a change in operating procedures to minimize the possibility of causing further damage.

The main principle behind the active damage mitigation is that if the actuators are located close to the damage location, the actuators should apply a strain out-

of-phase with the strain caused, in the damage location, by the external loads. This will essentially reduce the stress in the damaged area. Since the type of loading that can cause the stress is unknown, if the dynamic moment acting on the damaged region can be reduced over a wide frequency range, it can be said that the actuators are capable of stress alleviation for any loading condition.

1.7.3 Modal Based and Wave-type Vibration Energy Transmission for Active Control of Structures

It is essential to provide means to obtain vibration minimization and isolation in engineering structures and systems to enhance performance, maintain reliability, ensure prolonged life of operation, and to reduce the effects of undesirable structurally radiated noise. In engineering systems such as light space vehicles, satellites, and space radar systems with large flexible antennae and beam-like appendages, the importance of suppression of the transmission of vibration is imperative [37]. Reduction of vibration transmitted to the body of a car from an engine or reduction of vibration transmitted to the aircraft from jet engines and propellers are good examples of vibration suppression. One method typically used to predict vibration levels for active vibration control is from Finite Element Modal (FEM) formulations [37]. The dynamic response of the system to some forced excitation is calculated by determining the normal modes of the system explicitly and the total response obtained as a sum of the modal responses. The modes of the structure and damping are obtained experimentally from modal

analysis or determined numerically from finite element methods [37]. The structural vibration response is viewed in the form of normal modes and standing waves (mode shapes) within the structure. For controller design the analytical model is usually truncated and the design is based on the truncated model.

The modal/FEM methods are usually based on the first few modes, particularly when structural modes are distinctly spaced.

1.8 Preliminary Conclusions Regarding Smart Structures

A smart structure involves distributed actuators and sensors, and one or more microprocessors that analyze the responses from the sensors and use distributed-parameter control theory to command the actuators to apply localized strains to minimize system response. A smart structure has the capability to respond to a changing external environment (such as loads or shape changes) as well as to a changing internal environment (such as damage or failure). It incorporates smart actuators that allow the alteration of system characteristics as well as of system response in a controlled manner. Many types of actuators and sensors can be considered, such as piezoelectric materials. Numerous applications of smart structures technology to various physical systems are evolving to actively control vibration, noise, aeroelastic stability, damping, shape and stress distribution. Applications range from space systems, fixed-wing and

rotary-wing aircraft, automotive, civil structures and machine tools. Much of the early development of smart structures methodology was driven by space applications such as vibration and shape control of large flexible space structures, but now wider applications are envisaged for aeronautical and other systems. Applications of smart structures technology to aerospace and other systems are also expanding rapidly [52]. More information about smart structures can be found in the book called "Smart Material and Structures" by M.V. Gandhi and B.S. Thompson [79].

Chapter 2

Literature Review on Vibration of Smart Structures

2.1 General Overview of Vibration

The vibration of thin beams supported and clamped in different ways was first studied by Euler and Bernoulli in the middle of the 18^{th} century. Their approach is now called the thin beam theory or Euler-Bernoulli theory. Another important contribution to beam theory was given by Stephen Timoshenko [76] in the middle of the 20^{th} century. He developed an improved theory of vibration of beams which is now called thick beam theory or Timoshenko theory by considering the effects of rotary inertia and shear deformation.

In recent times, many investigations have been motivated by the engineering applications of vibration, such as the design of machines, foundations, structures and control systems. As mentioned by Gorman [6], no mechanical design should be complete without a free vibration analysis of beams. The vibration of beams has become a subject of great interest in the industrialized world.

In the study of free vibrations of continuous systems (such as beams), attention is typically concentrated on finding the eigenvalues (frequencies) and

corresponding eigenfunctions i.e. mode shapes. Determination of the motion of a system subsequent to its beginning with a known initial displacement and velocity was presented by Leissa in 1991 [70]. For general initial conditions, the subsequent motion of a typical point will not be simple harmonic. It will not even be periodic. Points of the beam will reach their maximum displacements at different times. The classical procedure for analyzing such motion, at least in the case of a linear system, is to express it as a superposition of the displacements of the free vibration modes. As a first test, Leissa considered a cantilever beam which initially was deflected by a moment applied at its end. Then he considered a concentrated force applied at the end and considered next the case of an initial deflection caused by a uniformly distributed load. He found that in his first case, the initial displacement caused by an end moment, the motion was nearly periodic. In the next two cases, the contributions of the second and higher modes to the motions were found to be smaller, and so the motions were also nearly periodic. From theory, the motion would be perfectly periodic only if the natural frequencies of the initiated modes are all rational multiples of each other and only a finite number of modes are initiated. Finally he suggested a new definition for vibration. He said that a vibration is a motion which is periodic, or almost periodic, in time, otherwise the motion simply falls into the broader category of dynamic response. In April 1996, Chan et al [79] published a paper concerning about a simply supported beam , which was partially loaded with distributed mass. His theoretical method is more accurate than the finite element method, especially at higher frequency modes.

Roy et al in 1995 [68] published a paper concerning the transient response of a cantilever beam subjected to an impulse load. In his paper, the effects of impulse duration, damping and location of application of loads were studied. Furthermore, the deflection and the stress histories and corresponding frequency responses were also discussed. The response of the system depends not only on system parameters such as mass, stiffness and the damping, but also on the duration of the impulse and point of application of the load. A comprehensive study has been carried out to investigate the influence of these parameters on the deflection and stress, and the effect of damping on the response.

Not only Euler-Bernoulli theory but also Timoshenko theory has been investigated experimentally by many people. Abbas and Irretier [72] investigated experimentally the combined effect of rotary inertia, shear deformation and root flexibility of a cantilever beam which is a Timoshenko beam. The experimental results show excellent agreement with theoretical methods.

Laura et al [73] has also presented analytical and experimental results for a vibrating Timoshenko cantilever beam carrying a mass at its free end. They also obtained a very satisfactory agreement between experimental and analytical results.

H.Abramovich [71] used a stainless steel beam to measure the natural frequencies of a Timoshenko cantilever beam and compared with analytical predictions. His experimental results were obtained by using two different methodologies.

(1) The beam was excited by using an electrodynamic exciter and the resonance was determined by using an accelerometer mounted on the tip of the beam and an oscilloscope.

(2) The beam was excited by using the impulse technique. The response of the beam was measured by an accelerometer mounted on its tip and stored by using a memory oscilloscope. The data was transferred on line to a PC which performs a Fourier transformation, yielding the natural frequencies of the beam.

Their experimental results yielded a fairly good agreement with the analytical predictions.

The propagation of bending waves under a moving single load was studied by A. Kunow-Baumhauer [69]. In his paper, 3 types of beams were studied, Euler-Bernoulli beam, a beam with shear deflection and a Timoshenko beam. The responses of the Euler- Bernoulli and the Timoshenko beam were studied under moving pressure wave excitation. The results were presented as dynamic amplification factors (DAF). Here a transient pressure wave load means neither a quasi-static load (described by the lowest frequency) nor a shock or impulse loading. A pressure wave load is between these 2 extreme cases. His paper presented an analytical approach to finding the response of a structure to a high speed pressure wave.

A simple supported beam was used in his work. A moving impulse load and a moving pressure wave starting from zero with constant velocity were separately studied. The response of beams under loads moving at high speed is very

different from those moving at slow speeds. For a moving impulse load the Euler-Bernoulli beam theory gives good results for the deflections if the propagation speed is small. Bending moments there are significant differences between the results of the Euler-Bernoulli and the Timoshenko theories while the difference between the response of a beam with shear deflection and that of a Timoshenko beam are small. The moment of inertia has only a small influence on the response. The response of a beam under a moving pressure wave is presented in terms of the maximum dynamic amplification factors (DAF) both for the deflections and the bending moments. If the Euler-Bernoulli theory is compared with the Timoshenko theory the differences between the DAF results are small. The influence of the load shape is important. If the load is asymmetrical and suddenly rising in the propagation direction, it nearly doubles the DAF as compared to that for a symmetrical load shape.

In 1997, the analysis of the Timoshenko beam traversed by uniform partially distributed moving masses was carried out by Esmailzadeh et al [81]. In their work, the equations of motion were solved by using finite difference method. The beam response, and the distribution of the shear force and bending moment along the beam have been considered. The results compare well with those reported in the literature for the limiting case in which the length of the load distribution reduces to zero and also the effects of shear deformation and rotary inertia are neglected.

Sato [62] investigated the free vibration of beams with changes of cross section. He used a simple beam with grooves for testing. As the ratio of the groove width to beam thickness increases, the analytical results may become incorrect.

Cawley and Ray [64] examined natural frequency changes in a beam due to cracks with changes caused by machined slots. Their results showed conclusively that the width of the machined slots must be taken into account, i.e., the geometry must be included in modeling and testing for damage.

In 1996 in Japan, work has been done by Yoshitsugufor Goto [82] [83] in developing experimental identification techniques for boundary conditions of a beam. These techniques permit the determination of the boundary conditions in terms of spring constants, damping coefficients, and equivalent masses and moments of inertia, using data of dynamic responses of a beam. The technique was applied to an actual beam. The responses obtained using the identified results were confirmed well with experiment. Yuji Sogabe [80], analyzed the transient vibrations of elastically connected double-beam systems taking into account the effects of shear deformation and rotary inertia in accordance with the Timoshenko beam theory. The Finite Integral Transform technique was used successfully and applied to the elastically coupled two Timoshenko beams having different cross sections and being made of different materials. After solving the boundary value problem, it was shown that there exist four series of eigenvalues and eigenfunctions. Transient responses due to impulsive loading as well as step loading was analyzed and compared with the case of the Euler-Bernoulli double-beam system. It was found that the Timoshenko double-beam

system behaves in a slightly different manner from that of Euler-Bernoulli double-beam system.

2.2 Vibration of Smart Structures

Adams [78] was the first to find that a state of damage in fiber-reinforced plastics could be detected by a reduction of stiffness and an increase in damping. In 1978, he presented a method for determining damage location by receptance analysis. Vibration measurements made at a single station in a structure can be used in conjunction with a suitable theoretical model to indicate both the location and the magnitude of a defect. Cawley and Adams [65] used finite-elememt analysis for finding the damage location. They were also the first to present the analytical and experimental results regarding piezoelectric actuators as elements of intelligent structures. In 1989, Tracy and Pardoen showed that the presence of delamination of a laminated beam, degraded the even-numbered vibration modes much more rapidly than the odd-numbered modes. In 1994 Abu S. Islam [63] used piezoceramic actuators to excited a composite beam at different sinusoidal frequencies, and used piezoceramic sensors to measure the response of the structure. By using these method, the damage in composite structures was detected. Section 2.2.1 describes the concept used in more details. Section 2.2.2 explains experimentally validated damage detection using non-modal based method .

2.2.1 Damage Detection By Structural Modal Analysis Using Collocated Piezoelectric Actuator/Sensors - An Electromechanical Approach

A single piezoceramic (PZT) patch bonded to a structure may be used as a collocated actuator/sensor for structural modal analysis. When activated by a voltage signal, the PZT element excites the structure as a result of its induced strain. The interaction between PZT and its host structure is governed by the mechanical impedance of the structure. If the applied electrical voltage and resulting electrical current (or the electrical transfer function) of the collocated PZT actuator/sensor are known, the mechanical impedance of the structure can be determined through an appropriate electromechanical model. Based on the measurement of the electric admittance of collocated actuator/sensors, the modal analysis technique utilizes thin piezoelectric patches bonded on structures as both sensor and actuator. A commercial electrical impedance analyzer is used to measure the electrical admittance of the PZT patch. Two corresponding algorithms, revised inverse Nyquist plane curve fitting and admittance matching-half power bandwidth approaches were presented for the extraction of modal parameters [63].

Experimental modal test is now a mature and standard technique in structure dynamic analysis. It usually consists of several independent stages: structure

excitation, measurement of driving force and vibrational response, formation of Frequency Response Function (FRF), and modal parameter extraction. The attachment of conventional transducers onto a testing structure may result in considerable errors in determining system parameters, especially with light-weight and flexible structures. The use of Laser Doppler Vibrometer and Eddy Current Sensor still needs attachment of a force gauge and shaker to the structure.

A piezoceramic patch may serve as both sensor and actuator at the same time as a result of piezoelectric effect and its converse. When bonded to a structure and driven by an alternating voltage, it imposes a bending moment on the structure through its longitudinal expansion and contraction, causing the structure to vibrate. This strain on the piezoceramic patch due to vibration of the structure then in turn produces a voltage and modulates the current flowing through the patch. The electric admittance of the bonded patch is much easier to measure than a mechanical transfer function for force input and displacement output. Because of the light weight and the low flexural stiffness of a PZT patch, the mass loading effect can usually be neglected and its stiffening effect can be easily compensated.

A generic model governing the electromechanical interaction of the actuator and the structure was derived and used to extract the structure admittance, or mobility at the position where the PZT is bonded [63].

All load-carrying members of structures continuously accumulate damage in their service. In order to ensure safe operating conditions it is necessary to monitor

the damage continuously and to take temporary corrective actions by redistributing the load to minimize the effects of such damage until the structure can be repaired. The consequences of damage in composite structures are change in stiffness, strength, and fatigue properties. Measurement of strength or fatigue properties during damage development is not feasible because both of these require destructive testing. However, stiffness can be measured frequently during damage development because it directly affects the dynamic response of the structure. This change in stiffness results in a decrease of the natural frequencies of the specimen. The measurement of natural frequencies of a structure at two more stages of its life therefore offers the possibility of detecting the presence and location of damage.

Using a piezoelectric actuator it is possible to excite the member at different sinusoidal frequencies and with a piezoelectric sensor the response of the member can be measured and the dynamic parameters of the structure can be evaluated. The advantage of using active materials for the system identification is that the condition of the structure can be continuously monitored. Generally there are 3 kinds of damage: fiber fracture, matrix cracking and delamination. Of these types of damage, only delamination was considered in a finite element model of the damaged structure which was used to calculate the theoretical change in frequencies for comparison with the experimental result. An alternate method is to train a neural network with dynamic responses that result from structures with known locations and types of defect. After sufficient training the network may be able to find the position and type of defect in a damaged

structural member. In [63] a back-propagation neural network has been trained with the frequencies of the first five modes obtained from modal analysis data (not transient) from piezoceramic sensors in both damaged and healthy composite beams.

2.2.2 Experimentally Validated Damage Detection Using A Non Modal Based Method.

A method for the non-destructive detection and location of damage using parameterized partial differential equations and Galerkin approximation techniques is presented by Banks et al [58]. The optimization method and enhanced least-square error minimization method were also used for their mathematical model. Experimental results were presented from tests on cantilevered aluminum beams damaged at different locations and with damage of different dimensions. It was demonstrated that the method can sense the presence of damage, and locate and characterize the damage to a satisfactory precision.

Piezoceramic patches can be used both as a sensor and actuator (i.e, they are collocated) for the damage detection experiments. The literature survey demonstrated the feasibility of using measured changes in vibration characteristics to detect damage by measuring the vibration response both

before and after the damage occurrence. The methods [58] do not consider damping effects or mode shape changes. Unlike many competing methods, the approach presented was independent of modal information from the structure. The method [58] was based on the fact that the damage to a structure will produce in some way changes in the structural mass, damping and stiffness properties. The changes in the physical coefficients of mass density, elastic modulus and damping coefficients can provide information regarding damage detection.

The detection is based on determining the shape function using observation of the system output response to excitation from the patches [58]. One response data set was generated for a beam with a centered circular hole at 2.413 cm away from the clamped end. The second response data was generated with a hole at 14.478 cm. Identical broadband input signals were applied and the time response data were plotted. Since the amount of change in the response due to the damage was very small, recorded data in a short time period would not provide enough information showing the difference caused by damages. On the other hand, higher vibrational modes were damped out in the response over a longer time period. Two experimental data sets were obtained. One recorded from an undamaged beam and one from a damaged beam.

Their mathematical model was assumed based on Euler-Bernoulli hypothesis and Kelvin-Voigt hypothesis (damping proportional to strain rate). The beam was subject only to forces and moments generated by actuating the patches.

The parameter estimation method was sensitive to small change due to the damage. However the size of the damages were all over-estimated.

The authors discovered that the beams' characteristics were slightly changed during the drilling process in a manner in which the change was not modeled in their equations. (e.g., changes in mass density around the holes due to shearing and stress, etc.)

Derivation of the governing equations and boundary conditions of laminated beam smart structures were developed in [60]. Sensor and actuator layers were included in the beam to facilitate vibration suppression. Two mathematical models, the shear-deformable (Timoshenko) model and the shear-indeformable (Euler-Bernoulli) model, were presented in [60]. The differential equations for the continuous system were approximated by utilizing finite element techniques. A cantilever laminated beam was investigated to assess the validity and the accuracy of the proposed models. Comparison between the two models was presented to show the advantages and the limitations of the proposed models. Since the Timoshenko beam theory is higher order than the Euler-Bernoulli theory, it is known to be superior in predicting the transient response of the beam.

A finite element formulation was presented for modeling the dynamic response of smart structures with embedded piezoelectric ceramic devices subjected to transient loading. Paper [50] was based on the concept of virtual work and a thin cantilever plate with piezoelectric devices is investigated.

Chapter 3

Physical Description and Mathematical Model for Transient Response Analysis

3.1 Introduction

The purpose of this thesis as mentioned before is to develop a non-destructive testing method which uses transient responses analysis to measure the degree of damage in a beam. The degree of damage is measured by the difference between transient responses of the tested beam and the undamaged beam. Before this primary objective can be realized for damages such as crack or joint loosening, two extreme cases were first analyzed. They are an undamaged clamped-clamped beam and a completely disconnected beam which is represented by a cantilever beam. A simple structure, a two beam system, was therefore chosen for this proof of concept using analytical and experimental methods. The location of damage was assumed to be in the middle of the clamped-clamped beam for simplicity. In this chapter physical description and mathematical model of the system is described.

3.2 Physical Description of The System

In order to detect any damage on a beam, the transient response to a forcing function of a beam with different boundary conditions is analyzed. Two sets of boundary conditions are considered, a clamped-clamped beam (perfectly connected beams) while the second is a Cantilever beam (totally disconnected beams).

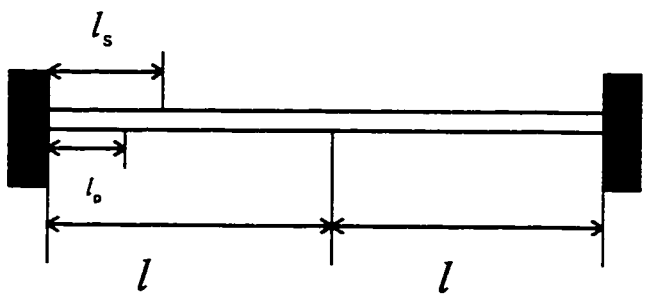

Fig 3.1 a. Clamped-clamped beam model of healthy beam system.

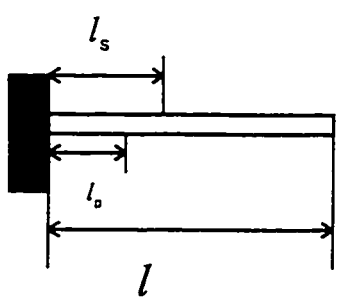

Fig 3.1 b. Cantilever beam as model of completely disconnected beam system.

These two boundary conditions were selected to represent a safe beam and a damaged beam. Other boundary conditions also could be selected, to represent partially damaged beam like fixed-pinned.

As shown in Fig 3.1, a thin aluminum beam with non-collocated piezoceramic sensor and two piezoceramic actuators which were fixed to the top and the bottom of the beam were used. In this figure l_s and l_p represent the sensor location and actuator location respectively. Specification of the beam and the locations of sensor and actuators are given in table 3.1.

Table 3.1 Physical Description of Beam

Beam of aluminum		
object type	symbols	unit
sensor diameter	Φ	20.68 mm
thickness	t_b	0.94 mm
width	w_b	25.34 mm
length	l	0.55 m
area	$A=w_b*t_b$	$23.8*10^{-6}$ m^2
moment of inertia	$I=w_b*t_b^3/12$	$1.75*10^{-12}$ m^4
Young's modulus	E	$70*10^9$ N/m^2
density	ϱ	$2.7*10^3$ Kg/m^3
shear modulus of elasticity	G	$26*10^9$ N/m^2

location of actuator	l_p	0.1315 m
location of sensor	l_s	0.1936 m

In order to find the dynamic specifications of the beam, vibration of the beam is analyzed theoretically and experimentally. Table 3.2 shows the first five natural frequencies of the cantilever and clamped-clamped beams obtained in theoretical analysis.

Table 3.2 Natural frequencies

Number of mode	Natural frequencies (Cantilever) rad/s	Natural frequencies (Clamped-Clamped) rad/s
First	16.13	25.53
Second	100.4	70.32
Third	281.3	138.1
Fourth	551.3	228.1
Fifth	912.6	340.7

Fig 3.3 and fig 3.4 shows the mode shapes of the first few modes for Cantilever and clamped-clamped beams. The forcing functions used in this study are a half sine wave, a full sine wave and ten or higher number of sine waves. Fig 3.5

shows these forcing function for input frequency of $1/(2\pi)$ Hz. Mathematical model of transient vibration of the beam is given in section 3.3 and experimental results of this system are given in Section 5.2.

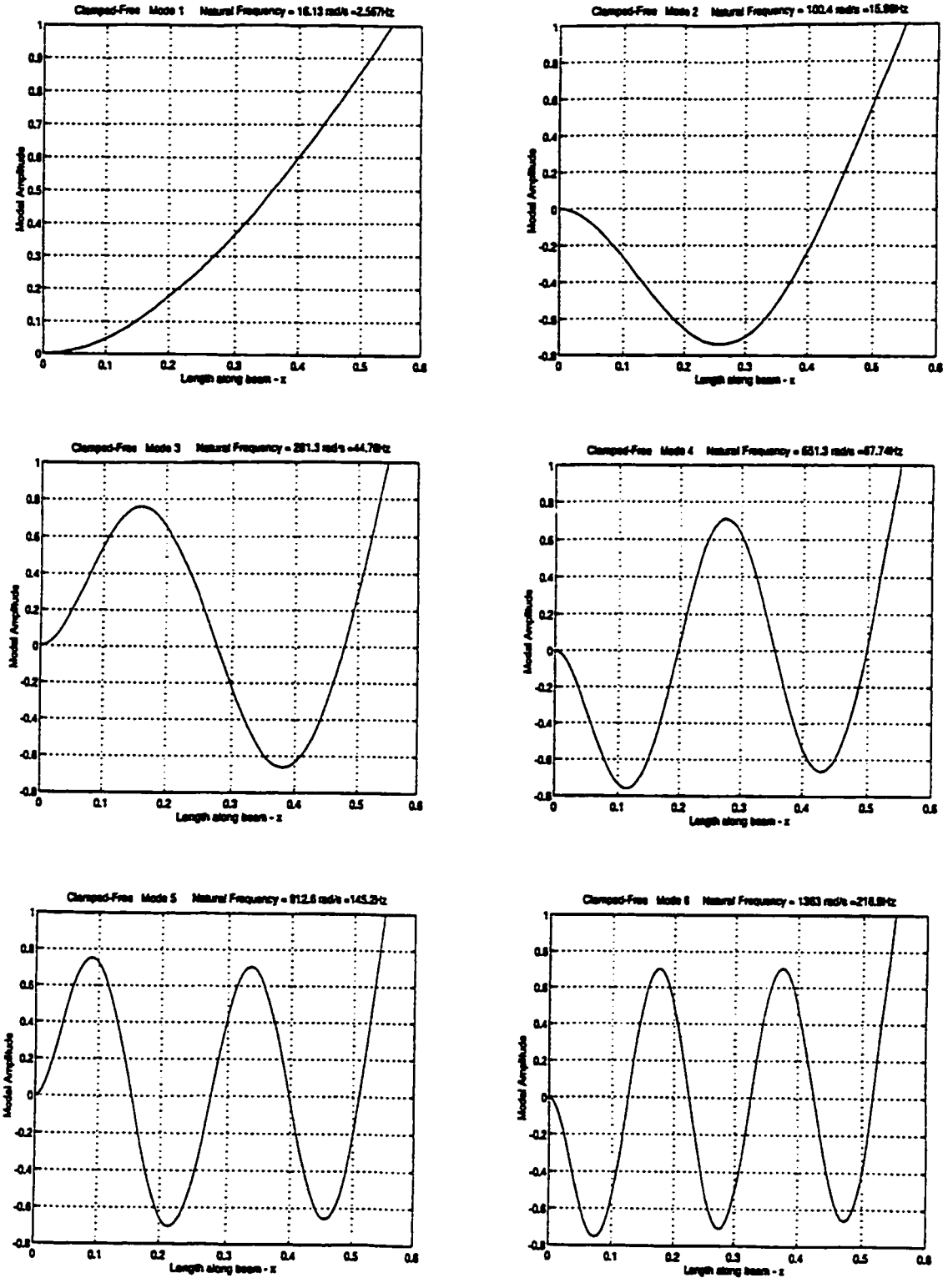

Fig 3.3 Mode shapes of the first six modes for Cantilever beam.

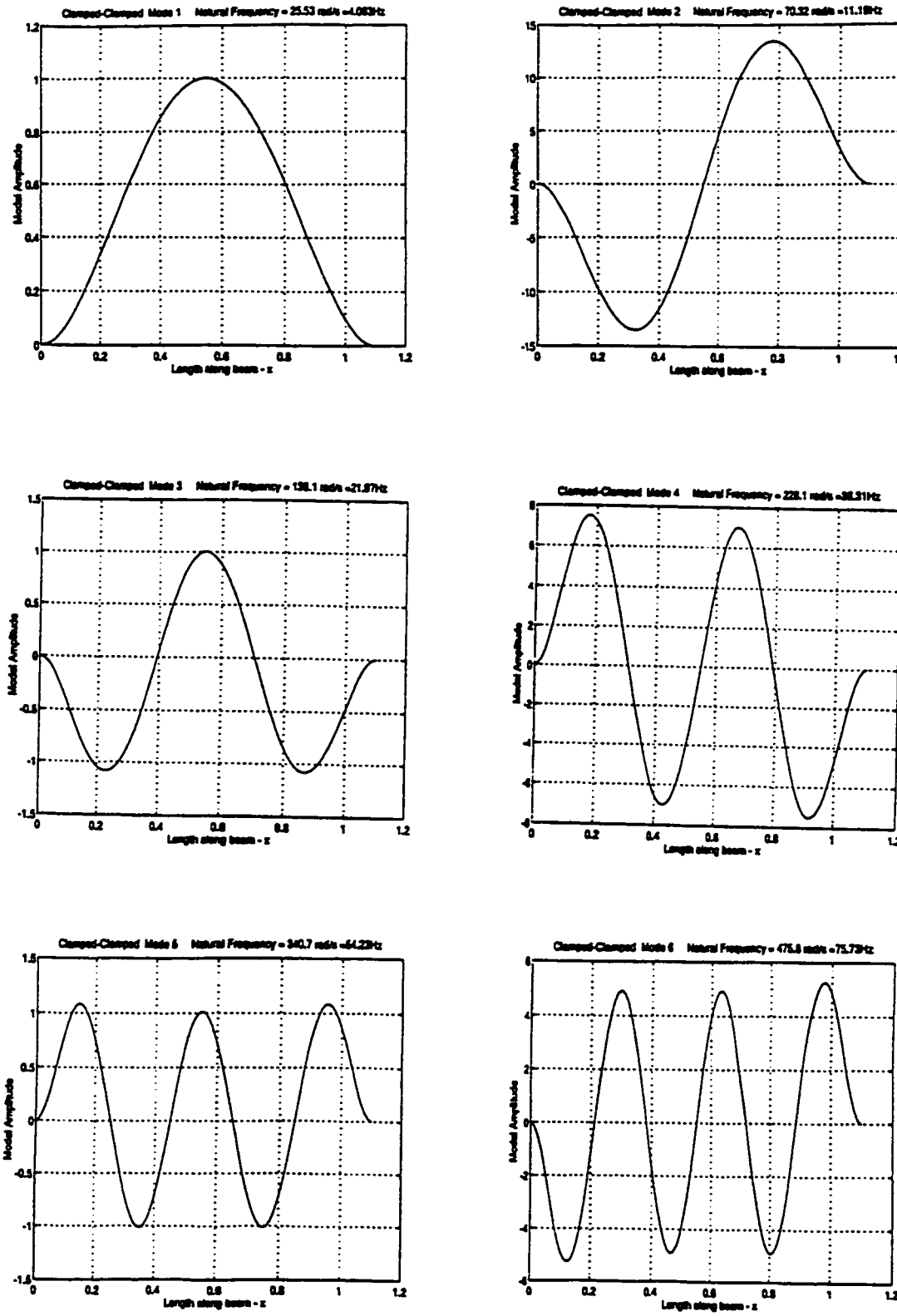

Fig 3.4 Mode shapes of the first six modes for Clamped-Clamped beam.

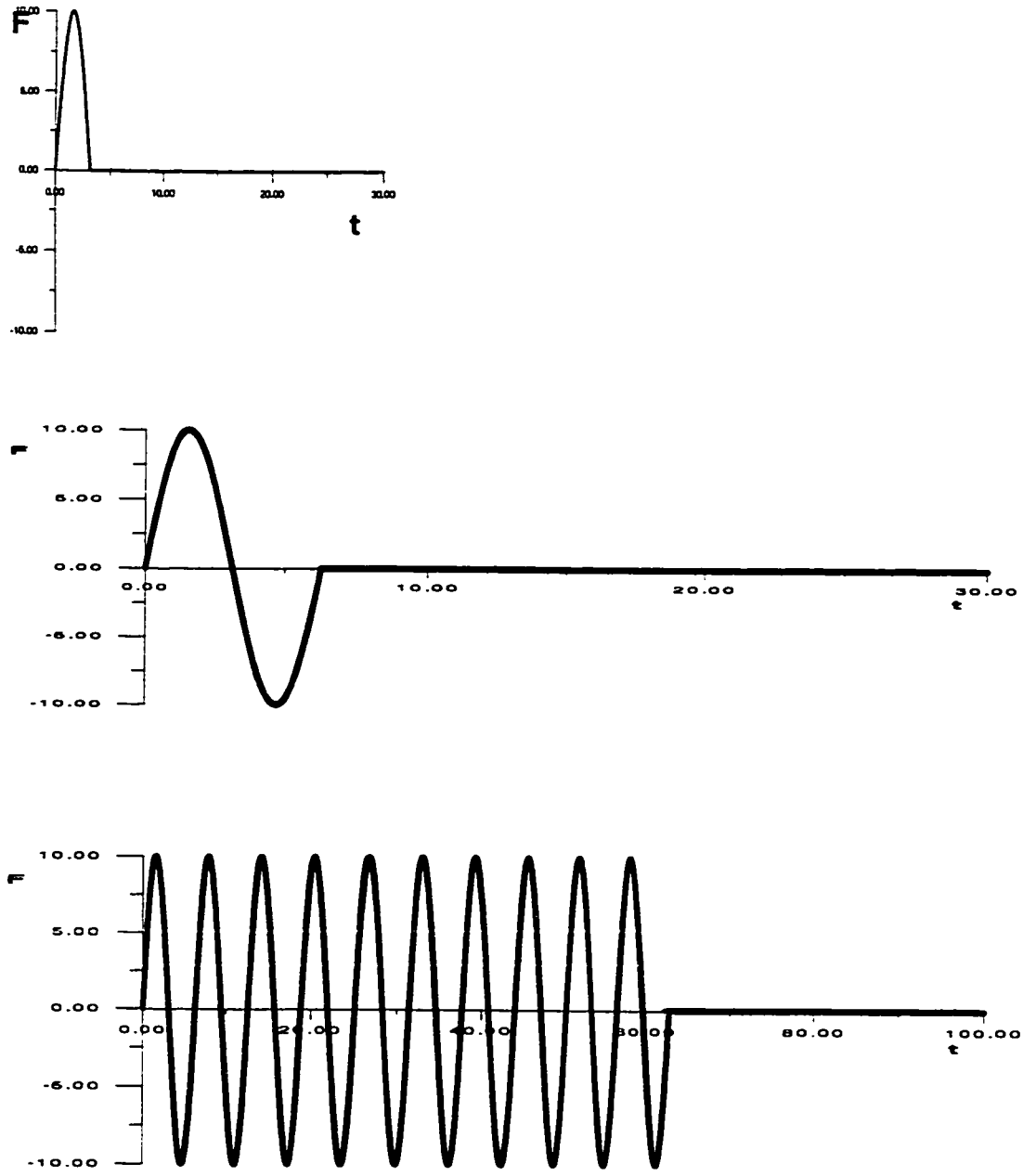

Fig 3.5 Different kind of forcing functions used in this study.

3.3 Analytical Model of Vibration of a Beam.

Vibration of a beam can be divided into longitudinal vibration and transverse vibration. The differential equation of longitudinal vibration for a given forcing function $F(x,t)$ is given as:

$$\frac{\partial^2 u}{\partial x^2} = \frac{1}{c^2}\frac{\partial^2 u}{\partial t^2} + \frac{F(x,t)}{c^2 M} \qquad (3.1)$$

This is similar to the equation for string vibration or the differential equation of the wave. The differential equation for transverse vibration of a beam with forcing function $F(x,t)$ generally can be derived based on two models. One is the thin beam (Euler Bernoulli) model and the other is the thick beam (Timoshenko) model.

The thin beam model or Euler Bernoulli equation is

$$a^2 \frac{\partial^4 y}{\partial x^4} + \frac{\partial^2 y}{\partial t^2} = \frac{F(x,t)}{\varrho AL} = \frac{f(x,t)}{\varrho A} \qquad (3.2)$$

In equation (3.1) and (3.2) the variables

u is the axial displacement in (m),

x is the position along the length of the beam in (m) ,

t is the time in (s),

$F(x,t)$ is the applied force in (N),

M is the total mass of the beam in (kg),

$c = \sqrt{\frac{E}{\varrho}}$ is the velocity of longitudinal wave propagation,

y is the transversal displacement,

E is Young's Modulus in (N/m^2),

I is the area moment of inertia of the beam about its thickness axis in (m^4),

ϱ is the density of the beam in (kg/m^3),

A is the cross-section area of the beam in (m^2),

L is the Length of the beam in (m),

$f(x,t)$ is Force per unit length in (N/m), and

$a = \sqrt{\frac{EI}{\varrho A}}$ is a coefficient in (m^2/s).

Thick beam theory or Timoshenko beam equation is obtained taking into consider on the rotary inertia and shear deformation. The results are :

$$-kAG\left(\frac{\partial \psi}{\partial x} - \frac{\partial^2 y}{\partial x^2}\right) + f(x,t) = \varrho A \frac{\partial^2 y}{\partial t^2} \tag{3.3}$$

$$EI\frac{\partial^2 \psi}{\partial x^2} - kAG\left(\psi - \frac{\partial y}{\partial x}\right) = \varrho I \frac{\partial^2 \psi}{\partial t^2} \tag{3.4}$$

By solving (3.3) for $\frac{\partial \psi}{\partial x}$ and substituting the result in (3.4), uncoupled Timoshenko beam model [76] is obtained.

$$\frac{EI}{\varrho A}\frac{\partial^4 y}{\partial x^4} + \frac{\partial^2 y}{\partial t^2} - \frac{I}{A}\left(1 + \frac{E}{kG}\right)\frac{\partial^4 y}{\partial x^2 \partial t^2} + \frac{\varrho I}{KGA}\frac{\partial^4 y}{\partial t^4} + \frac{EI}{\varrho k A^2 G}\frac{\partial^2 f}{\partial x^2} - \frac{I}{kA^2 G}\frac{\partial^2 f}{\partial t^2} = \frac{f(x,t)}{\varrho A} \tag{3.5}$$

The first two terms on the left hand side and the first term on the right hand side are common with Euler-Bernoulli beam model. The term $\frac{\varrho I}{KGA} = \frac{1}{\varpi_c}$, where ϖ_c is defined as cutoff frequency [78].

In Timoshenko equation, ψ represents the total angle change due to bending, k is the Timoshenko shear coefficient (which is equal to 5/6 for rectangular cross-section area and 9/16 for a circular cross-section area of the beams) and , G is the shear modulus (N/m^2).

In this research only transverse wave motion with the Euler-Bernoulli model is used due to the following 3 reasons:

(1) The beam used in this study is very thin and rotary inertia and shear deformation effects are not important.

(2) For this beam, based on the data given in table 3.1, the values of $\frac{\varrho I}{GAk} = 9.1629*10^{-15}, \frac{I}{A}\left(1+\frac{E}{Gk}\right) = 3.1108*10^{-7}, \frac{EI}{\varrho kA^2G} and \frac{I}{kA^2G}$ are very small, so they can be neglected.

(3) According to [78], since the input frequency of excitation is much below the cutoff frequency ($\varpi_c = \sqrt{\frac{kGA}{\varrho I}}$ =1.66 MHz) by at least a factor of 20, Euler-Bernoulli model is suitable for the beam used in this analytical and experimental study.

Several transient forcing functions were selected for this study as shown in section 3.2, i.e. half-sine pulse, one complete sine pulse and several sine waves. Two extreme conditions were considered: A) two beams are completely disconnected and B) two beams perfectly connected.

In the first case (A), completely disconnected beams can be reduced to a cantilever actuated beam model with length equal to just l given that the other

beam remains unactuated. The second case (B) corresponds to perfectly connected beams and can be considered as a clamped-clamped beams system with the length $L=2l$. In order to distinguish between the two boundary conditions, the transient response of the Euler-Bernoulli model must be derived analytically. First, the cantilever beam problem and then the clamped-clamped beam problem are solved.

For solving the Euler Bernoulli differential equation, as given in equation (3.2) (which is a fourth order partial differential equation), four boundary conditions and two initial conditions are needed. The boundary conditions and solution for two different cases are given as the following section.

3.3.1 Case A: The Clamped-Free Beam (Cantilever Beam)

Boundary Conditions for this beam can be defined as :

① $y(x,t)|_{x=0} = 0$ Displacement at clamped end =0.

② $\frac{\partial y(x,t)}{\partial x}|_{x=0} = 0$ Slope at clamped end =0.

③ $\frac{\partial^2 y(x,t)}{\partial x^2}|_{x=l} = 0$ Moment at free end =0.

④ $\frac{\partial^3 y(x,t)}{\partial x^3}|_{x=l} = 0$ Shear at free end =0.

For the transient response to the given forcing function, the beam is assumed to be initially at rest. Therefore the initial conditions are:

❶ $y(x,t)|_{t=0} = 0$

❷ $\frac{\partial y(x,t)}{\partial t}|_{t=0} = 0$

The acceleration due to the excitation force will be a sinusoidal signal of magnitude α (m/s^2) and frequency Ω (rad/s). This vertical acceleration in practice is produced by the two piezoceramic actuators which are connected to two opposite sides of the beam at the center point location x = l_p, therefore:

$$\frac{f(x,t)}{\varrho A} = \alpha \sin(\Omega t) \qquad \text{for } (x = l_p)$$

$$\frac{f(x,t)}{\varrho A} = 0 \qquad \text{elsewhere}$$

To calculate the mode shapes of the beam, normal mode vibration with no forcing function is considered, and by using separation of variable method ($y(x,t)=X(x)T(t)$) substituting this equation into the differential equation

$a^2 \frac{\partial^4 y}{\partial x^4} = -\frac{\partial^2 y}{\partial t^2}$, the following results can be obtained :

$$a^2 X'''' T = -X\ddot{T}$$

or

$$a^2 \frac{X''''}{X} = -\frac{\ddot{T}}{T} = \lambda^2$$

or

$$a^2 X'''' = \lambda^2 X$$

Solving the above equation, the result is

$$X(x) = C\cos\left(\sqrt{\frac{\lambda}{a}}x\right) + D\sin\left(\sqrt{\frac{\lambda}{a}}x\right) + E\cosh\left(\sqrt{\frac{\lambda}{a}}x\right) + F\sinh\left(\sqrt{\frac{\lambda}{a}}x\right)$$

Applying boundary conditions ① and ② give:

$C+E=0$

and

$D+F=0$

Applying boundary conditions ③ and ④ and with $z=\sqrt{\frac{\lambda}{a}}l$ the following two equations can be obtained:

$$E(\cosh z+\cos z)+F(\sinh z+\sin z)=0$$
$$E(\sinh z-\sin z)+F(\cosh z+\cos z)=0$$

These equations have a solution different from the obvious trivial solution $E=F=0$ if and only if

$$\begin{vmatrix}\cosh z+\cos z & \sinh z+\sin z\\ \sinh z-\sin z & \cosh z+\cos z\end{vmatrix}=0$$

i.e.

$$\cosh z\cos z=-1$$

therefore $z_1=1.8751$, $z_2=4.6941$, $z_3=7.8548$, $z_4=10.006$, $z_5=14.14,\ldots$

The rest of the approximate solution from T.C.Chang and R.R.Craig Jr. "Normal Modes of Uniform Beam",Proc. ASCE v95 n.EM4,1025-1031 (1969) [84] is in the form

$z_i=(i-1/2)\,\pi$

$$\lambda_i=\frac{az_i^2}{l^2}$$

when z has any one of the values z_1, z_2, z_3 ...

E and F have the corresponding values E_n and F_n

$$\frac{E_n}{F_n}=-\frac{\cosh z_n+\cos z_n}{\sinh z_n-\sin z_n}$$

or

$$\frac{E_n}{F_n} = -\frac{\sinh z_n + \sin z_n}{\cosh z_n - \cos z_n}$$

Since E and F must satisfy both of the above equations, we can select the first equation for convenience and let

$$\sigma_n = \frac{\sinh z_n - \sin z_n}{\cosh z_n + \cos z_n}$$

therefore

E_n=-C_n=-F_n/σ_n

F_n=-D_n

and

$$X_n(x) = -\frac{F_n}{\sigma_n}\left[\cosh \beta_n x - \cos \beta_n x - \sigma_n (\sinh \beta_n x - \sin \beta_n x)\right] \qquad (3.6)$$

where $\beta_n = \sqrt{\frac{\lambda_n}{a}} = \frac{z_n}{l}$

Since F_n and σ_n are constant values, we can replace them as a new constant value,

let $A_n = -\frac{F_n}{\sigma_n}$

The equation (3.6) for the mode shape is

$$X_n(x) = A_n\left[\cosh \beta_n x - \cos \beta_n x - \sigma_n (\sinh \beta_n x - \sin \beta_n x)\right] \qquad (3.7)$$

where

$$\sigma_n = \frac{\sinh \beta_n l - \sin \beta_n l}{\cosh \beta_n l + \cos \beta_n l}$$

and

$\cosh(\beta_n l)\cos(\beta_n l) = -1$

Since $a^2 X_n'''' = \lambda_n^2 X_n$, substituting into the equation of motion (3.2) we get:

$$(\ddot{T}_n + \lambda_n^2 T_n) X_n = \alpha \sin(\Omega t)\delta(x - l_p) \tag{3.8}$$

From orthogonality condition we have the following two equations:

$$\int_0^l X_n(x) X_m(x) dx = 0 \qquad \text{for } m \neq n$$

and

$$\int_0^l X_n^2(x) dx = 1 \qquad \text{for } m = n$$

Therefore substituting (3.7) into the orthogonality condition, we get

$$A_n^2 \int_0^l \left[\cosh\beta_n x - \cos\beta_n x - \sigma_n(\sinh\beta_n x - \sin\beta_n x)\right]^2 dx = 1$$

After integrating, we have

$$\begin{aligned} A_n^2 = {} & 8\beta_n / (-2e^{(-2\beta_n l)}\sigma_n - 4e^{(-\beta_n l)}\sin(\beta_n l) - e^{(-2\beta_n l)}\sigma_n^2 - e^{(-2\beta_n l)} \\ & - 4\cos(\beta_n l)e^{(\beta_n l)} + 8\sigma_n \cos^2(\beta_n l) - 4\sin(\beta_n l)e^{(\beta_n l)} + 8\beta_n l - 2e^{(2\beta_n l)}\sigma_n \\ & + 8\sigma_n \sin(\beta_n l)e^{(\beta_n l)} + e^{(2\beta_n l)}\sigma_n^2 + 4\sigma_n^2 \cos(\beta_n l)e^{(\beta_n l)} + 4e^{(-\beta_n l)}\cos(\beta_n l) \\ & - 4\sigma_n^2 \sin(\beta_n l)e^{(\beta_n l)} + 2e^{(2\beta_n l)} + 4\cos(\beta_n l)\sin(\beta_n l) - 8e^{(-\beta_n l)}\sigma_n \sin(\beta_n l) \\ & - 4e^{(-\beta_n l)}\sigma_n^2 \cos(\beta_n l) - 4e^{(-\beta_n l)}\sigma_n^2 \sin(\beta_n l) - 4\sigma_n^2 \cos(\beta_n l)\sin(\beta_n l) - 4\sigma_n) \end{aligned}$$

Simplifying this equation gives,

$$\begin{aligned} A_n^2 = {} & 4\beta_n / \{4\beta_n l + 2\sigma_n \cos(2\beta_n l) - 2\sigma_n \cosh(2\beta_n l) - 4\cosh(\beta_n l)\sin(\beta_n l) - 4\sigma_n^2 \cosh(\beta_n l)\sin(\beta_n l) \\ & + \sin(2\beta_n l) - \sigma_n^2 \sin(2\beta_n l) - 4\cos(\beta_n l)\sinh(\beta_n l) + 4\sigma_n^2 \cos(\beta_n l)\sinh(\beta_n l) + 8\sigma_n \sin(\beta_n l)\sinh(\beta_n l) \\ & + \sinh(2\beta_n l) + \sigma_n^2 \sinh(2\beta_n l)\} \end{aligned}$$

Multiplying the equation of motion (3.8) by $X_n(x)$ and integrating over the length of the beam:

$$\ddot{T}_n + \lambda_n^2 T_n = \alpha \sin \Omega t \int_0^l X_n(x)\delta(x - l_p)dx$$

or

$$\ddot{T}_n + \lambda_n^2 T_n = \alpha \sin \Omega t X_n(l_p) \quad (3.9$$

In order to solve the above non-homogeneous equation, a complementary function should be added to the particular solution.

The complementary function has the form of $T=C\cos(\lambda_n t)+D\sin(\lambda_n t)$

and then try the particular integral to be

$T= H\cos(\Omega t)+K\sin(\Omega t)$

and

$\ddot{T} = -H\Omega^2\cos(\Omega t)-K\Omega^2\sin(\Omega t)$

Substituting the particular integral into the original equation (3.9) we get

$H = 0$

and

$$K = \frac{\alpha X_n(l_p)}{\lambda_n^2 - \Omega^2}$$

The total solution for $T_n(t)$ is therefore

$$T_n(t) = C\cos\lambda_n t + D\sin\lambda_n t + \frac{\alpha X_n(l_p)}{\lambda_n^2 - \Omega^2}\sin\Omega t$$

To satisfy the initial conditions

$T(0)=0$ and $\dot{T}(0)=0$

we get

$C = 0$

and

$$D = \frac{-\alpha X_n(l_p)}{\lambda_n^2 - \Omega^2}\frac{\Omega}{\lambda_n}$$

Therefore by substituting C and D into equation (3.10) we get

$$T_n(t) = \frac{\alpha X_n(l_p)}{\lambda_n^2 - \Omega^2}\left(\sin\Omega t - \frac{\Omega}{\lambda_n}\sin\lambda_n t\right)$$

The complete solution for a continuous sinusoidal excitation at point l_p is

$$y(x,t) = \sum_{n=1}^{\infty}\left\{A_n\left[\cosh\beta_n x - \cos\beta_n x - \sigma_n(\sinh\beta_n x - \sin\beta_n x)\right]\frac{\alpha X_n(l_p)}{\lambda_n^2 - \Omega^2}(\sin\Omega t - \frac{\Omega}{\lambda_n}\sin\lambda_n t)\right\}$$

or

$$y(x,t) = \sum_{n=1}^{\infty}\frac{\alpha X_n(x) X_n(l_p)}{\lambda_n^2 - \Omega^2}(\sin\Omega t - \frac{\Omega}{\lambda_n}\sin\lambda_n t) \qquad (3.11)$$

Two sinusoidal pulse excitations are used:

Case 1: Half-sine pulse,

Case 2: Full -sine pulse.

For case 1, let $t_1 = \pi/\Omega$

To determine the solution for $t>t_1$ the superposition principle is used. We have

$$y(x,t) = \sum_{n=1}^{\infty}\{\frac{\alpha X_n(x) X_n(l_p)}{\lambda_n^2 - \Omega^2}[\sin\Omega t - \frac{\Omega}{\lambda_n}\sin\lambda_n t + \sin\Omega(t-t_1) - \frac{\Omega}{\lambda_n}\sin\lambda_n(t-t_1)]\}$$

After arrangement, we have

$$y(x,t) = \sum_{n=1}^{\infty}\{\frac{\alpha X_n(x) X_n(l_p)}{\lambda_n^2 - \Omega^2}[2\sin\left(\frac{2\Omega t - \pi}{2}\right)\cos(\frac{\pi}{2}) - \frac{\Omega}{\lambda_n}2\sin\left(\frac{2\lambda_n t - \lambda_n\pi/\Omega}{2}\right)\cos(\frac{\lambda_n}{\Omega}\frac{\pi}{2})]\}$$

and simplifying, we get

$$y(x,t) = \sum_{n=1}^{\infty}\{\frac{2\alpha X_n(x) X_n(l_p)}{\Omega^2 - \lambda_n^2}\frac{\Omega}{\lambda_n}\sin\left(\lambda_n t - \frac{\lambda_n}{\Omega}\frac{\pi}{2}\right)\cos(\frac{\lambda_n}{\Omega}\frac{\pi}{2})\} \qquad \text{for } t > t_1 \qquad (3.12)$$

For $t<t_1$, equation (3.11) remains unchanged. Therefore, we have

$$y(x,t)=\sum_{n=1}^{\infty}\left\{A_n\left[\cosh\beta_n x-\cos\beta_n x-\sigma_n\left(\sinh\beta_n x-\sin\beta_n x\right)\right]\frac{\alpha X_n(l_p)}{\lambda_n^2-\Omega^2}\left(\sin\Omega t-\frac{\Omega}{\lambda_n}\sin\lambda_n t\right)\right\}$$

After simplifying, the equation becomes

$$y(x,t)=\sum_{n=1}^{\infty}\frac{\alpha X_n(x)X_n(l_p)}{\lambda_n^2-\Omega^2}\left(\sin\Omega t-\frac{\Omega}{\lambda_n}\sin\lambda_n t\right)\qquad \text{for } t<t_1 \qquad (3.13)$$

For case 2 (a complete sine wave)

let $t_1=\pi/\Omega$

To determine the solution for $t>2\,t_1$ the superposition principle is used:

$$y(x,t)=\sum_{n=1}^{\infty}\left\{\frac{\alpha X_n(x)X_n(l_p)}{\lambda_n^2-\Omega^2}\left[\sin\Omega t-\frac{\Omega}{\lambda_n}\sin\lambda_n t-\sin\Omega(t-2t_1)+\frac{\Omega}{\lambda_n}\sin\lambda_n(t-2t_1)\right]\right\}$$

or

$$y(x,t)=\sum_{n=1}^{\infty}\left\{\frac{\alpha X_n(x)X_n(l_p)}{\lambda_n^2-\Omega^2}\left[2\cos(\Omega t-\pi)\sin\pi+2\frac{\Omega}{\lambda_n}\cos(\lambda_n t-\lambda_n\frac{\pi}{\Omega})\sin(-\frac{\lambda_n\pi}{\Omega}\right]\right\}$$

After simplifying, the equation becomes

$$y(x,t)=\sum_{n=1}^{\infty}\left\{\frac{2\alpha X_n(x)X_n(l_p)}{\Omega^2-\lambda_n^2}\frac{\Omega}{\lambda_n}\cos\left(\lambda_n t-\frac{\lambda_n}{\Omega}\pi\right)\sin(\frac{\lambda_n}{\Omega}\pi)\right\}\qquad \text{for } t>2t_1 \qquad (3.14)$$

For $t<2t_1$. Equation (3.11) remains unchanged. Therefore we have

$$y(x,t)=\sum_{n=1}^{\infty}\left\{A_n\left[\cosh\beta_n x-\cos\beta_n x-\sigma_n\left(\sinh\beta_n x-\sin\beta_n x\right)\right]\frac{\alpha X_n(l_p)}{\lambda_n^2-\Omega^2}\left(\sin\Omega t-\frac{\Omega}{\lambda_n}\sin\lambda_n t\right)\right\}$$

or

$$y(x,t)=\sum_{n=1}^{\infty}\frac{\alpha X_n(x)X_n(l_p)}{\lambda_n^2-\Omega^2}\left(\sin\Omega t-\frac{\Omega}{\lambda_n}\sin\lambda_n t\right)\qquad \text{for } t<2t_1 \qquad (3.$$

3.3.2 Case B: The clamped-clamped beam

Euler Bernoulli Equation is

$$a^2 \frac{\partial^4 y}{\partial x^4} + \frac{\partial^2 y}{\partial t^2} = \frac{f(x,t)}{\varrho A}$$

where (3.16)

$$a = \sqrt{\frac{EI}{\varrho A}}$$

The four boundary conditions are:

① $y(x,t)|_{x=0} = 0$ Displacement at one clamped end =0.

② $\frac{\partial y(x,t)}{\partial x}|_{x=0} = 0$ Slope at one clamped end =0.

③ $y(l,t) = 0$ Displacement at the other clamped end =0.

④ $\frac{\partial y(x,t)}{\partial x}|_{x=l} = 0$ Slope at the other clamped end =0.

and the two initial conditions are :

❶ $y(x,t)|_{t=0} = 0$

❷ $\frac{\partial y(x,t)}{\partial t}|_{t=0} = 0$

The forcing function is

$\frac{f(x,t)}{\varrho A} = \alpha \sin(\Omega t)$ for $(x = l_p)$

$\frac{f(x,t)}{\varrho A} = 0$ elsewhere

Similar to the cantilever situation to calculate the mode shape assume $y(x,t)=X(x)T(t)$ and substituting this equation into the differential equation

$a^2\frac{\partial^4 y}{\partial x^4}=-\frac{\partial^2 y}{\partial t^2}$ gives:

$$a^2 X'''' T = -X\ddot{T}$$

or

$$a^2\frac{X''''}{X}=-\frac{\ddot{T}}{T}=\lambda^2$$

or

$$a^2 X'''' = \lambda^2 X$$

Solving the above equation, the result is

$$X(x)=C\cos\left(\sqrt{\frac{\lambda}{a}}x\right)+D\sin\left(\sqrt{\frac{\lambda}{a}}x\right)+E\cosh\left(\sqrt{\frac{\lambda}{a}}x\right)+F\sinh\left(\sqrt{\frac{\lambda}{a}}x\right) \qquad (3.17)$$

Applying boundary condition ① and ② give

$E=-C$

and

$F=-D$

Let $\beta=\sqrt{\frac{\lambda}{a}}$. Equation (3.17) becomes

$$X(x)=C(\cos\beta x-\cosh\beta x)+D(\sin\beta x-\sinh\beta x)$$

Applying boundary conditions and give the following two equations

$$C(\cos\beta l-\cosh\beta l)+D(\sin\beta l-\sinh\beta l)=0$$
$$C(\sin\beta l+\sinh\beta l)+D(-\cos\beta l+\cosh\beta l)=0$$

For $z=\beta l$, a solution for the constant C, D (different from zero) can be obtained when the determinant equal to zero:

$$\begin{vmatrix} -(\cos z+\cosh z) & \sin z-\sinh z \\ \sin z+\sinh z & -\cos z+\cosh z \end{vmatrix}=0$$

or

$$\cosh z\cosh z=1$$

The lowest consecutive roots are

z_1=4.730 , z_2=7.853 , z_3=10.996 , z_4=14.137 , z_5=17.279 , ...

The rest of them can be approximated by the formula $z_i=(i+1/2)\pi$

When z has any one of the values z_1, z_2, z_3 .... the corresponding values of C and D are

$$\frac{C_n}{D_n}=\frac{-(\sin\beta_n l-\sinh\beta_n l)}{\cos\beta_n l-\cosh\beta_n l}$$

or

$$\frac{C_n}{D_n}=\frac{-(-\cos\beta_n l+\cosh\beta_n l)}{\sin\beta_n l+\sinh\beta_n l}$$

Choosing the first equation for convenience and letting $\sigma_n=\frac{\cosh\beta_n l-\cos\beta_n l}{\sinh\beta_n l-\sin\beta_n l}$, the results are:

C_n=-D_n/σ_n

E_n=D_n/σ_n

F_n=-D_n

Therefore the mode shape is

$$X_n(x)=\frac{D_n}{\sigma_n}\left[\cosh\beta_n x-\cos\beta_n x-\sigma_n(\sinh\beta_n x-\sin\beta_n x)\right] \qquad (3.18)$$

Similarly D_n and σ_n are constant value, they can be replaced as another constant value

$$A_n = \frac{D_n}{\sigma_n}$$

Substituting $a^2 X_n'''' = \lambda_n^2 X_n$ in the equation of motion (3.16) we get

$$(\ddot{T}_n + \lambda_n^2 T_n) X_n = \alpha \sin(\Omega t)\delta(x - l_p) \qquad (3.19)$$

From orthogonality condition (now *L=2l*) we can write

$$\int_0^L X_n(x) X_m(x) dx = 0 \qquad \text{for } m \neq n$$

and

$$\int_0^L X_n^2(x) dx = 1 \qquad \text{for } m = n$$

Therefore, substituting (3.18) into the orthogonality condition, we get:

$$A_n^2 \int_0^L [\cosh\beta_n x - \cos\beta_n x - \sigma_n(\sinh\beta_n x - \sin\beta_n x)]^2 dx = 1$$

After some calculations, we get

$$A_n^2 = 4\beta_n / \{4\beta_n L + 2\sigma_n \cos(2\beta_n L) - 2\sigma_n \cosh(2\beta_n L) - 4\cosh(\beta_n L)\sin(\beta_n L) - 4\sigma_n^2 \cosh(\beta_n L)\sin$$
$$+ \sin(2\beta_n L) - \sigma_n^2 \sin(2\beta_n L) - 4\cos(\beta_n L)\sinh(\beta_n L) + 4\sigma_n^2 \cos(\beta_n L)\sinh(\beta_n L) + 8\sigma_n \sin(\beta_n L)\sinh$$
$$+ \sinh(2\beta_n L) + \sigma_n^2 \sinh(2\beta_n L)\}$$

Multiply the equation of motion (3.19) by $X_n(x)$ and integrating over the length of the beam, we have

$$\ddot{T}_n + \lambda_n^2 T_n = \alpha \sin\Omega t \int_0^L X_n(x)\delta(x - l_p) dx$$

or

$$\ddot{T}_n + \lambda_n^2 T_n = \alpha \sin\Omega t X_n(l_p) \qquad (3.20)$$

In order to solve the above non-homogeneous solution, a complementary function should be added to the particular solution.

The complementary function has the form of $T=C\cos(\lambda_n t)+D\sin(\lambda_n t)$

The particular integral has the form of :

$$T= H\cos(\Omega t)+K\sin(\Omega t)$$

or $$\ddot{T} = -H\Omega^2\cos(\Omega t)-K\Omega^2\sin(\Omega t)$$

Substituting the particular integral into the original equation (3.20), we get

$$H = 0$$

and

$$K = \frac{\alpha X_n(l_p)}{\lambda_n^2 - \Omega^2}$$

The complete solution for $T_n(t)$ is then become as follows

$$T_n(t) = C\cos\lambda_n t + D\sin\lambda_n t + \frac{\alpha X_n(l_p)}{\lambda_n^2 - \Omega^2}\sin\Omega t \qquad (3.21)$$

Same as before, to satisfy the initial conditions, we have :

$$C = 0$$

and

$$D = \frac{-\alpha X_n(l_p)}{\lambda_n^2 - \Omega^2}\frac{\Omega}{\lambda_n}$$

Equation (3.21) becomes

$$T_n(t) = \frac{\alpha X_n(l_p)}{\lambda_n^2 - \Omega^2}\left(\sin\Omega t - \frac{\Omega}{\lambda_n}\sin\lambda_n t\right)$$

The total solution for a continuous sinusoidal excitation at point l_p is therefore

$$y(x,t)=\sum_{n=1}^{\infty}\left\{A_n\left[\cosh\beta_n x-\cos\beta_n x-\sigma_n(\sinh\beta_n x-\sin\beta_n x)\right]\frac{\alpha X_n(l_p)}{\lambda_n^2-\Omega^2}(\sin\Omega t-\frac{\Omega}{\lambda_n}\sin\lambda_n t)\right\}$$

or

$$y(x,t)=\sum_{n=1}^{\infty}\frac{\alpha X_n(x)X_n(l_p)}{\lambda_n^2-\Omega^2}(\sin\Omega t-\frac{\Omega}{\lambda_n}\sin\lambda_n t) \qquad (3.22)$$

Same as for clamped-free beam, two sinusoidal pulse excitations are used. They are:

Case 1: Half-sine pulse

Case 2: Full -sine pulse

For case 1, let $t_1=\pi/\Omega$

To determine the solution for $t>t_1$ the superposition principle is used. We have

$$y(x,t)=\sum_{n=1}^{\infty}\{\frac{\alpha X_n(x)X_n(l_p)}{\lambda_n^2-\Omega^2}[\sin\Omega t-\frac{\Omega}{\lambda_n}\sin\lambda_n t+\sin\Omega(t-t_1)-\frac{\Omega}{\lambda_n}\sin\lambda_n(t-t_1)]\}$$

or

$$y(x,t)=\sum_{n=1}^{\infty}\{\frac{\alpha X_n(x)X_n(l_p)}{\lambda_n^2-\Omega^2}[2\sin\left(\frac{2\Omega t-\pi}{2}\right)\cos(\frac{\pi}{2})-\frac{\Omega}{\lambda_n}2\sin\left(\frac{2\lambda_n t-\lambda_n\pi/\Omega}{2}\right)\cos(\frac{\lambda_n}{\Omega}\frac{\pi}{2})]\}$$

After simplifying, the equation becomes

$$y(x,t)=\sum_{n=1}^{\infty}\{\frac{2\alpha X_n(x)X_n(l_p)}{\Omega^2-\lambda_n^2}\frac{\Omega}{\lambda_n}\sin\left(\lambda_n t-\frac{\lambda_n}{\Omega}\frac{\pi}{2}\right)\cos(\frac{\lambda_n}{\Omega}\frac{\pi}{2})\} \qquad \text{for } t>t_1 \qquad (3.23)$$

For $t<t_1$, equation (3.22) remains unchanged. Therefore, we have:

$$y(x,t)=\sum_{n=1}^{\infty}\left\{A_n\left[\cosh\beta_n x-\cos\beta_n x-\sigma_n(\sinh\beta_n x-\sin\beta_n x)\right]\frac{\alpha X_n(l_p)}{\lambda_n^2-\Omega^2}(\sin\Omega t-\frac{\Omega}{\lambda_n}\sin\lambda_n t)\right\}$$

or

$$y(x,t)=\sum_{n=1}^{\infty}\frac{\alpha X_n(x)X_n(l_p)}{\lambda_n^2-\Omega^2}(\sin\Omega t-\frac{\Omega}{\lambda_n}\sin\lambda_n t) \qquad \text{for } t<t_1 \qquad (3.24)$$

For case 2 (a complete sine wave)

let $t_1=\pi/\Omega$

To determine the solution for $t>2\,t_1$ the superposition principle is used. We have:

$$y(x,t)=\sum_{n=1}^{\infty}\{\frac{\alpha X_n(x)X_n(l_p)}{\lambda_n^2-\Omega^2}[\sin\Omega t-\frac{\Omega}{\lambda_n}\sin\lambda_n t-\sin\Omega(t-2t_1)+\frac{\Omega}{\lambda_n}\sin\lambda_n(t-2t_1)]\}$$

or

$$y(x,t)=\sum_{n=1}^{\infty}\{\frac{\alpha X_n(x)X_n(l_p)}{\lambda_n^2-\Omega^2}[2\cos(\Omega t-\pi)\sin\pi+2\frac{\Omega}{\lambda_n}\cos(\lambda_n t-\lambda_n\frac{\pi}{\Omega})\sin(-\frac{\lambda_n\pi}{\Omega}]\}$$

or

$$y(x,t)=\sum_{n=1}^{\infty}\{\frac{2\alpha X_n(x)X_n(l_p)}{\Omega^2-\lambda_n^2}\frac{\Omega}{\lambda_n}\cos\left(\lambda_n t-\frac{\lambda_n}{\Omega}\pi\right)\sin(\frac{\lambda_n}{\Omega}\pi)\}\qquad \text{for } t>2t_1 \qquad (3.2$$

For $t<2t_1$, equation (3.22) remains unchanged. Therefore we have:

$$y(x,t)=\sum_{n=1}^{\infty}\left\{A_n[\cosh\beta_n x-\cos\beta_n x-\sigma_n(\sinh\beta_n x-\sin\beta_n x)]\frac{\alpha X_n(l_p)}{\lambda_n^2-\Omega^2}(\sin\Omega t-\frac{\Omega}{\lambda_n}\sin\lambda_n t)\right\}$$

or

$$y(x,t)=\sum_{n=1}^{\infty}\frac{\alpha X_n(x)X_n(l_p)}{\lambda_n^2-\Omega^2}(\sin\Omega t-\frac{\Omega}{\lambda_n}\sin\lambda_n t)\qquad \text{for } t<2t_1 \qquad (3.2$$

3.3.3 Alternative Laplace Transform - Normal - Mode Expansion Method.

In order to verify our solutions and make sure they are correct an alternative Laplace Transform method is also used.

As a continuation of last section (3.3.2), we consider the Clamped-Clamped case first.

Applying Laplace transform w.r.t. t in the Euler-Bernoulli equation, it gives

$$a^2\bar{y}''''(x,s)+s^2\bar{y}(x,s)=\frac{\bar{f}(x,s)}{\varrho A} \qquad (3.27)$$

Expanding $\bar{y}(x,s),\bar{f}(x,s)$ in a series of normal modes $Y_n(x)$, we have:

$$\bar{y}(x,s) = \sum_{n=1}^{\infty} a_n(s) Y_n(x)$$

and

$$\bar{f}(x,s) = \sum_{n=1}^{\infty} b_n(s) Y_n(x) \qquad (3.28)$$

where

$$X_n(x) = A_n Y(x) = A_n \left[\cosh \beta_n x - \cos \beta_n x - \sigma_n (\sinh \beta_n x - \sin \beta_n x)\right]$$

and $$\sigma_n = \frac{\cosh \beta_n l - \cos \beta_n l}{\sinh \beta_n l - \sin \beta_n l} \qquad (3.29)$$

From equation (3.28) we must be able to expand an arbitrary function in an infinite series of known function $\{Y_n(x)\}$.

Equations (3.28) bear little or no resemblance to the terms of a Fourier Series, however the required expansions can be carried out using orthogonality of the Y's which is guaranteed by the Theorem 5 on p519 [77] summarized in section 3.3.4.

Before applying the theorem, we need to remember the following relationship between X and Y:

$$X_n'''' = \frac{\lambda_n^2}{a^2} X_n$$

and

$$Y_n'''' = \frac{\lambda_n^2}{a^2} Y_n$$

The following variables and constants are used in the theorem:

$r(x)=1,\ q(x)=0,\ p(x)=1,\ \psi=\lambda^2/a^2$

$a=0, b=L$

$a_1=1, \alpha_1=0$

$b_1=1, \beta_1=0$

$a_2=1, \alpha_2=0$

$b_2=1, \beta_2=0$

The set $\{Y_n(x)\}$ is orthogonal w.r.t. $p(x)=1$.

Multiplying (3.28) by $Y_n(x)$ and integrating from 0 to L, we have

$$b_n = \frac{\int_0^L \bar{f}(x,s)Y_n(x)dx}{\int_0^L Y_n^2(x)dx} = \frac{\int_0^L \bar{f}(x,s)Y_n(x)dx}{\frac{1}{A_n^2}\int_0^L X_n^2(x)dx} = A_n^2 \int_0^L \bar{f}(x,s)Y_n(x)dx \qquad (3.30)$$

Substituting (3.28) and (3.30) into (3.27) we get:

$$a^2 \sum_{n=1}^{\infty} a_n(s)Y_n''''(x) + s^2 \sum_{n=1}^{\infty} a_n(s)Y_n(x) = \frac{1}{\varrho A}\sum_{n=1}^{\infty} b_n(s)Y_n(x)$$

or

$$\sum_{n=1}^{\infty} a^2 a_n(s)Y_n''''(x) + s^2 a_n(s)Y_n(x) = \frac{1}{\varrho A}\sum_{n=1}^{\infty} b_n(s)Y_n(x)$$

Remembering the relationship:

$Y_n'''' = \beta_n^4 Y_n(x)$

and

$$a_n(s) = \frac{b_n(s)}{A\varrho(a^2\beta_n^4 + s^2)},$$

We get

$$\bar{y}(x,s) = \frac{1}{\varrho A}\sum_{n=1}^{\infty}\left(\frac{A_n^2}{(a^2\beta_n^4 + s^2)}\right)\int_0^L \bar{f}(x,s)Y_n(u)du \qquad (3.31)$$

Taking inverse Laplace Transform, equation (3.31) becomes

$$y(x,t) = \frac{1}{\varrho A}\sum_{n=1}^{\infty}\frac{A_n Y_n(x)}{\lambda_n}\int_0^L A_n Y_n(u)du\int_0^t f(u,\tau)\sin[\lambda_n(t-\tau)]d\tau$$

where $f(x,t) = F_0\sin(\Omega t)\delta(x-l_p)$

or

$$y(x,t) = \frac{F_0}{\varrho A}\sum_{n=1}^{\infty}\frac{X_n(x)}{\lambda_n}X_n(l_p)\int_0^t\sin(\Omega\tau)\sin(\lambda_n t-\lambda_n\tau)d\tau$$

Since

$$\int_0^t\sin(\Omega\tau)\sin(\lambda_n t-\lambda_n\tau)d\tau = \frac{\sin(\Omega t)\lambda_n - \sin(\lambda_n t)\Omega}{\lambda_n^2-\Omega^2}$$

and

$F_0 = \alpha\varrho A$

therefore

$$y(x,t) = \sum_{n=1}^{\infty}\frac{\alpha X_n(x)X_n(l_p)}{\lambda_n^2-\Omega^2}(\sin(\Omega t)-\sin(\lambda_n t)\frac{\Omega}{\lambda_n}) \qquad (3.32)$$

The above equation (3.32) is the same as (3.22), the equation of Case B.

Similarly, one can use the same Laplace transform to proof for the cantilever beam.

In this case, we have the following values to substitute into the theorem in the section 3.3.4:

$r(x)=1,\ q(x)=0,\ p(x)=1,\ \psi = \frac{\lambda^2}{a^2}$

$a=0,\ b=l\ ;$

$a_1=1,\ \alpha_1=0;$

$b_1=0,\ \beta_1=-1;$

$a_2=1,\ \alpha_2=0;$

$b_2=0,\ \beta_2=-1.$

Using similar procedure as clamped-clamped beam above we have

$$y(x,t)=\sum_{n=1}^{\infty}\left\{A_n\left[\cosh\beta_n x-\cos\beta_n x-\sigma_n(\sinh\beta_n x-\sin\beta_n x)\right]\frac{\alpha X_n(l_p)}{\lambda_n^2-\Omega^2}(\sin\Omega t-\frac{\Omega}{\lambda_n}\sin\lambda_n t)\right\}$$

or

$$y(x,t)=\sum_{n=1}^{\infty}\frac{\alpha X_n(x)X_n(l_p)}{\lambda_n^2-\Omega^2}(\sin\Omega t-\frac{\Omega}{\lambda_n}\sin\lambda_n t)$$

The result is the same as (3.11) with $\sigma_n=\dfrac{\sinh z_n-\sin z_n}{\cosh z_n+\cos z_n}$.

Therefore we have shown that the mathematical equations for both Case A and Case B are correct.

3.3.4 Expansion Theorem

Given

$$\frac{d^2[r(x)y^{"}]}{dx^2}+[q(x)+\psi p(x)]y=0$$

where *r(x)* and *p(x)* are continuous on the closed interval *[a,b]*. *q(x)* is continuous at least on the open interval *(a,b)*, and at the same time

satisfying the boundary conditions

$$a_1y(a)-\alpha_1(ry^{"})^{'}\Big|_{x=a}=0$$
$$b_1y(b)-\beta_1(ry^{"})^{'}\Big|_{x=b}=0$$
$$a_2y^{'}(a)-\alpha_2(ry^{"})\Big|_{x=a}=0$$
$$b_2y^{'}(b)-\beta_2(ry^{"})\Big|_{x=b}=0$$

where neither a_i and α_i nor b_i and β_i are both zero and if y_1, y_2, y_3 are nontrivial solution corresponding to ψ_n then $\{y_n(x)\}$ form a system orthogonal with respect to weight function *p(x)* over the interval *(a,b)*.

3.4 Some General Information About Piezoelectric Effect.

A piezoceramic (PZT), short for Lead Zirconate Titanate, exhibits a bi-directional "piezoelectric" effect. When motion is in only one direction and the stress T and the electric field E are chosen as the intensive variables, the electromechanical interaction between the stress, strain, the electric field and flux density is governed by the following constitutive equations [41]:

$$S_{ij} = S^{E}_{ijkl} T_{kl} + d_{kij} E_k$$

$$D_i = d_{ikl} T_{kl} + \varepsilon^{T}_{ik} E_k$$

where i, j, k, l takes on values 1, 2, 3 or (x,y,z)

S_{ij} = strain tensor

T_{kl} = stress in PZT along the y-axis

E_k = electric field

D_i = dielectric displacement

S^{E}_{ijkl} = the complex mechanical compliance at zero electric field

d_{kij} = the piezoelectric constant at zero stress

ε^{T}_{ik} = permittivity

3.5 Mathematical Description of Wave Characteristics in Structures

A propagating wave incident upon a discontinuity can be further determined by the reflected and transmission coefficients. One dimensional flexural wave propagation is considered here for development of matrices for incident near field, reflection and transmission matrices. Considering an Euler-Bernoulli thin beam neglecting shear deformation and rotary inertia along the x-axis, the governing differential equation, is given by

$$EI\frac{\partial^4 y}{\partial x^4}+m\frac{\partial^2 y}{\partial t^2}=f(x,t)$$

where *EI* and *m* are flexural rigidity and mass per unit length of the beam and *f(x,t)* is the applied force/moment per unit length.

If *f=0*, a solution of the form $y=e^{-st}$ of the governing differential equation gives

$$y(x)=a_F^+e^{-ikx}+a_F^-e^{ikx}+a_N^+e^{-kx}+a_N^-e^{kx}$$

where k wavenumber

a_F^+, a_F^- coefficients regarding positive traveling and negative traveling waves respectively;

a_N^+, a_N^- coefficients regarding positive and negative attenuating waves respectively which decay exponentially and can be ignored at large distances.

In the presence of a discontinuity, the near field wave gives rise to [37]

transmitted wave: $a^{+} = \begin{bmatrix} a^{+} \\ a_N^{+} \end{bmatrix}$

reflected waves: $a^{-} = \begin{bmatrix} a^{-} \\ a_N^{-} \end{bmatrix}$

In matrix form the displacement, slope, bending moment and shear force is given by [37]

$$\begin{Bmatrix} y \\ \frac{1(\partial y)}{k(\partial x)} \\ \frac{M}{EIk^2} \\ \frac{V}{EIk^3} \end{Bmatrix} = \begin{bmatrix} 1 & 1 & 1 & 1 \\ -i & -1 & i & 1 \\ 1 & -1 & 1 & -1 \\ -i & 1 & i & -1 \end{bmatrix} \cdot \begin{bmatrix} a^{+} \\ a^{-} \end{bmatrix} \cdot \begin{bmatrix} e^{-ikx} & 0 & 0 & 0 \\ 0 & e^{-kx} & 0 & 0 \\ 0 & 0 & e^{-ikx} & 0 \\ 0 & 0 & 0 & e^{-kx} \end{bmatrix}$$

For the active beam structure, the piezoelectric actuators apply moments which result in discontinuities in the moment and produce waves into the beam. The amplitude vector for a piezoelectric patch is given by [37]

$$m_p = \begin{bmatrix} 1 \\ -1 \end{bmatrix} \frac{M}{4EIk^2}$$

Where M is the piezoelectric moment with respect to the actuator location.

The goal of the active control architectures, is therefore to use pzt sensors to sense the wave parameters which are used in control optimization schemes to produce manipulating signals to the pzt actuators, which in turn produce necessary excitations to destructively cancel the incident disturbance waves.

Chapter 4

Theoretical Results and Observations

4.1 Introduction

The solution of the Euler-Bernoulli equation as presented in section 3.3 was used to find the effects of different transient forcing functions on cantilever and clamped-clamped beams. For the simulations in this thesis, first five modes of vibration are used. These results as presented in this chapter were used to compare the responses for different boundary conditions in order to detect differences. Based on the graphs of these results, several observations were noticed and discussed. Section 4.2 presents the shapes of the beams due to the different forcing functions and their wave motion. In section 4.3, effects of different frequencies on time history of beam vibration are presented. Also reasons for selecting a proper frequency are given. The results of time response of transient forcing functions with several cycles for two different beams, clamped-clamped with length equal to $2l$ and cantilever with length of l, are presented and discussed in section 4.4.

4.2 Shape response of the beams and their wave motion.

In order to see the vibration shape of the beams, a coarse plot for each figure is used with eleven sampling points along the position of each beam. For the beam of length equal to $2l$, the distance between two points correspond to 0.1 meter, while in the case of length equal to l, the distance corresponds to 0.05 meter.

Fig 4.1 and Fig 4.2 represent displacement of the lateral vibration versus position of a clamped-clamped beam with the length of $2l$ at different specific time with an excitation force of one sine pulse with frequencies of 100 Hz and 1000 Hz respectively. As it can be seen from these graphs, the wave traveled to the end of the beam in approximately 0.035 second and started to return.

Fig 4.3 and Fig 4.4 represent displacement of the lateral vibration versus position of a cantilever beam with length of l at different specific time with one sine pulse excitation of frequencies of 100 Hz and 1000 Hz. Fig 4.5 and Fig 4.6 show the complete 3-Dimensional overview of clamped-clamped beam and cantilever beam respectively with one sine pulse excitation of frequency of 1000 Hz.

In comparing Fig 4.1 with Fig 4.3 and also Fig 4.2 with Fig 4.4, they show that the time of transverse wave traveling to the end takes approximate 0.035 sec for clamped-clamped beam while for the cantilever beam the time of transverse wave traveling to the end takes approximate 0.02sec. This is nearly half for the case of clamped-clamped beam. The time of transverse wave reflection can be used to detect the difference between several boundary conditions and as a

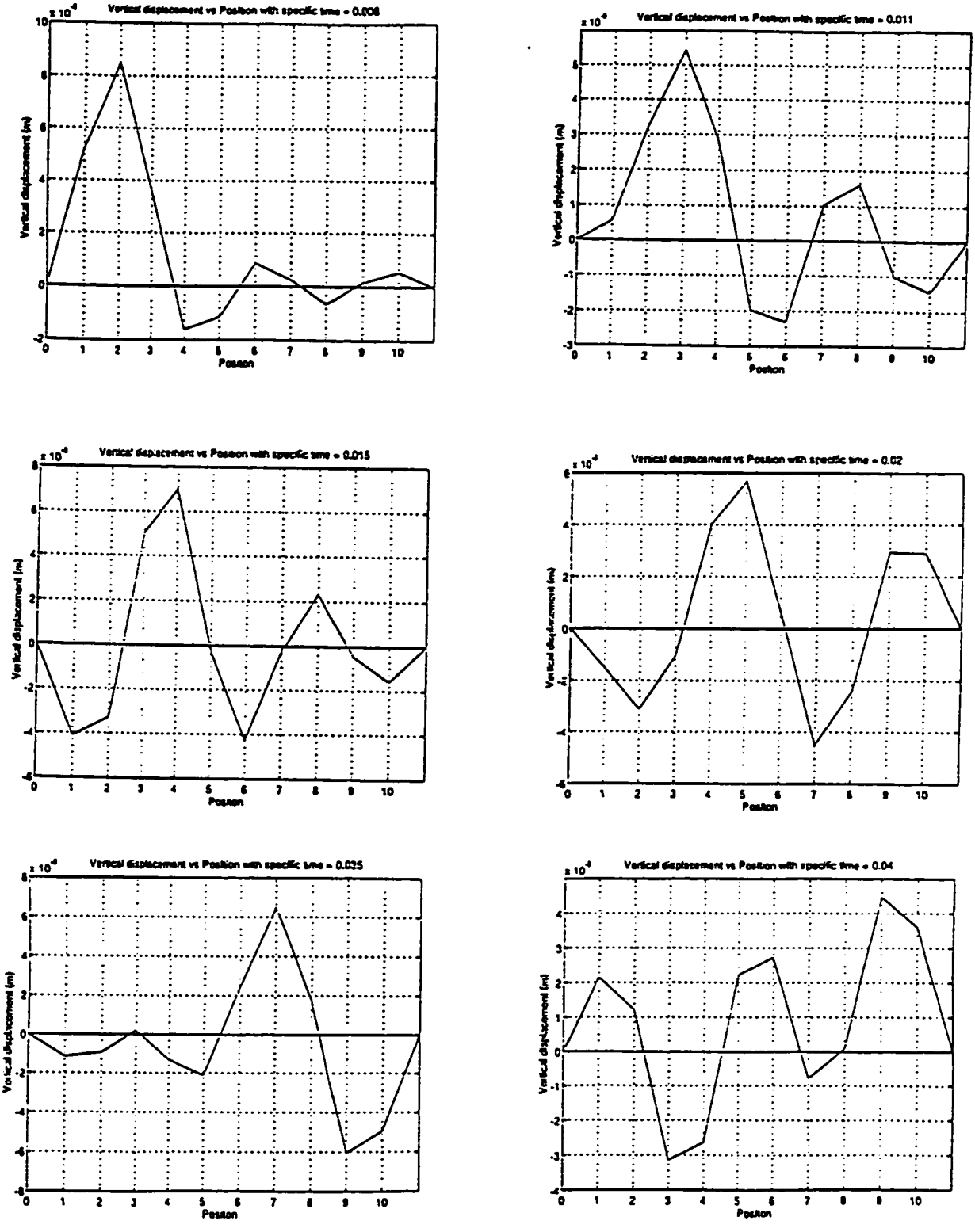

Fig 4.1 Displacement of lateral vibration versus position of a clamped-clamped beam with length of $2l$ at different specific time (in second) with an excitation force of one sine pulse with frequency of 100 Hz.

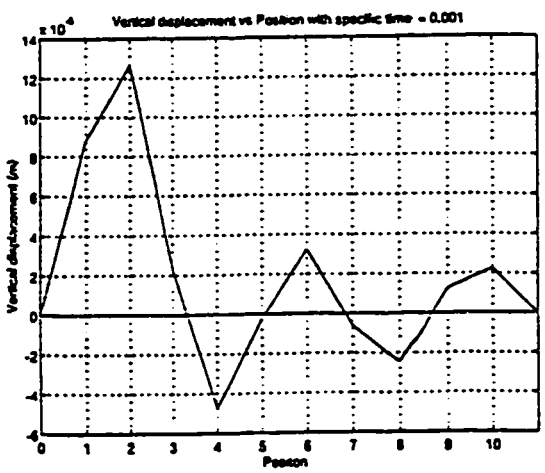

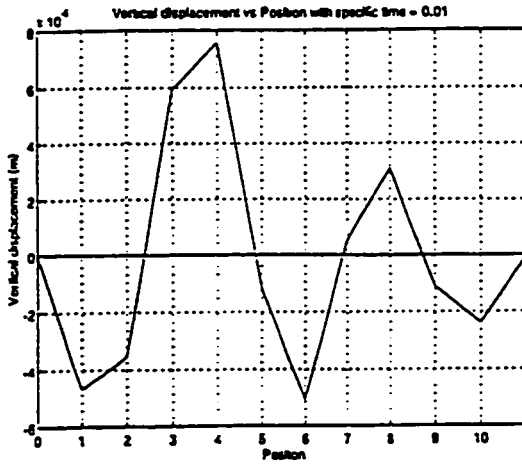

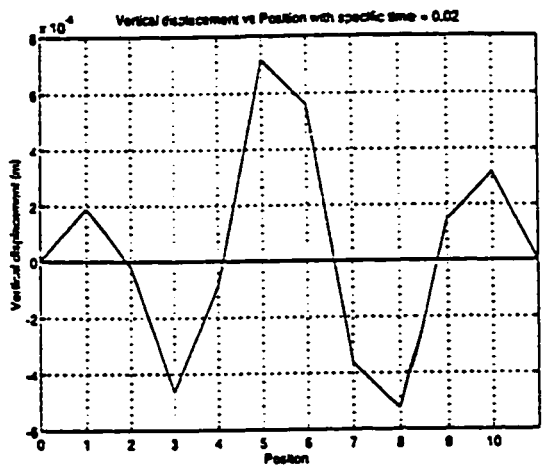

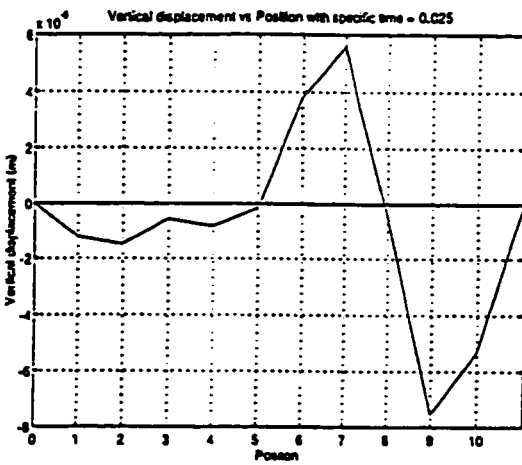

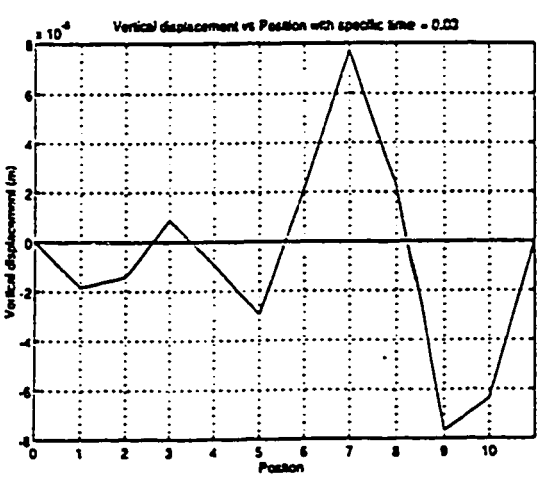

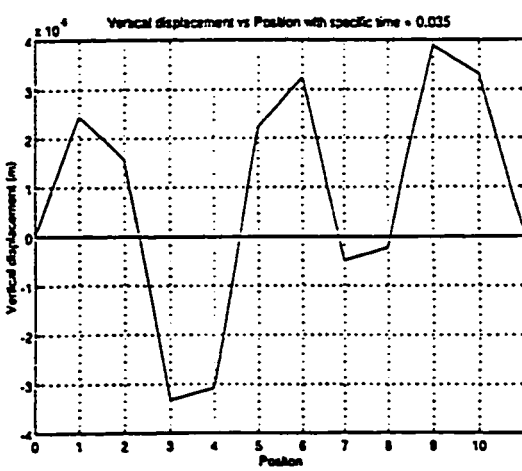

Fig 4.2 Displacement of lateral vibration versus position of a clamped-clamped beam with length of $2l$ at different specific time (in second) with an excitation force of one sine pulse with frequency of 1000 Hz.

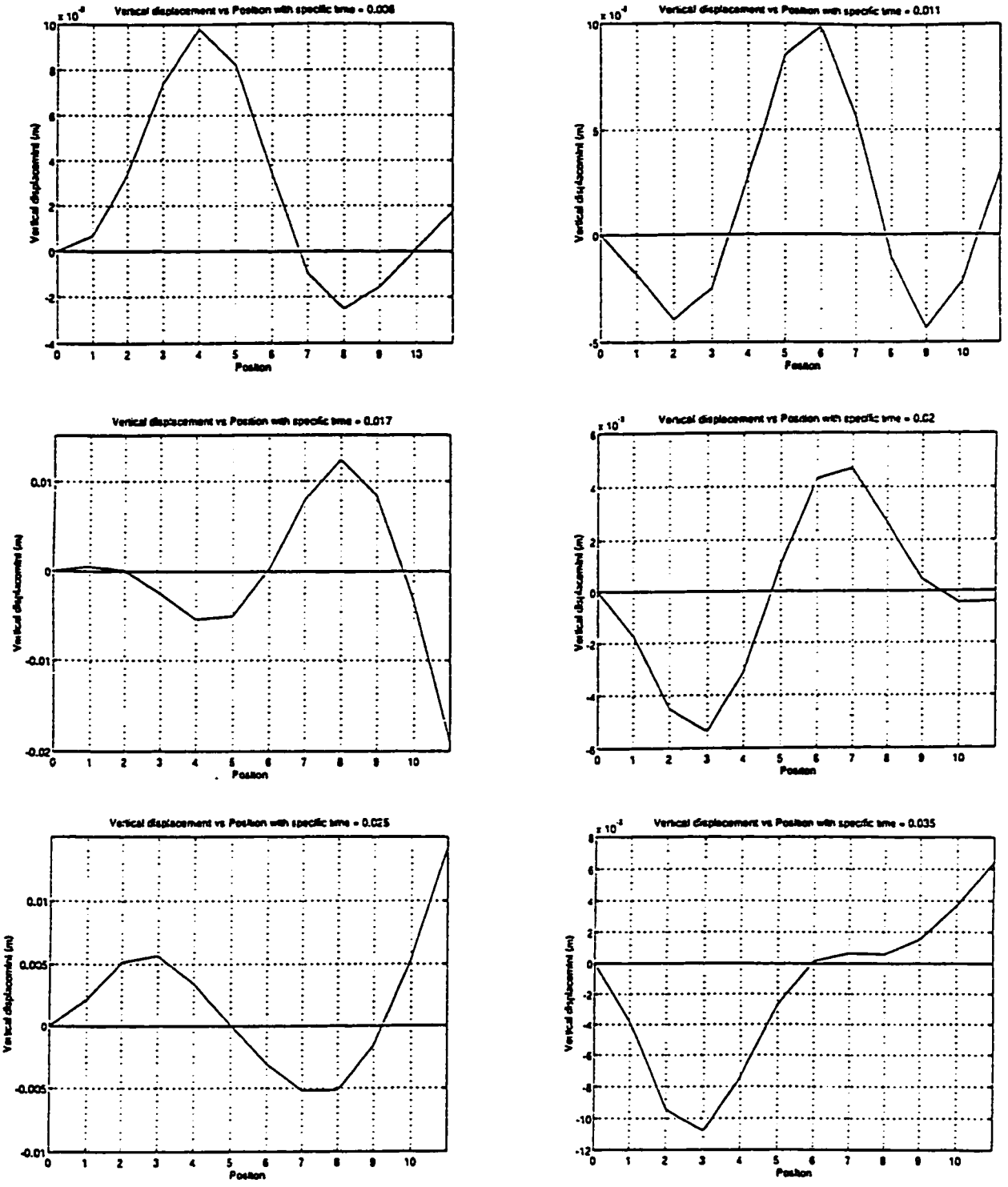

Fig 4.3 Displacement of lateral vibration versus position of a cantilever beam with length of l at different specific time (in second) with an excitation force of one sine pulse with frequency of 100 Hz.

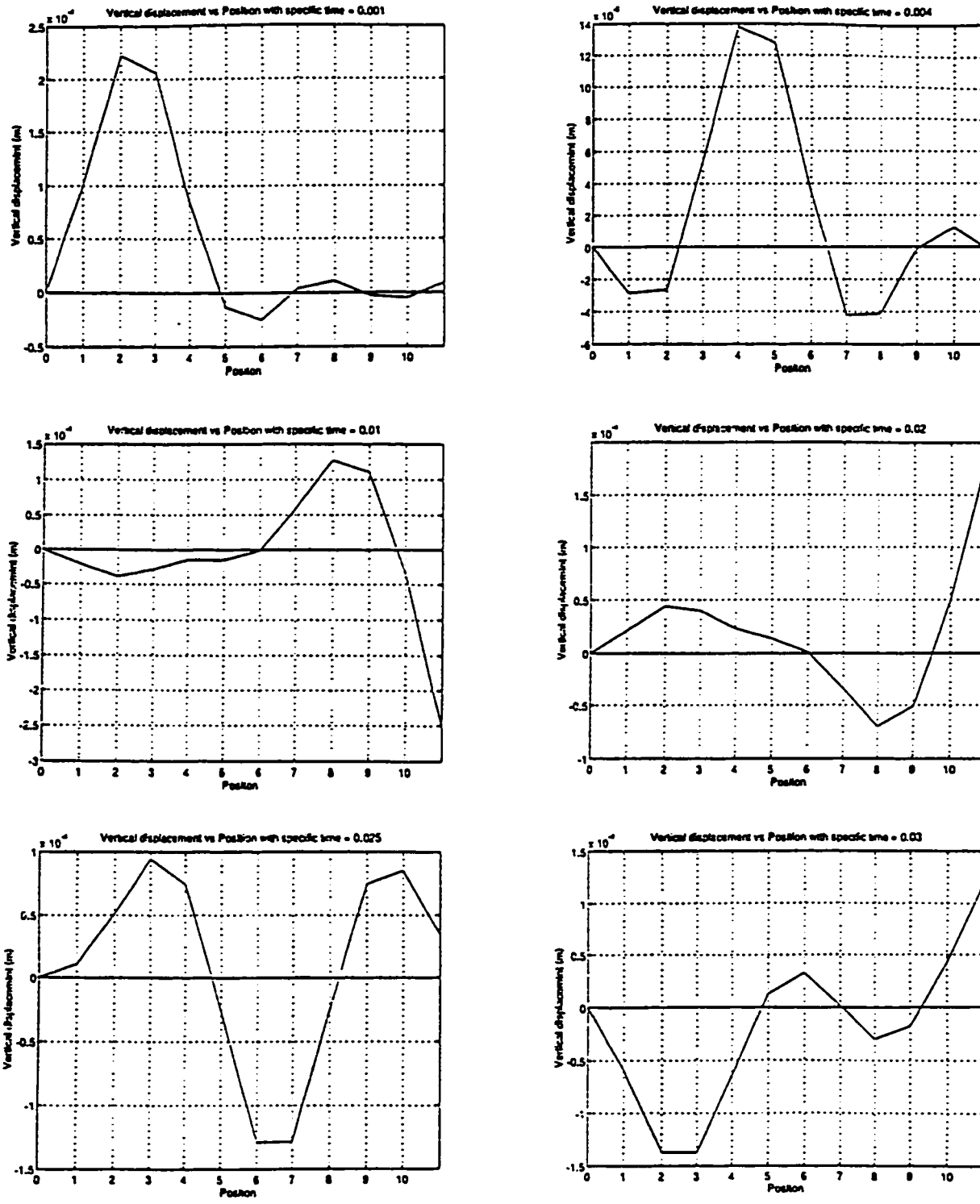

Fig 4.4 Displacement of lateral vibration versus position of a cantilever beam with length of l at different specific time (in second) with an excitation force of one sine pulse with frequency of 1000 Hz.

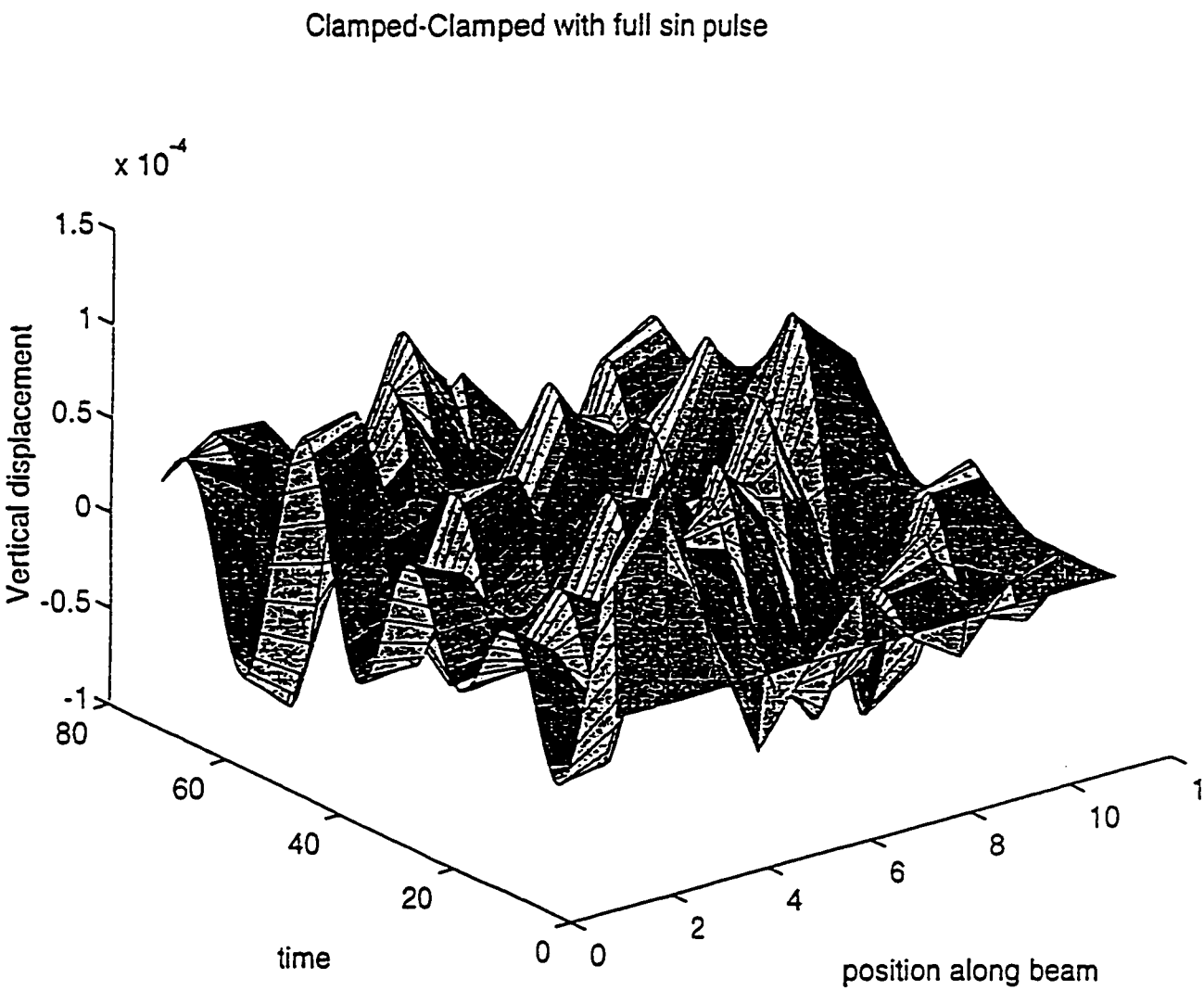

Fig 4.5 Three dimensional graph of a clamped-clamped beam with an excitation force of one sine pulse with frequency of 1000 Hz.

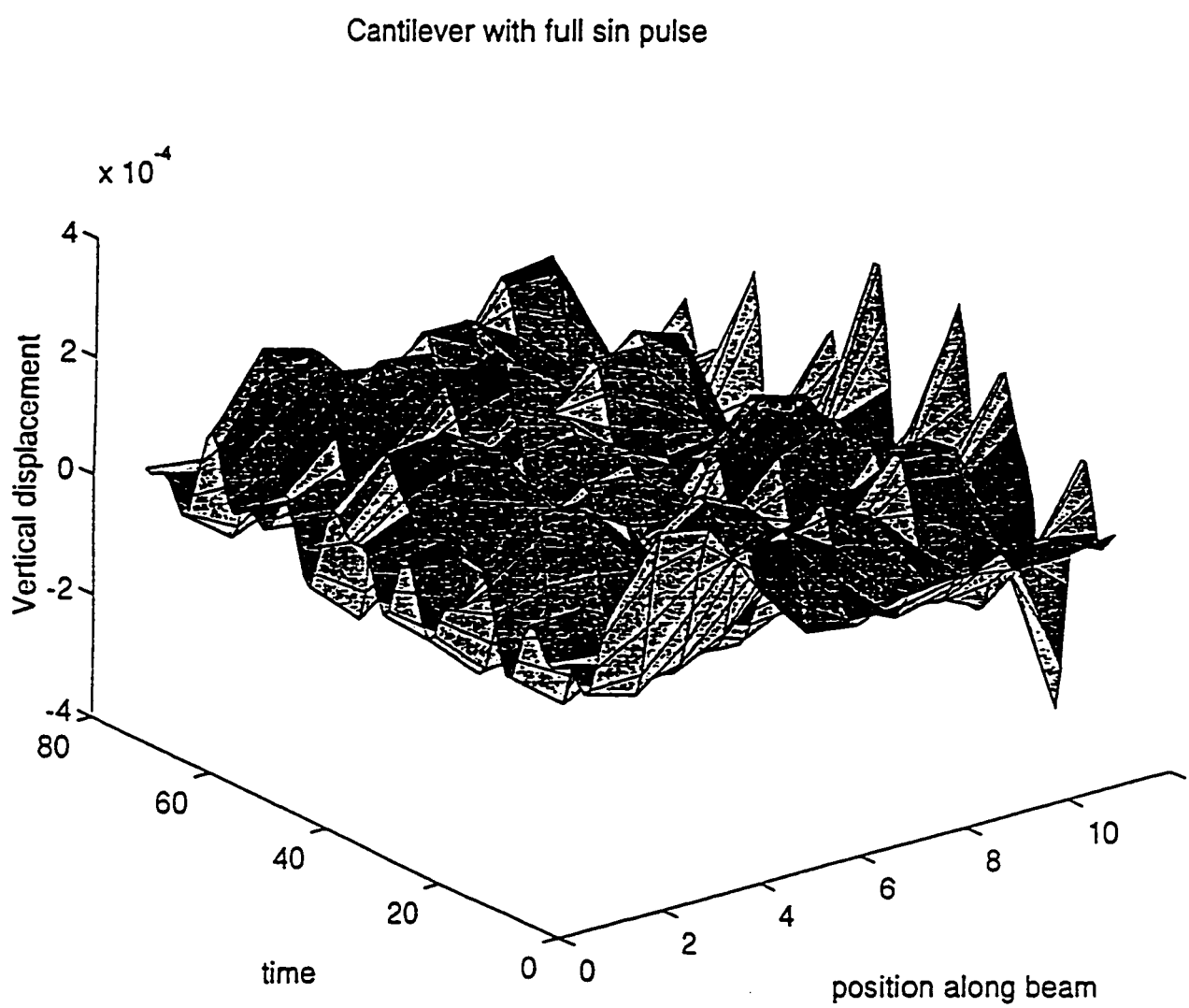

Fig 4.6 Three dimensional graph of a cantilever beam with an excitation force of one sine pulse with frequency of 1000 Hz.

result can be used to monitor any deflected parts. The results of the above simulation correspond to experimental results for a beam with eleven sensors along the beam to measure the vibration response. By using just one sensor, we cannot distinguish which transverse wave is the first reflected pulse that needs to be measured. The above observation shows that the transverse vibration of the beam is different from vibration of a string. Only a very fast monitoring system would detect the propagation of excitation. The alternative approach is to measure the time response at a single sensor location. Results of this approach are given in section 4.3 and section 4.4.

4.3 Effect of different frequencies with transient excitation.

Fig 4.7 and Fig 4.8 show the effect of different frequencies on the response of clamped-clamped beam of length $2l$ and cantilever of length l respectively. In both cases we assume that l_p and l_s, as shown in Fig 3.1, are not equal. Fig 4.9 shows the difference between responses of clamped-clamped and cantilever beams.

In comparing the results shown in Figures 4.7, 4.8 and 4.9, we can state that if the frequency of excitation increased by a factor of 10, the amplitude of vibration is decreased by approximately a factor of 100.

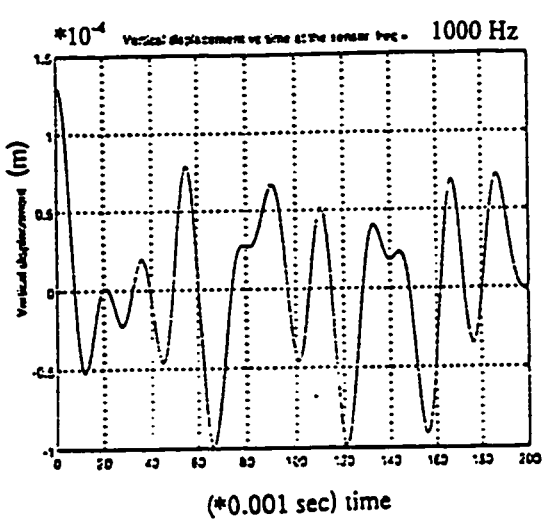

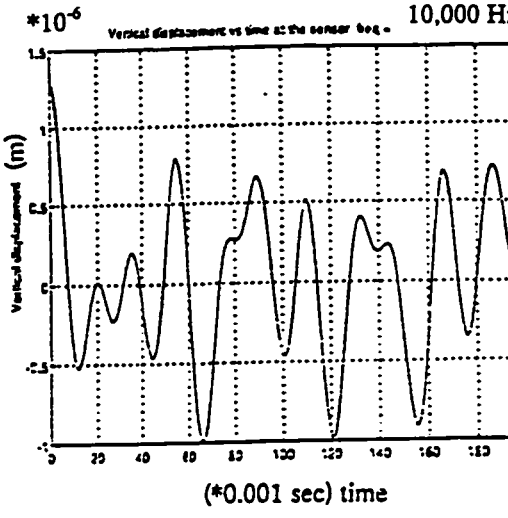

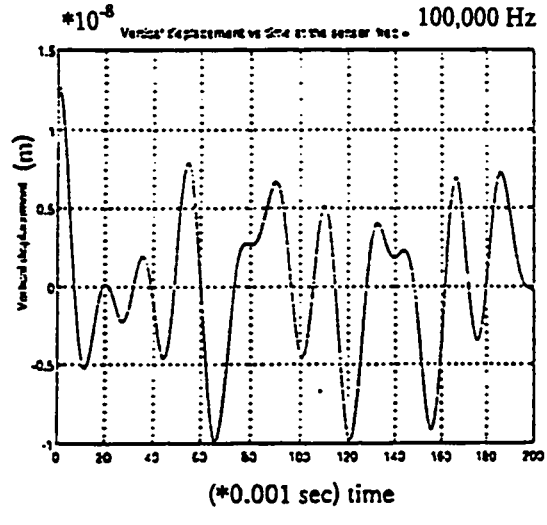

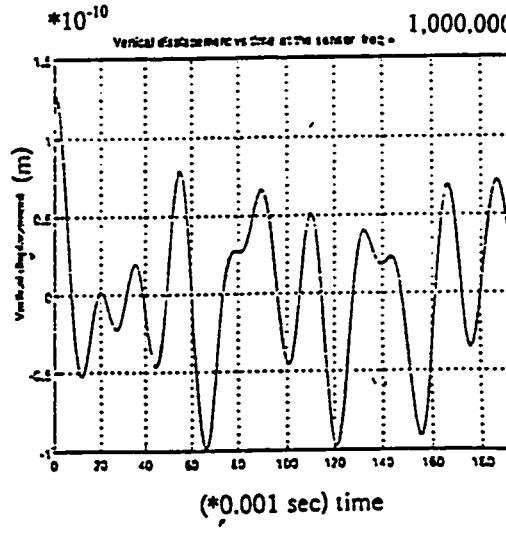

Fig 4.7 Effect of different frequencies on the response of a clamped-clamped beam (length =2*l*) with one sine pulse excitation when $l_p \neq l_s$

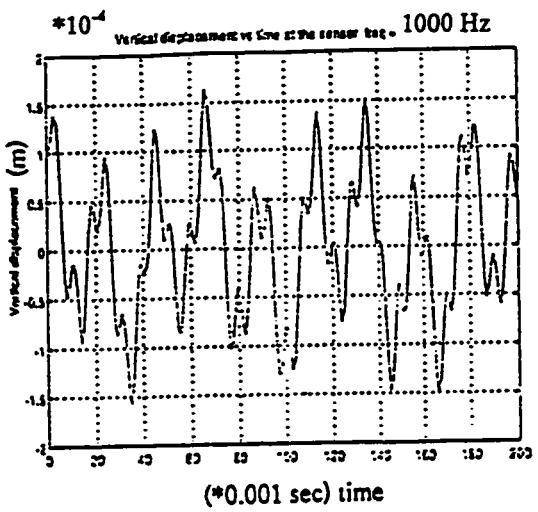

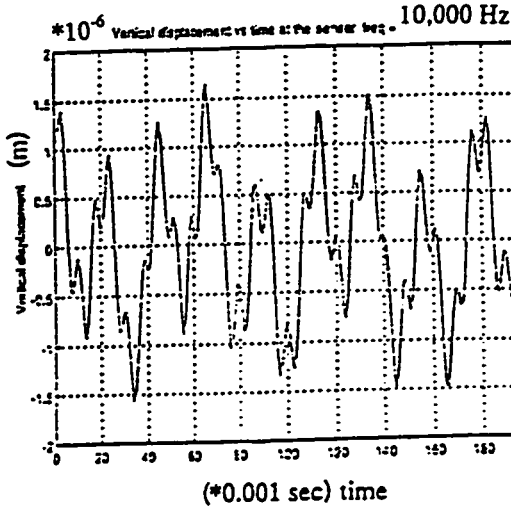

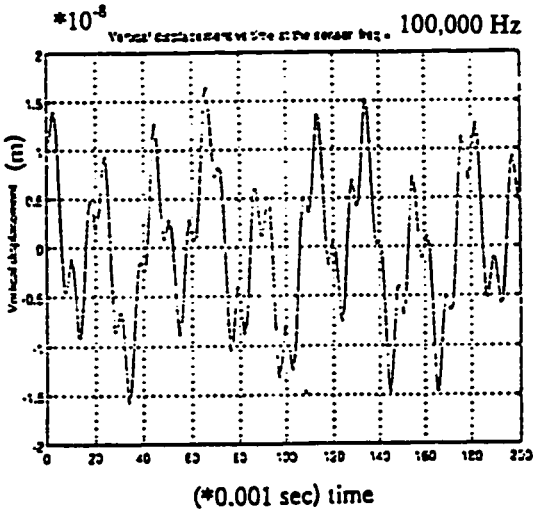

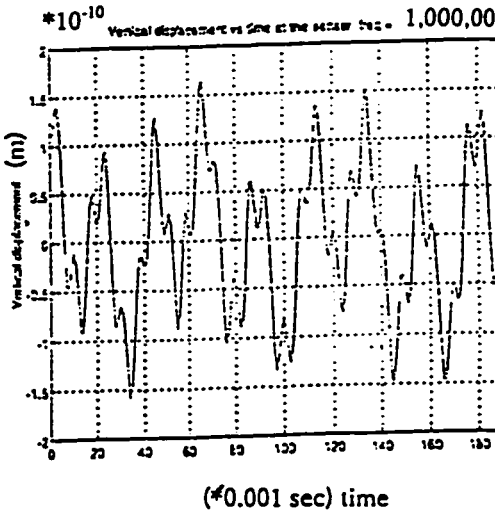

Fig 4.8 Effect of different frequencies on the response of a cantilever beam (length = l) with one sine pulse excitaion when $l_p \neq l_L$

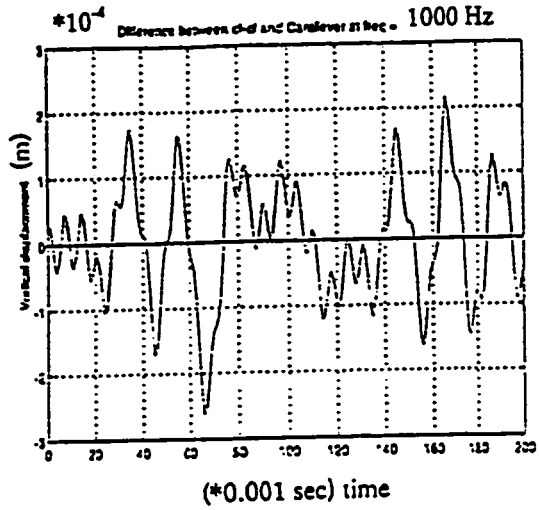

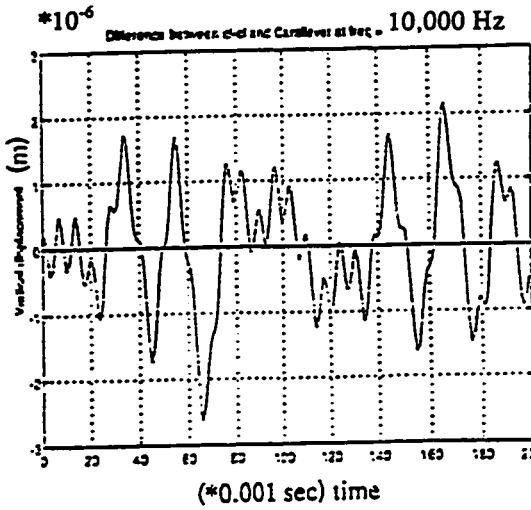

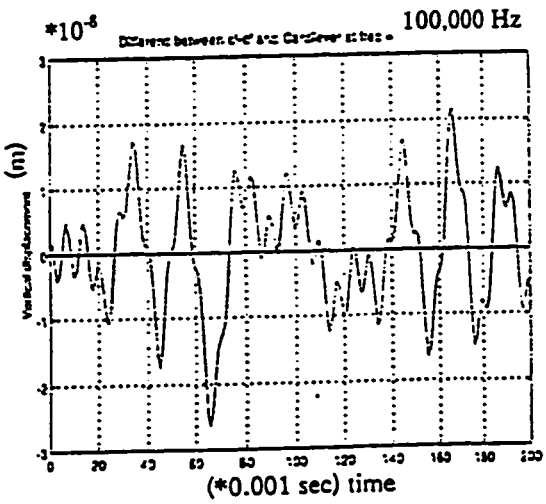

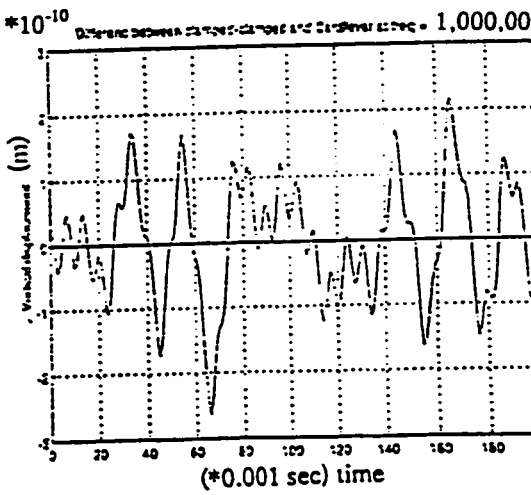

Fig 4.9 Effect of different frequencies on the difference between Fig 4.7 and Fig 4.8.

As mentioned in section 3.3, we need to select the excitation frequency much lower than the cutoff frequency by at least a factor of 20, where the cutoff frequency is given by $\varpi_c = \sqrt{\frac{kGA}{\rho I}}$; for our beam ϖ_c is approximately 1.66 MHz. The maximum frequency is computed to be 83133.1 Hz and any frequency below this value and higher than 2500 Hz is suitable. The lower limit is selected based on the time of traveling wave to the end of the cantilever beam and reflected back which is about 0.04 sec. Therefore the last two graphs of Fig 4.7 to Fig 4.9 are not accurate enough to represent the system responses. However, the trends of the responses can be seen. The frequency selected and used in this analysis was 4000 Hz.

4.4 Transient Time Response to Pulse Excitation.

Fig 4.10 and Fig 4.11 show the effect of number of excitation cycles on the response of clamped-clamped beam with lengths of $2l$ and cantilever beam with length of l at selected frequency of 4000 Hz, respectively.

In comparing the results shown in Figures 4.10 and 4.11, we can observe that if the number of complete cycles is increased by a factor of 10 the amplitude of vibration is increased by a factor of approximately 10.

From these observations, it can be concluded that a lower frequency of harmonic sinusoidal excitation and higher number of cycles can be used to amplify the excitation input signal and can be acted as an useful amplifier.

A piezoceramic actuator can also be used as a sensor and sometimes can be more sensitive than a separate sensor to measure the vibration response. In this case, the position of sensor and actuator are the same. This is called collocation and a switch is needed to change between actuating and sensing. This will allow the piezoceramic patch to be used both as an actuator and as a sensor. In order to be consistent with experimental results, we selected l_s equal to l_p and we used collocation in this analysis.

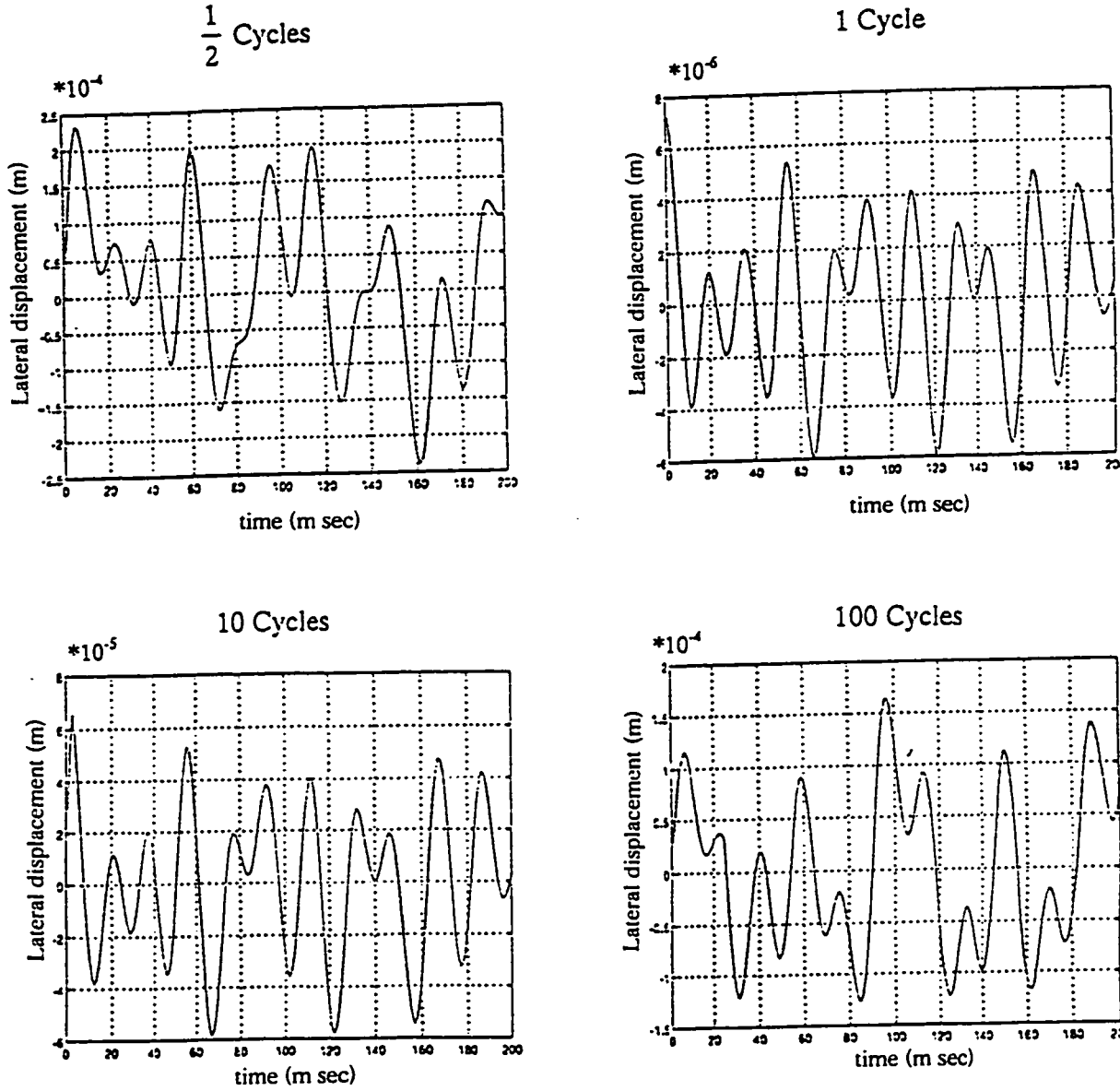

Fig 4.10 Effect of number of excitation cycles on the response of clamped-clamped beam with length equal to $2l$ when $l_p = l_s$ for excitation frequency of 4000 Hz.

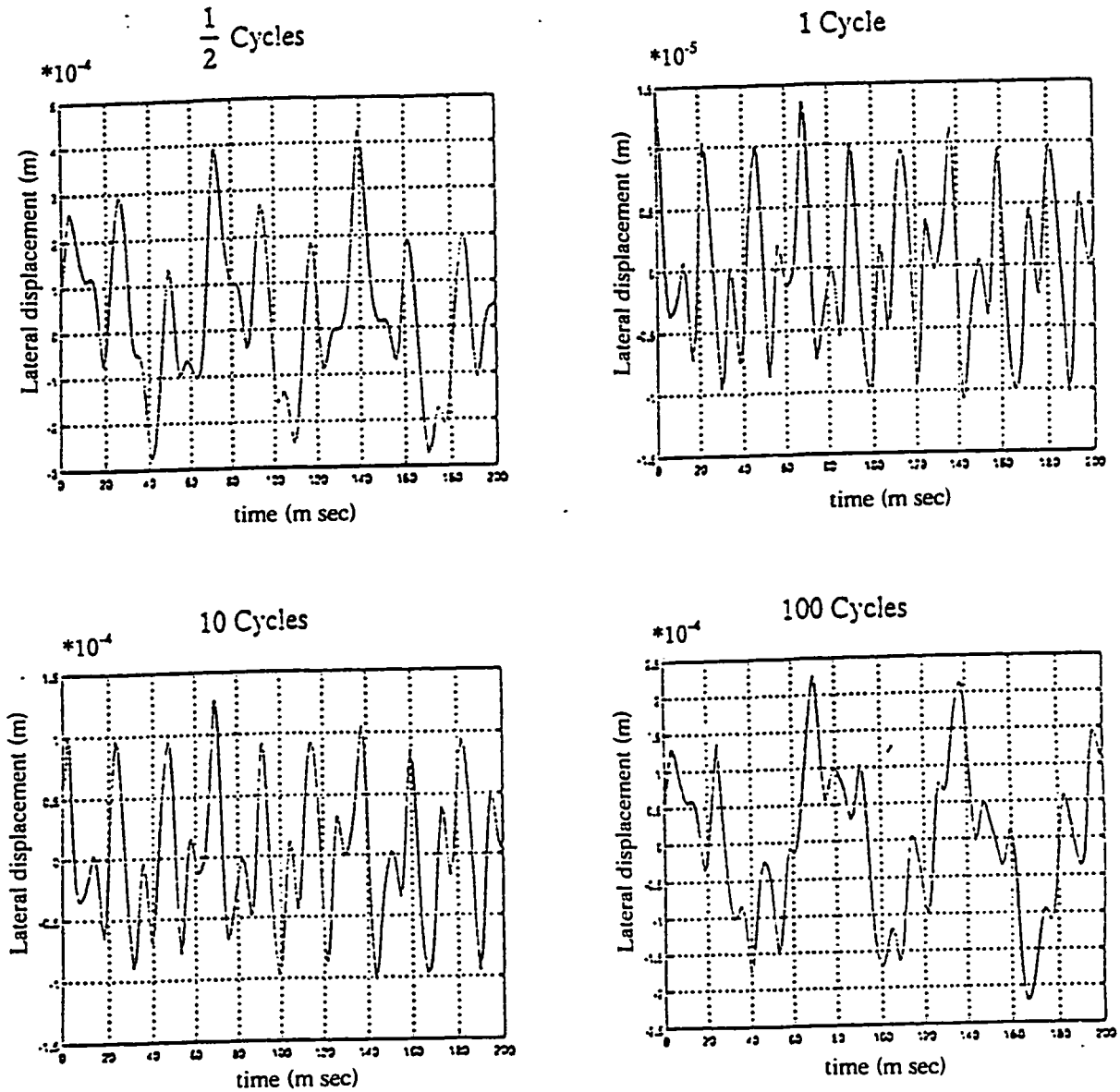

Fig 4.11 Effect of number of excitation cycles on the response of cantilever beam with length equal to l when $l_p = l_s$ for excitation frequency of 4000 Hz.

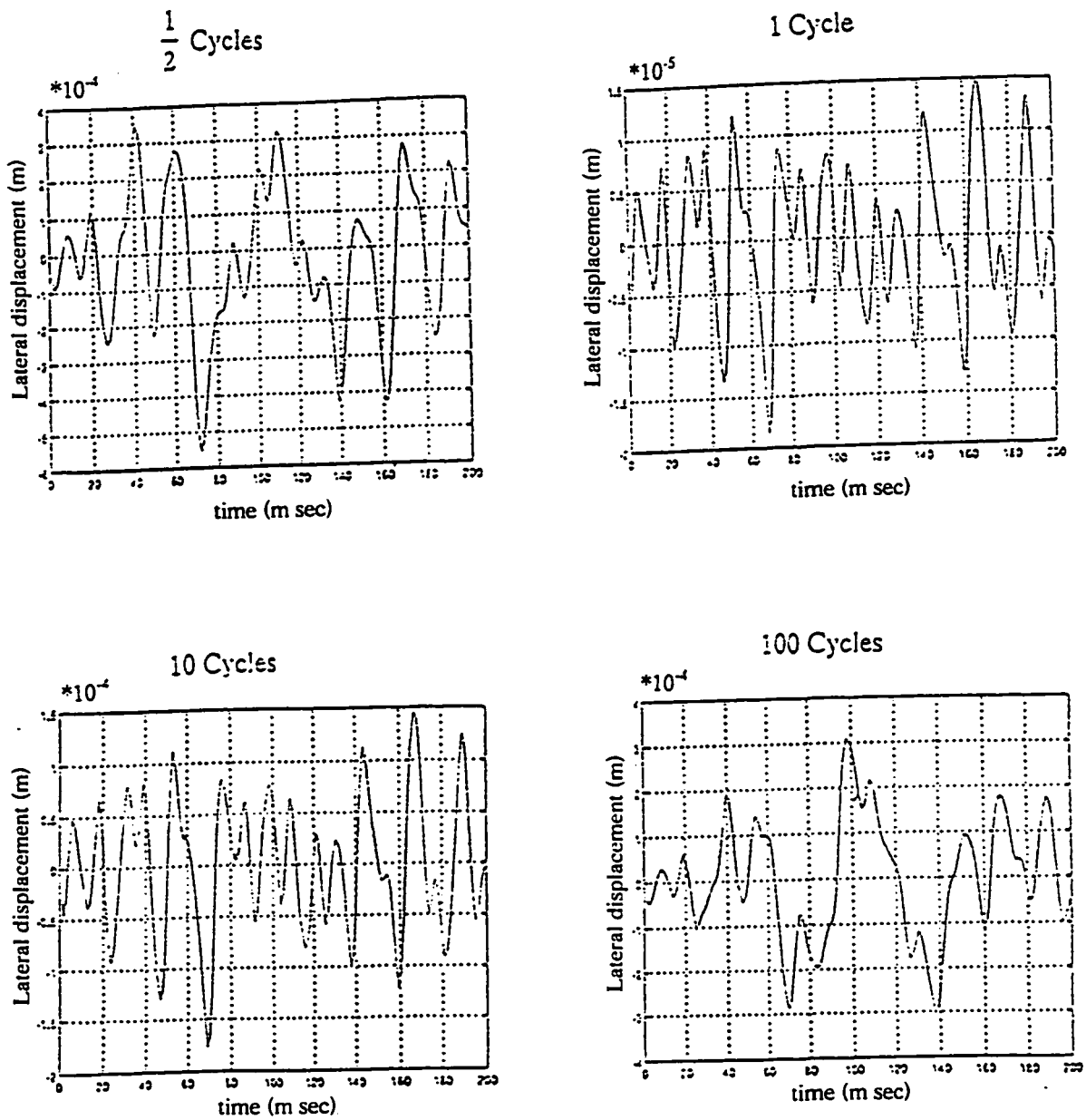

Fig 4.12 Effect of number of excitation cycles on the difference between clamped-clamped beam (Fig 4.10) and cantilever beam (Fig 4.11) for excitation frequency of 4000 Hz.

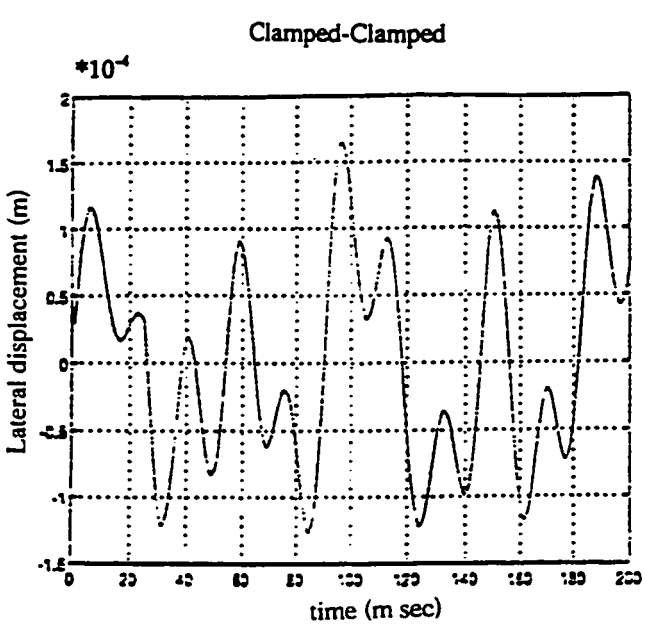

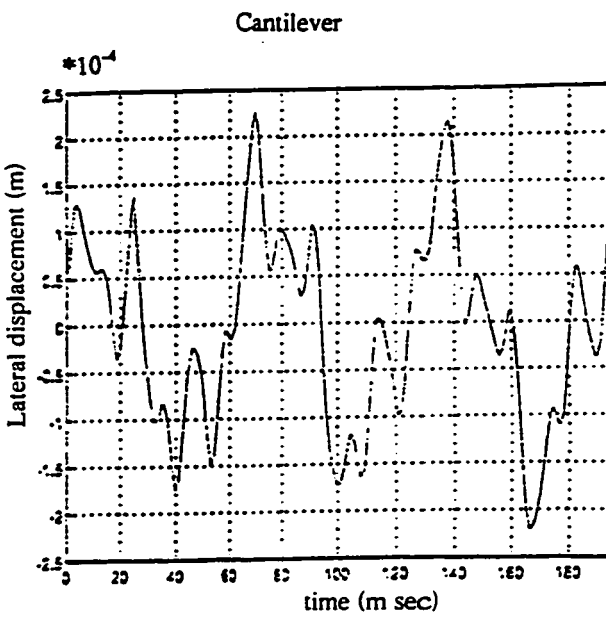

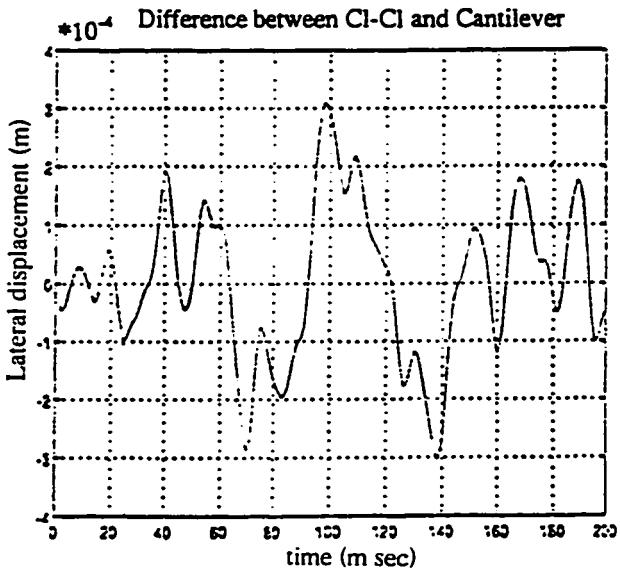

Fig 4.13 Responses of the clamped-clamped beam with $2l$ length, cantilever beam and their difference with a pulse excitation of 100 cycles of a sinusoidal input of 4000 Hz

By exciting the beams with the same forcing function but changing the boundary values, the response of the systems are completely changed. For this reason, changes in the boundary condition of the beam are recognized and, as a result, any damaged connection can be detected. The graph of the difference of their responses will be used as an indicator of the degree of damage. If the difference is zero, it means that the clamped-clamped beam is still connected perfectly and there is no damage on the beam.

Fig 4.12 shows the effects of the number of excitation cycles on the difference between clamped-clamped beam, Fig 4.10, and cantilever beam, Fig 4.11. Fig 4.13 shows very clearly that there is a great difference between, the response of a safe beam (clamped-clamped beam) and the response of a damage beam (Cantilever beam).

Since the graph of the difference between clamped-clamped and cantilever beams has both positive and negative values, an index of safety can be defined as the sum of the square of the lateral vibration displacement difference between clamped-clamped and cantilever as given in Figures 4.9 and 4.12. The index of safety can be chosen as follows:

$$IS = \sqrt{\sum (y_{cl-cl} - y_{cant})^2} \qquad (4.1)$$

where

y_{cl-cl} is the lateral vibration displacement of clamped-clamped beam

and y_{cant} is the lateral vibration displacement of cantilever beam.

Table 4.1 shows the values of index of safety between a safe beam and a completely disconnected beam.

Table 4.1 Reference Table

Corresponding figure number	Different between end conditions	Number of excitation cycles	Frequency of excitation (Hz)	Index of safety, *IS* (mm)
4.9	cl-cl 2*l* and cantilever	1	1000	1.28
4.9	cl-cl 2*l* and cantilever	1	10000	0.0128
4.12	cl-cl 2*l* and cantilever	½	4000	2.755
4.12	cl-cl 2*l* and cantilever	1	4000	0.0952
4.12	cl-cl 2*l* and cantilever	10	4000	0.9082
4.12	cl-cl 2*l* and cantilever	100	4000	1.842

In the next chapter, experimental results will be shown for 100 cycles of 4000 Hz sinusoidal excitation. Experimental results confirmed that it is possible to distinguish between clamped-clamped and cantilever beams using the proposed method. These results justify further study in monitoring any state of the boundary conditions.

Chapter 5

Experimental Setup and Results

This chapter is divided into two sections. Section 5.1 presents the specifications of the equipment while section 5.2 presents the experimental results.

5.1 Experimental Setup Specifications.

Fig 5.1.1 shows the equipment set up used in this research. This setup includes beams with piezoelectric sensor, piezoelectric actuators, a PC, a power supply, and a dSPACE digital signal processor, (DSP) .

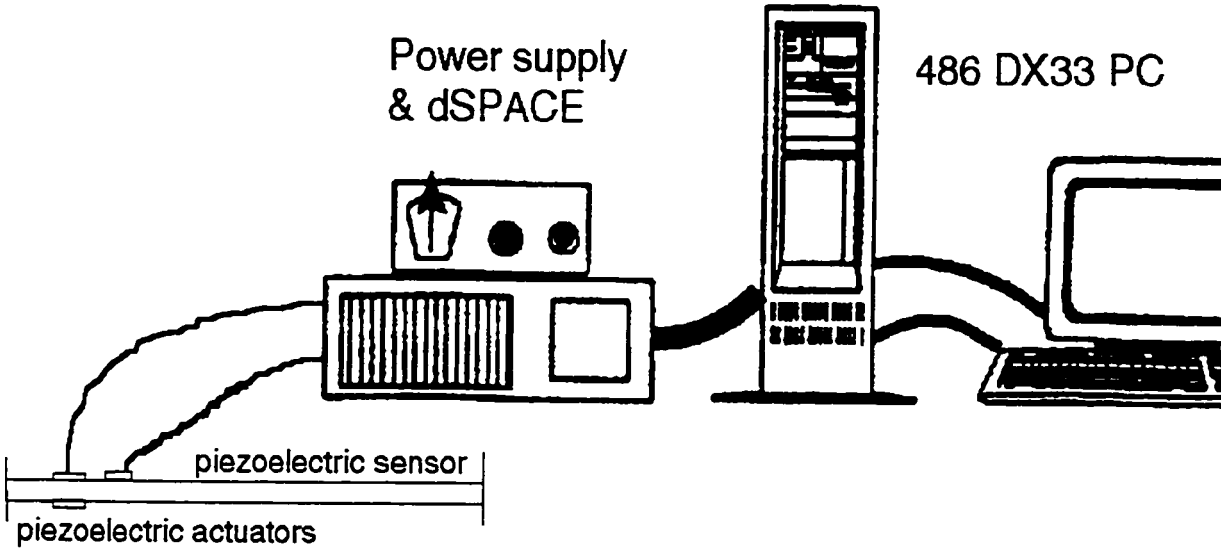

Fig 5.1.1 General physical layout of equipment

The sensor which was used in this research was not sensitive enough to measure the vibration response to excitations without any amplifier. Therefore, the piezoceramic patch of the actuator, which was very sensitive, was used as an actuator and as a sensor. As a result of this, a mechanical switch was used during the excitation period to connect the signal generating line to actuator and afterward switch to connect the signal receiving line to actuator. The modified configuration now becomes a collocated actuator and sensor. The result of this configuration shows a better response than the previous configuration. Subsection 5.1.1 and 5.1.2 will described the digital signal processor and system software very briefly, whereas subsection 5.1.3 and 5.1.4 will describe the piezoelectric sensor and piezoelectric actuator characteristics and specifications.

5.1.1 dSPACE Digital Signal Processor

dSPACE contains a number of cards, among which 2 cards are more important than others and are often used in this research. They are :

DS2001 card,	the analog to digital converter.
DS2101 card,	the digital to analog converter.

More detail information can be found in DS2002 and DS2101 User's Guide [85].

5.1.2 System Software

Three pieces of software were used in this experimental study. They are summarized below:

1. SED30

   A setup software used to setup all the boards as desired by the user and to create a setup file.

2. MON30

   This is a utility program which loads and evaluates the setup file and the object code modules and downloads the object module into dSPACE.

3. TRACE30

   This software can trace in real time any variable of the object code from DS1002 digital signal processing board.

5.1.3 Piezoelectric Sensor

The property possessed by some materials that become electrically charged when subjected to a mechanical stress is called Piezoelectricity. These materials also show the reverse effect by undergoing mechanical deformation due to the application of an electric field.

Material characteristics of piezoelectric ceramics depend on the direction of the applied electric field, displacement, stress and strain. The direction of

polarization is generally designated as the z-axis. The axes x, y and z are respectively represented as 1, 2 and 3 directions and the shear about these axes are represented as 4, 5 and 6 as shown in the figure 5.1.2 below.

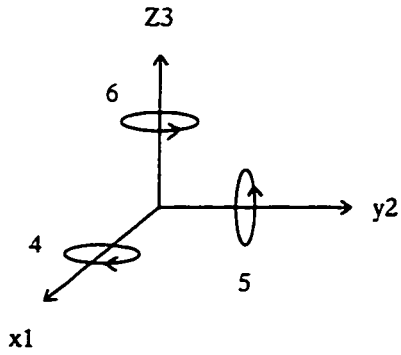

Fig 5.1.2 Direction x, y, z represented as 1,2,3, whereas 4,5,6 represent the corresponding shear direction

The complete symbols and terminology are referred to the piezoelectric Ceramics catalogue on p3, p6 , p7 and p9 of [86]. With the above mentioned direction, the first subscript gives the direction of the electrical field associated with the voltage applied or the charge produced and the second subscript gives the direction of mechanical stress or strain.

The table 5.1 below gives a general description of the superscripts used in [86].

Table 5.1 General description of the superscripts used.

Parameters	Symbol	Condition
Stress	T	Mechanically Clamped
Field	E	Electrical Short Circuit
Displacement	D	Electrical Open Circuit
Strain	S	Mechanically Clamped

The sensor used are BM400. BM400 with lead zirconate titanate composition, low dielectric loss and excellent piezoelectric properties. These properties make it attractive for applications requiring large mechanical drive amplitudes. The material can also be exposed to highly repetitive quasi-static loads.

The sensor used in this research was provided by Sensor Technology, Collingwood, Ontario.

5.1.4 Piezoelectric Actuator.

A piezoelectric actuator is a device consisting of a number of piezoelectric elements in a stack. The elements are generally connected in parallel either through the electrode structure or the insertion of brass electrodes between the elements. When a voltage is applied to the assembly, it produces small displacements with a high force capability.

The actuator is used in this research is also manufactured and provided by the Sensor Technology, Collingwood, Ontario.

The key features of the piezoelectric actuators are :

1. Compact and light weight
2. Solid state
3. 50% conversion efficiency
4. Fast response
5. Displacement proportional to applied voltage
6. Large force
7. Broad operating temperature range
8. Excellent stability

Some material characteristics of the actuator are

Dielectric Constant	$k^T_{33} = 1400$
Ageing (Change/Time Decade)	-6%
Loss Factor	0.2%
Charge Coefficient	$d_{33} = 280*10^{-12}$ C/N
Voltage Limits	7500V/cm
Compliance	$s_{33}^E = 15*10^{-12} m^2/N$

5.2 Experimental Results

When one cycle of excitation at 4000 Hz with limited amplitude is used, the duration of excitation is only 0.25 m sec. This cannot excite the beam with enough energy. In this case a high voltage power amplifier is needed when using piezoelectric or piezoceramic material to activate the actuator. Also due to the presence of noise a charge amplifier is needed to amplify the signals from the sensor before they can be measured and recorded. However, due to the limitation of our equipment, it was not possible to use those amplifiers. The alternative way was to use low frequency excitation and a higher number of cycles as a means of amplifying the input signal to the actuator as mentioned in section 4.4. Subsequently, all experimental results are based on 4000 Hz frequency with 100 cycles for amplifying the input signal to produce responses detectable by the measuring device. Also, since the sensor available for this experiment was not sensitive enough without an amplifier, the actuator which was much more sensitive to actual signals was used for the actuating and for sensing the vibration of the beam.

In order to show the repeatability of the experimental results, each experiment was repeated several times and two sets of data for tests are presented in this section. All the figures presented in this chapter are qualified with (a) and (b), where (a) refers to the first test result and (b) refers to the second test result. Fig 5.2.1 shows the time response of clamped-clamped beam with length $2l$. While

Fig 5.2.2 shows the time response of cantilever beam with length equal to l. Each division on the x-axis of all graphs corresponds to 0.001 second and each division on the y-axis represents the voltage measured from the sensor.

Comparing Figures 5.2.1 and 5.2.2, it is obvious that there is a great difference between clamped-clamped beam and cantilever beam. The graph of response difference between these two end conditions is also shown in Fig 5.2.3. The results prove that it is possible to distinguish between those two end conditions very easily. Fig 5.2.4 shows experimental results of the difference in response of a safe beam at two different times represented by the difference between test 1 respond and test 2 respond of a clamped-clamped beam. Fig 5.2.5 shows experimental results of the difference between a safe beam (clamped-clamped beam) and damaged beam (Cantilever beam) in the same scale as in Fig 5.2.4 for comparison.

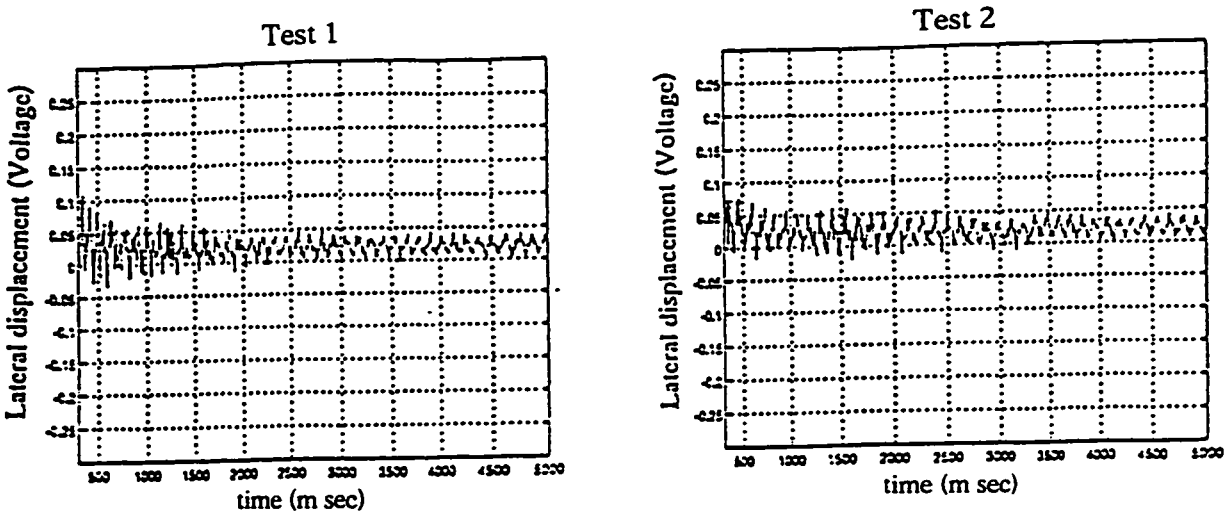

Fig 5.2.1 Experimental time response of clamped-clamped beam with length equal to $2l$.

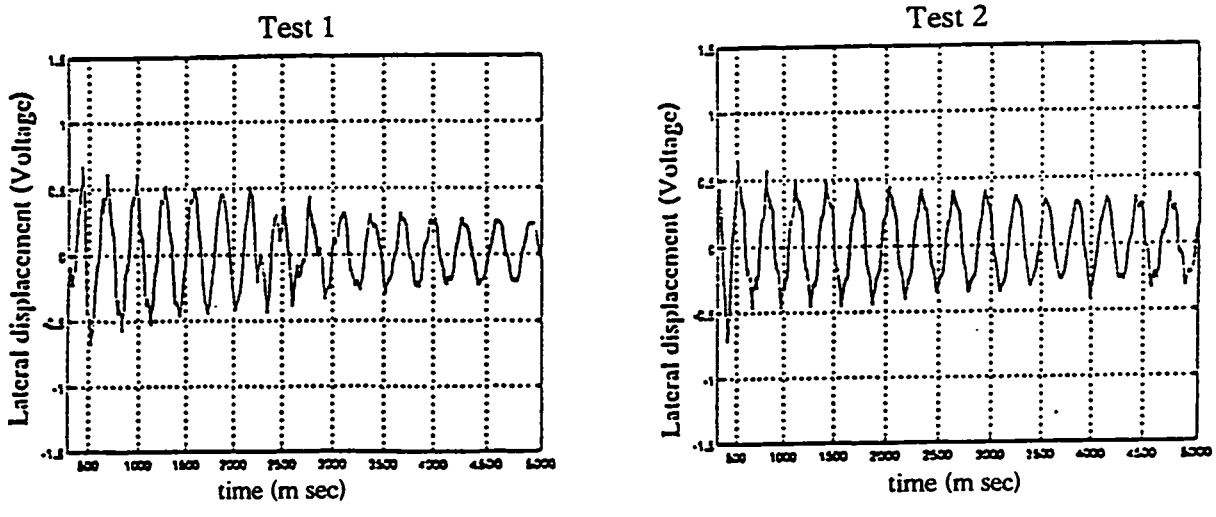

Fig 5.2.2 Experimental time response of cantilever beam with length equal to l.

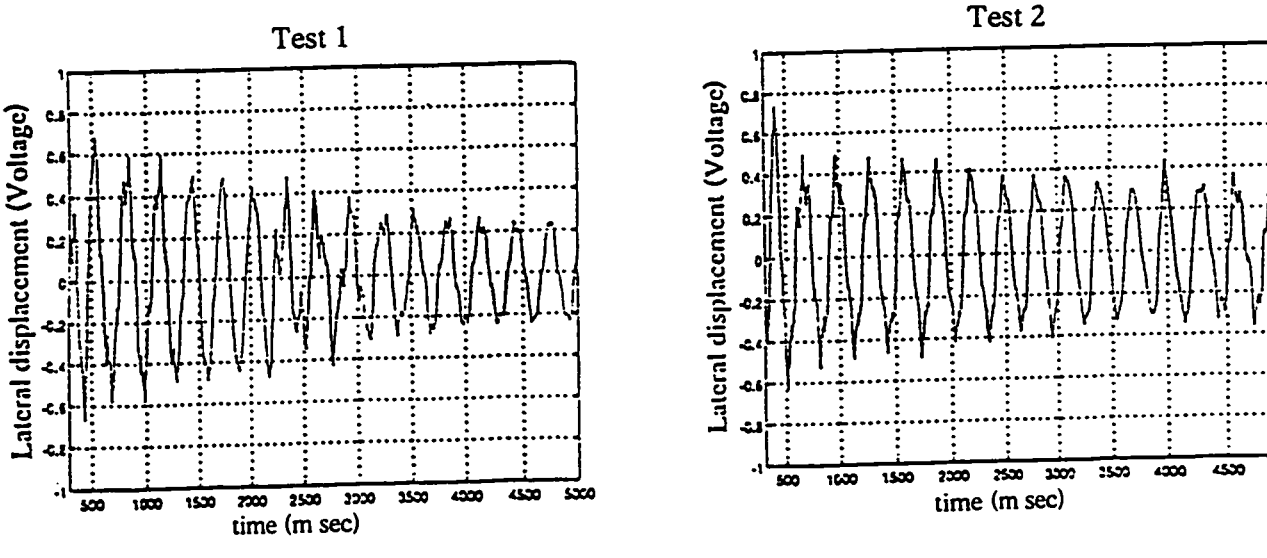

Fig 5.2.3 Experimental difference between clamped-clamped (Fig 5.2.1) and cantilever (Fig 5.2.2).

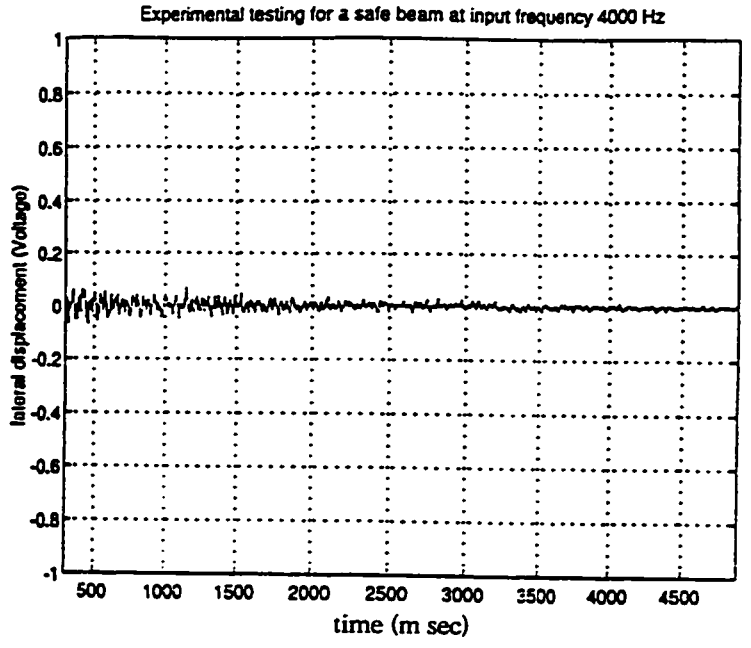

Fig 5.2.4 Difference in response of a safe beam at two different times.

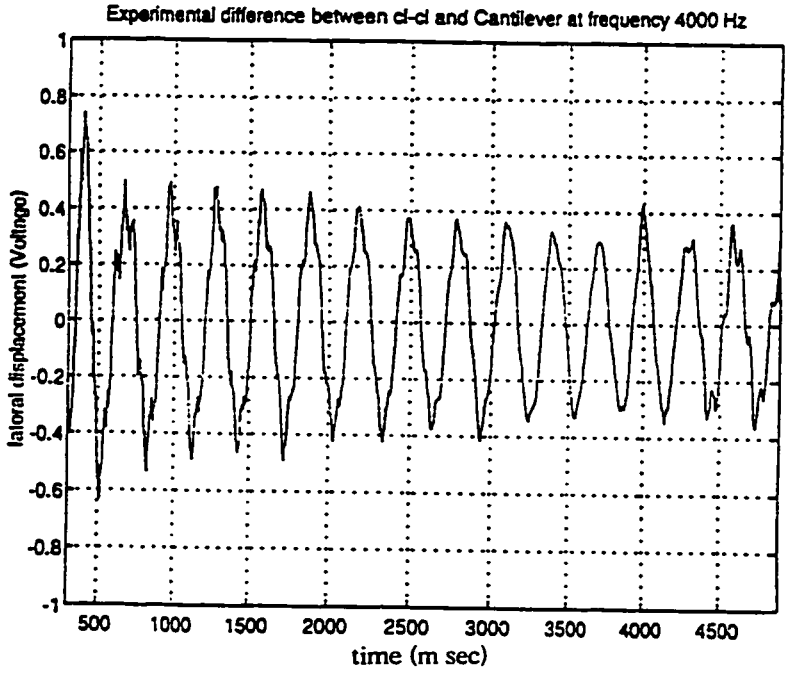

Fig 5.2.5 Difference between a safe beam (clamped-clamped beam) and damage beam (Cantilever beam).

Table 5.2 presents the index of safety for experimental results for different beam conditions.

Table 5.2 Reference Table from Experimental Data

Corresp-onding figure number	Different between end condition	Number of excitation cycle	Frequency of excitation	Index of safety *IS* (Volt)
5.2.3 a	cl-cl 2*l* and cantilever	100	4000	20.4
5.2.3 b	cl-cl 2*l* and cantilever	100	4000	20.7
5.2.4	cl-cl (test1) and cl-cl (test2)	100	4000	1.2
5.2.5	cl-cl 2*l* and cantilever	100	4000	20.7

For reducing the actual noise compared to the sensor's useful signal, a second order Butterworth digital filter, with cutoff frequency of 100 Hz, was designed using the digital signal processing system and was used in the experiment.

Due to the limitations when using a mechanical switch, the time taken to switch from actuator to sensor during the experiment may not be the same for each test. As a result, starting points for various tests were not coincident. Therefore the index of safety may not be accurate enough to compare experimental with simulation results. In addition, the units in experimental results and in theoretical results were not the same.

However, the results proved that the concept which was used in this research is satisfactory. The above proposed method is the most simple way of doing non destructive testing.

Chapter 6

Conclusions

The following observations result from theoretical and experimental studies. From the theoretical results given in chapter 4, it could be observed that, by increasing the number of cycles of the harmonic excitation, the amplitude of lateral vibration increases. Also, the increase of the value of frequency of excitation is inversely proportional to the square of the amplitude of vibration. As a result, low frequency of harmonic sinusoidal excitation and a higher number of cycles can be used to amplify the input signal.

Frequency and amplitude of free vibration of a continuous system similar to a beam depends on two factors. These factors are 1) boundary conditions and 2) initial transient forcing function and the location of the applied force that gives a specific initial condition for the system.

By exciting the beams with the same initial forcing function but changing the boundary values, the responses of the systems are completely changed. To determine exactly the type of boundary change, we defined a reference index of safety. Values of this index for different kinds of boundaries were compared for theoretical and for experimental results.

From this concept by comparing these values, any damaged or loose connection can be detected. For preliminary analysis, two extreme cases were considered:

(1) two beams, each with length of l, which were perfectly connected

(2) two beams completely disconnected, modeled by a Cantilever beam with length equal to l.

All experimental results were based on signals with 100 cycles of 4000 Hz sinusoidal excitation. The method was the same for other numbers of sinusoidal cycles for the excitation force. Time response graphs for each of these extreme cases were obtained. In addition, the difference between the responses for the two end conditions was analyzed.

The index of safety was introduced, based on the sum of the square of the lateral vibration displacement difference between any two different boundary conditions. This index is a quantitative measure of the safety of the beam and it is particularly useful for digital computer simulation studies. The degree of failure depends on how large the index of safety is. As a result, the larger the index of safety, the larger was the change in the beams connection.

From the theoretical results, the lateral vibration of the beam as a function of locations was obtained and analyzed as a measure of failure detection. Experimentally, these results were not possible to obtain with only one sensor. Therefore in this research, the time response data which indicate in a significant way the change in the beam was used.

Chapter 7

Recommendations

Four suggestions emphasize on experimental setup and one on theoretical simulation and mathematical formulation:

1) Higher order Timoshenko beam theory should be used for further simulation study of a short and a thicker beam. In this case, the effects of shear deformation and rotary inertia will be taken into account. The differences between the Euler-Bernoulli and Timoshenko increase as the thickness of the beam increases.
2) Voltage and charge amplifiers are needed for inputting the signal to the actuator and measuring the output of signal from the sensor in order to reduce the effect of noise on the signals.
3) Sensors must be precise enough to measure the response of the beam since the vibration for clamped-clamped beam is very small. If collocated sensor and actuator are used, i.e. one piezoelectric patch as sensor and actuator, an electrical timer switch is necessary to separate the time for sensing and for actuating.
4) In addition to a piezoelectric sensor, an accelerometer can also be useful for measuring the transverse vibration of the beam, in order to distinguish

between transverse and longitudinal vibrations. These two types of vibrations are normally mixed together and may not be measured separately by only one piezoelectric sensor.

5) At least two beams with piezoceramics sensors and actuators should be used during testing in order to verify the performance of equipment, because one beam may have build up fatigue effects or may have buckled after many times of testing, especially when the beam is very thin. Also, responses of two identical beams could be compared for repeatability of results.

Chapter 8

Appendix

8.1 References

1. Craig A. Rogers, An Introduction to Intelligent Material Systems and Structures. *Intelligent Structures, Elsevier Applied Science Publishers Ltd., 1990, pp. 3-37.*

2. Edward F. Crawley, Intelligent Structures for Aerospace: A Technololgy Overview and Assessment. *AIAA Journal Vol. 32, No 8, Aug 1994, pp1689-1699.*

3. F.P. Sun,Z. Chaudhry, C. Liang and C.A. Rogers, Truss Structure Integrity Identification Using PZT Sensor-Actuator. *Journal of Intelligent Material Systems and Structures, Vol. 6 -Jan 1995, pp134-139.*

4. D.S. Necsulescu & J. de Carufel, Finite Elements Model Based Predictive Control of Smart Structures. *3rd International Conference, Dynamics and Control of Structures in Space 27-31st May 1996, pp 253-274..*

5. Roy R. Craig, Jr , Structural Dynamics An Introduction to Computer Methods,Wiley Press.

6 Daniel J. Gorman, Free Vibration analysis of beams and shafts, *John Wiley and Son, 1975.*

7. Ronald Soeterboek, Predictive Control - A Unified Approach, Prentice Hall, 1995.

8. Ben K Wada, James L Fanson, Gun-Shing Chen, Chin-Po Kuo, Adaptive Structures : Space Systems. *Intelligent Structures, Elsevier Applied Science Publishers Ltd., 1990, pp 66-89.*

9. Firdaus E. Udwadia, New Methods in the Intelligent Control of Large-scale Continuous Systems. *Intelligent Structures, Elsevier Applied Science Publishers Ltd., 1990, pp 230-243.*

10. R.A. Manning, Structural Damage Detection Using Active Members and Neural Networks. *AIAA Journal Vol 32 No.6:Technical Notes pp 1331-1333.*

11. Mohamed Kaouk, David C. Zimmerman, Structural Damage Assessment Using a Generalized Minimum Rank Perturbation Theory. *AIAA Journal Vol 32, No4, April 1994, pp 836-842.*

12. Shawn E. Burke and James E. Hubbard, Jr., Active Vibration Control of a Simply Supported Beam Using a Spatially Distributed Actuator. *IEEE Control Systems Magazine, Aug, 1987, pp 25-30.*

13. Izhak Sheinman, Damage Detection in Framed Structures. *AIAA Journal Vol 32, No. 5 : Technical Notes pp 1103-1105.*

14. Edward F. Crawley and Javier de Luis, Use of Piezoelectric Actuators as Elements of Intelligent Structures. *AIAA Journal Vol 25, No. 10, Oct 1987, pp 1373-1385.*

15. C. Liang, F. P. Sun and C. A. Rogers, Coupled Electro-Mechanical Analysis of Adaptive Material Systems - Determination of the Actuator

Power Consumption and System Energy Transfer. *Journal of Intelligent Material Systems and Structures, Vol 5 - Jan 1994, pp 12-20.*

16. Tae W. Lim, Thomas A. L. Kashangaki, Structural Damage Detection of Space Truss Structures Using Best Achievable Eigenvectors. *AIAA Journal, Vol 32, No. 5, May 1994, pp 1049-1057.*

17. K. F.Graff, Wave Motion in Elastic Solids, Clarendon Press Oxford 1975.

18. Padma Akella, Xin Chen, Declan Hughes, John T. Wen, Modeling and Control of Smart Structures with Bonded Piezoelectric Sensors and Actuators: A Passivity Approach. *Mathematics and Control in Smart Structures, edited by H. Thomas Banks, Elsevier Applied Science Publishers Ltd. Vol.2192, pp 108-119.*

19. H. T. Banks and Yun Wang, Distributed Parameter System Models for Damage Detection and Location in Smart Material Structures. *Mathematics and Control in Smart Structures, edited by H. Thomas Banks Elsevier Applied Science Publishers Ltd. Vol.2192, pp199-209.*

20. Daryoush Allaei, An Efficient Mathematical Model for Interfaces between the Host Structure and Smart Devices, *Mathematics and Control in Smart Structures, edited by H. Thomas Banks, Elsevier Applied Science Publishers Ltd. Vol.2192, pp 262-271.*

21. T.W. McCray, H.H.Cudney, Modeling the Dynamics of Removable and Reusable Piezoelectric Patch-type Actuators. *Mathematics and Control in Smart Structures, edited by H. Thomas Banks, Elsevier Applied Science Publishers Ltd. Vol.2192 pp254-261.*

22. Jae-Hwan Kim, Vasundara V. Varadan and Vijay K. Varadan, Finite Element Modeling of a Finite Piezoelectric Sensor/Actuator Embedded in

a Fluid-Loaded Plate. *Mathematics and Control in Smart Structures, edited by H. Thomas Banks, Elsevier Applied Science Publishers Ltd., Vol.2192, pp273-280.*

23. S.Y. Hong, V.V. Varadan and V.K. Varadan, Prediction of modal responses for optimal selection of actuator positions in rectangular plate. *Smart Structures and Materials 1994 - Smart Materials, Vijay K. Varadan SPIE - The International Society for Optical Engineering Vol 2189, pp 202-207*

24. Daniel J. Inman, James P. Calamita, Modal Estimates for the Physical Parameters of A Programmable Structure. *Mathematics and Control in Smart Structures, edited by H. Thomas Banks, Elsevier Applied Science Publishers Ltd. Vol.2192, pp 190-197.*

25 Chen Liang, Fanping Sun, and Craig A. Rogers, Electro-mechanical Impedance Modeling of Active Material Systems. *Mathematics and Control in Smart Structures, edited by H. Thomas Banks, Elsevier Applied Science Publishers Ltd. Vol.2192, pp 232-253.*

26. Amy M. Jakubowski John J. Helferty and David S. Bayard, Development of a Recursive ZAP Controller with Specific Applications in Flexible Space Structures. *Mathematics and Control in Smart Structures, edited by H. Thomas Banks, Elsevier Applied Science Publishers Ltd. Vol.2192, pp 176-187.*

27. C. Chung Won and Jeff L. Sulla, Experiments on the Linearization of a Piezoelectric Strut. *Mathematics and Control in Smart Structures, edited by H. Thomas Banks, Elsevier Applied Science Publishers Ltd., Vol.2192, pp 168-175.*

28. Jeanne M. Sullivan, James E. Hubbard, Jr., Shawn E. Burke, Distributed Transducer Design for Plates: Spatial Shape and Shading as Design Parameters. *Mathematics and Control in Smart Structures, edited by H. Thomas Banks, Elsevier Applied Science Publishers Ltd. Vol.2192 pp132-144.*

29. Canadian Space Agency and Lockheed Martin Electronic Systems Canada, Health Performance Monitoring and Enhancement of Space Structures Study,Document No. 990000528,30/4/1996

30 Terry Hinnerichs and David Martinez, Vibration Control for Precision Manufacturing at Sandia National Laboratories. *Smart Structures and Materials 1995 edited by C. Robert Crowe- Industrial and Commercial Applications of Smart Structures Technologies Vol.2447, pp 115-130.*

31 V.G. DeGiorgi, P. Matic, G.C. Kirby III, Recent Studies on Integrated Smart Materials. *Smart Structures and Materials 1995 - Industrial and Commercial Applications of Smart Structures Technologies, edited by C. Robert Crowe, Vol.2447, pp 206-217.*

32 Patricia S. Han, Bradley A. Cleveland and Fred S. Tsuchiya, Remotely Queried Embedded Sensors in Composite Structures. *Smart Structures and Materials 1995 edited by C. Robert Crowe- Industrial and Commercial Applications of Smart Structures Technologies Vol.2447, pp229-236.*

33 D.S. Flamm, L.P. Heck, P.J. Titterton, W.C. Nowlin, J.A. Olkin, K.C. Chou, Control System Design for the SPICES Smart Structure Demonstrations. *Smart Structures and Materials 1995 ,edited by C. Robert Crowe,- Industrial and Commercial Applications of Smart Structures Technologies Vol.2447, pp 237-248.*

34 F.P. Sun, C. Liang and C.A. Rogers, Structural Modal Analysis using Collocated Piezoelectric Actuator/Sensors - an electromechanical approach. *Smart Structures and Materials 1994 edited by Nesbitt W. Hagood, - Smart Structures and Intelligent Systems Vol. 2190, pp 238-249.*

35 C. Liang, F. P. Sun, and C. A. Rogers, Development of an Actuator Power Factor Meter for Experimental Determination of the Optimal Actuator Location on Complex Structures. *Smart Structures and Materials 1994 - Smart Structures and Intelligent Systems Vol. 2190 pp262-274 by Nesbitt W. Hagood.*

36 David J. Warkentin, Edward F. Crawley, Power Flow and Amplifier Design for Piezoelectric Actuators in Intelligent Structures. *Smart Structures and Materials 1994, edited by Nesbitt W. Hagood, - Smart Structures and Intelligent Systems Vol. 2190 pp283-294.*

37 Kwaku O. Prakah-Asante and Kevin C. Craig, Investigation of Modal Based and Wave-type Vibration Energy Transmission for Active Control of Structures. *Smart Structures and Materials 1994 - Smart Structures and Intelligent Systems Vol. 2190 pp295-306 by Nesbitt W. Hagood.*

38 John E. Meyer, Shawn E. Burke, James E. Hubbard Jr. , Distributed and Discrete Transducer Spatial Design for Finite-Element-Modeled Flexible Structures. *Smart Structures and Materials 1994 - Smart Structures and Intelligent Systems Vol. 2190 pp369-380 by Nesbitt W. Hagood.*

39 Sunil Kumar Agrawal,K. Nagaraja, Control of Shapes of Elastic Plates Using Embedded Piezoelectric Actuators. *Smart Structures and Materials 1994 - Smart Structures and Intelligent Systems Vol. 2190 pp463-470 by Nesbitt W. Hagood.*

40 Suwei Zhou, Chen Liang and C. A. Rogers, A Dynamic Model of Piezoelectric Actuator-driven Thin Plates. *Smart Structures and Materials 1994 - Smart Structures and Intelligent Systems Vol. 2190 pp550-562 by Nesbitt W. Hagood.*

41 Abu S. Islam and Kevin C. Craig, Active Damage Mitigation in Composite Structure by Actuation of Piezoceramic Patches. *Smart Structures and Materials 1994 - Smart Structures and Intelligent Systems Vol. 2190 pp611-622 by Nesbitt W. Hagood.*

42 George C. Kirby, Douglas K. Lindner, Peter Matic, Michael Mirmak, Mode Shape Distortions due to Piezoceramic Actuators and Implications for Control. *Smart Structures and Materials 1994 - Smart Structures and Intelligent Systems Vol. 2190 pp647- 657 by Nesbitt W. Hagood.*

43 Don Edberg, Andreas von Flotow, Philip Cha, Bruce Fisher, Lisa Gann, Andy Roe, Jon Soberg, Ground-testing of a Microgravity Isolation System. *Smart Structures and Materials 1994 - Smart Structures and Intelligent Systems Vol. 2190 pp759-771 by Nesbitt W. Hagood.*

44 Douglas K. Lindner, George Kirby, Dan Sable, Power Converters and Power Systems for Piezoelectric Actuators. *Smart Structures and Materials 1994 - Smart Structures and Intelligent Systems Vol. 2190 pp262-274 by Nesbitt W. Hagood.*

45 Spillman, William B Jr., Sensing and Processing for Smart Structures. *Proceedings of the IEEE. v84 n1 Jan 1996 pp 68-77.*

46 Udd, Eric, Fiber Optic Smart Structures. *Proceedings of the IEEE. v84 n1 Jan 1996. pp 60-67.*

47 Wyman, Vic, Smart Work could Rewrite Design Rules, *Professional Engineering v8 n17 Oct 4 1995. pp 26-27.*

48 Lee, Gwo-Shiang, System Identification and Control of Smart Structures using Neural Networks. *Acta Astronautica. v38 n4-8 Feb-Apr 1996. pp 269-276.*

49 Kalamkarov, Alexander L. Drozdov, Aleksey D. , Mathematical Modeling of Smart Structures. *Proceedings of SPIE- The International Society for Optical Engineering. v2715 1996. pp 626-637.*

50 Lim, Young-Hun, Varadan,Vasundara V. Varadan, Vijay K., Finite Element Modeling of the Transient Response of Smart Structures. *Proceedings of SPIE - The International Society for Optical Engineering. v2175 1996. pp 233-242.*

51 Damle, Rajendra R. Rao, Vittal S., Control of Linear Smart Structural Systems using Neural Networks. *Proceedings of SPIE - The International Society for Optical Engineering. v2715 1996 pp 28-40.*

52 Chopra, Inderjit, Review of Current Status of Smart Structures and Integrated Systems. *Proceedings of SPIE - The International Society for Optical Engineering. v2717 1996. pp 20-62.*

53 Culshaw, Brian, Smart Structures Activities Worldwide. *Proceedings of SPIE - The International Society for Optical Engineering v2717 1996. pp 2-17.*

54 Spillman, W B Jr. Sirkis, J S. Gardiner, P T, Smart Materials and Structures : what are they? *Smart Materials & Structures. v5 n3 Jun 1996. pp 247-254.*

55 Spillman, W B Jr. , Smart Structures and Fiber Optic Technology for 21st Century Control Applications. *Proceedings of the 1996 International Gas Turbine and Aeroengine Congress & Exhibition. Burmingham, UK 19960610-19960613. conference Code 45083.*

56 Udd, Eric, Fiber Optic Smart Structures, *Proceedings of the IEEE. v84 n6 Jun 1996. pp 884-894.*

57 Udd, Eric, Applications of Fiber Optic Smart Structures, *Optics & Photonics News. v7 n5 May 1996. pp 16-22.*

58 Banks, H T. Inman, D J. Leo, D J. Wang, Y., Experimentally Validated Damage Detection Theory in Smart Structures. *Journal of Sound & Vibration. v191 n5 Apr 18 1996. pp 859-880.*

59 Yousefi-Koma, Aghil, Vukovich, George, Non-collocated Active Traveling Wave Control of Smart Structures using Distributed Transducers. *IEEE Conference on Control Applications - Proceedings 1996.pp 297-302.*

60 Aldraihem, Osama J. Wetherhold, Robert C. Singh, Tarunraj, Intelligent Beam Structures : Timoshenko Theory vs. Euler-Bernoulli Theory. *IEEE Conference on Control Applications - Proceedings 1996. pp 976-981.*

61 August, James A. Joshi, Shiv p. Smart Structures Applications for Hypersonic Vehicles, *Proceedings of SPIE - v2721 1996 pp 50-57.*

62 H.Sato , Free Vibration of Beams with Abrupt Changes of Cross-section. *Journal of Sound and Vibraion 89 1993, pp 59-64.*

63 A.Isman and K.Craig, Damage Detection in Composite Structures using Piezoelectric Materials, *Smart Mater. Struct Vol 3 1994, pp 318-328*

64 P. Cawley and R. Ray, A Comparison of the Natural Frequency Changes Produced by Cracks and Slots, *ASME Journal Vibration, Acoustics, Stress and Reliability in Design 110 1988, pp 366-370*

65 P. Cawley and R.D. Adams, The Location of Defects in Structures from Measurements of Natural Frequencies, *Journal of strain Analysis 14 1979, pp 49-57.*

66 R. D. Adams, P. Cawley, C.J. Pye and B.J. Stone , A Vibrational Technique for Non-destructively Assessing the Integrity of Structures. *Journal Mechanical Engineering Science 20 1978, pp 93-100.*

67 D. Armon, Y.Ben-Hain and S. Braun, Crack Detection in Beams by Rank-Ordering of Eigenfrequency Shifts, *Mechanical Systems and Signal Processing 8 1994 pp 81-92.*

68 P.K. Roy and N. Ganesan, Transient Response of a Cantilever Beam subjected to an Impulse load. *Journal of Sound and Vibration 183 1995 pp 873-880.*

69 A. Kunow-Baumhauer, The Response of a Beam to a Transient Pressure Wave Load. *Journal of Sound and Vibration, 92 1984 pp 491-506.*

70 A.W.Leissa and M.I. Sonalla, Vibrations of Cantilever Beams with Various Initial Conditions. *Journal of Sound and Vibration 150 1991 pp 83-39.*

71 H.Abramovich, A Note on Experimental Investigation on a Vibrating Timoshenko Cantilever Beam. *Journal of sound and vibration 1993 vol 160 pp 167-171.*

72 B.A.H.Abbas and H. Irretier , Experimental and Theoretical Investigations of the Effect of Root Flexibility on the Vibration Characteristics of Cantilever Beams. *Journal of sound and vibration 1989 130 pp 353-362.*

73 P.A.A. Laura, R.E. Rosst, L.Ercoli and S. La Malfa , Analytical and Experimental Investigation on a Vibrating Timoshenko Beam Clamped at One End and Carrying a Finite Mass at the Other. *Applied Mechanics Reviews 1991 44 (11) Part 2, pp 171-173.*

74 D. Inman, Engineering Vibration, *Prentice Hall, 1994*

75 W. Thomson, Laplace Transformation, *Pentice Hall, 1960,*

76 S. Timoshenko, D.H. Young, W. Weaver, Vibration Problems in Engineering, *John Wiley, 1974.*

77 Wylie and Barrett, Advanced Engineering Mathematics, *Mc.Graw- Hill, 1995.*

78 V.A. Spector and H. Flashner, Flexible Manipulator Modeling for Control System Development. *J. Guidance vol 12,No. 6 1989, pp 943-945.*

79 K.T. Chan, et al , Free Vibration of Simply Supported Beam Partially Loaded with Distributed Mass. *Journal of Sound and Vibration v191 n4 Apr 1996 pp 590-597.*

80 Yuji Sogabe, Transient Vibration Analysis of Elastically Connected Timoshenko Double-Beam Systems. *Nippon Kikai Gakkai Ronbunshu, C Hen v62 n594 Feb 1996 pp 429-437.*

81 Esmailzadeh et al, Vibration Analysis of a Timoshenko Beam Subjected to a Travelling mass. *Journal of Sound and Vibration Jan 1997 pp 615-628.*

82 Yoshitsugu Goto, Experimental Identification Technique for Boundary Conditions of a Beam (when boundary conditions are linear), *Nippon Kikai Gakkai Ronbunshu, C Hen v60 n570 Feb 1994 pp 482-489.*

83 Yoshitsugu Goto, Experimental Identification Technique for Boundary Conditions of a Beam (confirmation of applicability of the technique, and its application to a rolling bearing), *Nippon Kikai Gakkai Ronbunshu, C Hen v62 n597 May 1996. pp 1797-1804.*

84 T.C. Chang, R.R. Craig Jr., Normal Modes of Uniform Beam, *Proc. ASCE V95 n. EM4,1969 pp1025-1031.*

85 dSPACE digital signal processing and control engineering GmbH, DS2002 and DS2101 user's Guide, Document Version 1.1, *An der Schonen Aussicht 2, D-4790 Paderborn, West Germany.*

86 Sensor Technology, BM Hi-Tech Division, Piezoelectric Ceramics Catalogue.

87 D. Necsulescu, Health Monitoring of Space Structures Using High Frequency Mechanical Impedance Estimation, *Final Report, CSA, 1996.*

8.2 Computer Programs

```
%-- This program (Exathsin.m) has been written to simulate the
%-- solution for Cantilever beam with half sin pulse excitation.

format long;
a=1.38;
l=0.55;
lp=0.1315;
% ls=lp; % Collocated
% ls=0.1936;
%--Where input frequency is in Hz, Variable name Freq----

freq=4000;
omea=2*pi*freq;

rho=2.7*10^3;
A=23.8*10^(-6);
F0=10;
alpha=F0/(rho*A);
ht1=pi/omea;
z(1)=1.8751;
z(2)=4.6941;
z(3)=7.8548;
z(4)=10.996;
z(5)=14.14;

x=1;
t=1;
ht=0.00000005;

nt=80;
nx=11;
hx=l/nx;
for i=1:5
 lm(i)=a*(z(i)/l)^2;
 b(i)=z(i)/l;
 sig(i)=(sinh(b(i)*l)-sin(b(i)*l))/(cosh(b(i)*l)+cos(b(i)*l));

den=(4*b(i)*l+2*sig(i)*cos(2*b(i)*l)-2*sig(i)*cosh(2*b(i)*l)...
 -4*cosh(b(i)*l)*sin(b(i)*l)-4*sig(i)^2*cosh(b(i)*l)*sin(b(i)*l)+sin(2*b(i)*l)...
-sig(i)^2*sin(2*b(i)*l)-4*cos(b(i)*l)*sinh(b(i)*l)+4*sig(i)^2*cos(b(i)*l)...
*sinh(b(i)*l)+8*sig(i)*sin(b(i)*l)*sinh(b(i)*l)+sinh(2*b(i)*l)...
+sig(i)^2*sinh(2*b(i)*l));

 A(i)=sqrt(4*b(i)/den);

Xls(i)=A(i)*(cosh(b(i)*ls)-cos(b(i)*ls)-sig(i)*(sinh(b(i)*ls)...
      -sin(b(i)*ls)));


Xlp(i)=A(i)*(cosh(b(i)*lp)-cos(b(i)*lp)-sig(i)*(sinh(b(i)*lp)...
      -sin(b(i)*lp)));
```

```
end
u=zeros(nt,nx);
for j=1:nt
   for k=1:nx
        for i=1:5
          x=k*hx;
          t=j*ht;
          XX(i)=A(i)*(cosh(b(i)*x)-cos(b(i)*x)-sig(i)*(sinh(b(i)*x)-sin(b(i)*x)));
          if t>ht1
             u(j,k)=u(j,k)+2*(alpha*XX(i)*Xlp(i))/(omea^2-lm(i)^2)...
             *omea*sin(lm(i)*t-lm(i)*pi/(2*omea))...
             *cos(lm(i)*pi/(2*omea))/lm(i);
          end
          if t<ht1
             u(j,k)=u(j,k)+(alpha*XX(i)*Xlp(i))/(lm(i)^2-omea^2)...
             *(sin(omea*t)-omea*sin(lm(i)*t)/lm(i));
          end
        end
   end
end
%-------------------------------------------------------
% Calculate the value of response
% for j=1:nt
%   for k=1:nx
%      u(j,k);
%   end
% end
j=1;
%-------------------------------------------------------
% Plotting 3-D graph
%figure(1)
%surfl(u)
%title(['Cantilever with half sin pulse (Exact Sol)'])
%xlabel('position along beam');
%ylabel('time');
%zlabel('Vertical displacement');
%-------------------------------------------------------
% Plotting Vertical displacement vs Position along beam
%  for j=1:nt
%     for k=1:nx
%        x(k)=[k];
%        y(k)=[u(j,k)];
%     end
%     figure(j+1)
%     plot(x,y)
%     title(['Vertical displacement vs Position',' j= ', num2str(j)])
%     ylabel('Vertical displacemtnt')
%     xlabel('Positon')
%     grid
%  end
%-------------------------------------------------------
% Plotting displacement vs position with a specific time

% time =0.09;
% t= time;
```

```
%   for k=1:nx

%         ysum=0;
%         for i=1:5
%            x=k*hx;
%              XX(i)=A(i)*(cosh(b(i)*x)-cos(b(i)*x)-sig(i)*(sinh(b(i)*x)-sin(b(i)*x)));
%            if time>ht1
%               ysum=ysum+2*(alpha*XX(i)*Xlp(i))/(omea^2-lm(i)^2)...
%               *omea*sin(lm(i)*t-lm(i)*pi/(2*omea))...
%               *cos(lm(i)*pi/(2*omea))/lm(i);
%            end
%            if time<ht1
%               ysum=ysum+(alpha*XX(i)*Xlp(i))/(lm(i)^2-omea^2)...
%               *(sin(omea*t)-omea*sin(lm(i)*t)/lm(i));
%            end
%         end
%         yy(k)=ysum;
%   end
% for k=1:nx
%        x(k)=[k];
%        y(k)=[yy(k)];
% end
%    figure(j+1)
%    plot(x,y)
%    title(['Vertical displacement vs Position with specific',' time = ', num2str(time)])
%    ylabel('Vertical displacemtnt')
%    xlabel('Positon')
%    grid
%-------------------------------------------------------------
% Plotting displacement vs time at the sensor location

% steptime=0.001;
% for n=1 : 200
%   t=n*steptime;

%         ysum=0;
%         for i=1:5
%            if t>ht1
%               ysum=ysum+2*(alpha*Xls(i)*Xlp(i))/(omea^2-lm(i)^2)...
%               *omea*sin(lm(i)*t-lm(i)*pi/(2*omea))...
%               *cos(lm(i)*pi/(2*omea))/lm(i);
%            end
%            if t<=ht1
%               ysum=ysum+(alpha*Xls(i)*Xlp(i))/(lm(i)^2-omea^2)...
%               *(sin(omea*t)-omea*sin(lm(i)*t)/lm(i));
%            end
%
%         end
%         yy(n)=ysum;
% end
% for n=1:200
%        x(n)=[n];
%        y2(n)=[yy(n)];
% end
%    figure(j+1)
```

```
%    plot(x,y2)
%    title(['Vertical displacement vs time at the sensor',' freq = ', num2str(freq),' Hz'])
%    ylabel('Vertical displacement')
%    xlabel('Time')
%    grid
%-------------------------------------
```

```
%-- This program (Exhclams.m) has been written to simulate the
%-- solution for clamped-clamped beam with half sin pulse excitation.
format long;
a=1.38;
l=0.55*2;
lp=0.1315;
ls=lp; % Collocated
% ls=0.1936;
%--------Where input frequency is in Hz, Variable name freq---

freq=4000;
omea=2*pi*freq;

rho=2.7*10^3;
A=23.8*10^(-6);
F0=10;
alpha=F0/(rho*A);
ht1=pi/omea;
z(1)=4.730;
z(2)=7.853;
z(3)=10.996;
z(4)=14.137;
z(5)=17.279;

x=1;
t=1;
ht=0.002;

nt=70;
nx=11;
hx=l/nx;
for i=1:5
  lm(i)=a*(z(i)/l)^2;
  b(i)=z(i)/l;
  sig(i)=(cosh(b(i)*l)-cos(b(i)*l))/(sinh(b(i)*l)-sin(b(i)*l));

den=(4*b(i)*l+2*sig(i)*cos(2*b(i)*l)-2*sig(i)*cosh(2*b(i)*l)...
  -4*cosh(b(i)*l)*sin(b(i)*l)-4*sig(i)^2*cosh(b(i)*l)*sin(b(i)*l)+sin(2*b(i)*l)...
-sig(i)^2*sin(2*b(i)*l)-4*cos(b(i)*l)*sinh(b(i)*l)+4*sig(i)^2*cos(b(i)*l)...
*sinh(b(i)*l)+8*sig(i)*sin(b(i)*l)*sinh(b(i)*l)+sinh(2*b(i)*l)...
+sig(i)^2*sinh(2*b(i)*l));

  A(i)=sqrt(4*b(i)/den);

Xls(i)=A(i)*(cosh(b(i)*ls)-cos(b(i)*ls)-sig(i)*(sinh(b(i)*ls)...
      -sin(b(i)*ls)));

Xlp(i)=A(i)*(cosh(b(i)*lp)-cos(b(i)*lp)-sig(i)*(sinh(b(i)*lp)...
      -sin(b(i)*lp)));
end
u=zeros(nt,nx);
for j=1:nt

    for k=1:nx
          for i=1:5
```

```
            x=k*hx;
            t=j*ht;
            XX(i)=A(i)*(cosh(b(i)*x)-cos(b(i)*x)-sig(i)*(sinh(b(i)*x)-sin(b(i)*x)));
            if t>ht1
               u(j,k)=u(j,k)+2*(alpha*XX(i)*Xlp(i))/(omea^2-lm(i)^2)...
               *omea*sin(lm(i)*t-lm(i)*pi/(2*omea))...
               *cos(lm(i)*pi/(2*omea))/lm(i);
            end
            if t<ht1
               u(j,k)=u(j,k)+(alpha*XX(i)*Xlp(i))/(lm(i)^2-omea^2)...
               *(sin(omea*t)-omea*sin(lm(i)*t)/lm(i));
            end
         end
   end
end
%-------------------------------------------------------------
% Calculate the value of response
%for j=1:nt
%   for k=1:nx
%      u(j,k);
%   end
%end
j=1;
%-------------------------------------------------------------
% Plotting 3-D graph

% figure(1)
% surfl(u)
% title(['Clamped-Clamped with half sin pulse (Exact Sol)'])
% xlabel('position along beam');
% ylabel('time');
% zlabel('Vertical displacement');

%-------------------------------------------------------
% Plotting Vertical displacement vs Position along beam
%  for j=1:nt
%     for k=1:nx
%        x(k)=[k];
%        y(k)=[u(j,k)];
%     end
%     figure(j+1)
%     plot(x,y)
%     title(['Vertical displacement vs Position',' j= ', num2str(j)])
%     ylabel('Vertical displacemtnt')
%     xlabel('Positon')
%     grid
%  end
%-------------------------------------------------------
% Plotting displacement vs position with a specific time

% time =0.0055;
% t= time;
%   for k=1:nx
%
%        ysum=0;
```

```
%        for i=1:5
%           x=k*hx;

%           XX(i)=A(i)*(cosh(b(i)*x)-cos(b(i)*x)-sig(i)*(sinh(b(i)*x)-sin(b(i)*x)));
%           if time>ht1
%              ysum=ysum+2*(alpha*XX(i)*Xlp(i))/(omea^2-lm(i)^2)...
%              *omea*sin(lm(i)*t-lm(i)*pi/(2*omea))...
%              *cos(lm(i)*pi/(2*omea))/lm(i);
%           end
%           if time<ht1
%              ysum=ysum+(alpha*XX(i)*Xlp(i))/(lm(i)^2-omea^2)...
%              *(sin(omea*t)-omea*sin(lm(i)*t)/lm(i));
%           end
%        end
%        yy(k)=ysum;
%   end
% for k=1:nx
%       x(k)=[k];
%       y(k)=[yy(k)];
% end
%    figure(j+1)
%    x=[0,x];
%    y=[0,y];
%    plot(x,y)
%    title(['Vertical displacement vs Position with specific',' time = ', num2str(time)])
%    ylabel('Vertical displacemtnt')
%    xlabel('Positon')
%    grid
%-------------------------------------------------------------
% Calculate the velocity of transverse wave
% t=ht1/2;
% ticouter=0;
% for i=1:5
%  ticouter=ticouter+(alpha*Xlp(i)^2*omea*(cos(omea*t)-cos(lm(i)*t))/(lm(i)^2-omea^2));
%end
%  den=ticouter;
%timetake=(l-lp)/den
%-------------------------------------------------------------
% Plotting displacement vs time at the sensor location

% steptime=0.001;
% for n=1 : 200
%   t=n*steptime;

%        ysum=0;
%        for i=1:5

%           if t>ht1
%              ysum=ysum+2*(alpha*Xls(i)*Xlp(i))/(omea^2-lm(i)^2)...
%              *omea*sin(lm(i)*t-lm(i)*pi/(2*omea))...
%              *cos(lm(i)*pi/(2*omea))/lm(i);
%           end
%           if t<=ht1
%              ysum=ysum+(alpha*Xls(i)*Xlp(i))/(lm(i)^2-omea^2)...
%              *(sin(omea*t)-omea*sin(lm(i)*t)/lm(i));
```

```
%              end
%            end
%            yy(n)=ysum;
% end
% for n=1:200
%          x(n)=[n];
%          y1(n)=[yy(n)];
% end
%     figure(j+1)
%     plot(x,y1)
%     title(['Vertical displacement vs time at the sensor',' freq = ', num2str(freq),' Hz'])
%     ylabel('Vertical displacement')
%     xlabel('Time')
%     grid
%-------------------------------------------------------------
```

```
%-- This program (Exatcsin.m) has been written to simulate the
%-- solution for Cantilever beam with 1 full sin pulse excitation.

format long;
a=1.38;
l=0.55;
lp=0.1315;
 ls=lp;  % Colloated
% ls=0.1936;
%------Where input frequency is in Hz, Variable name freq----
freq=4000;
omea=2*pi*freq;

rho=2.7*10^3;
A=23.8*10^(-6);
F0=10;
alpha=F0/(rho*A);

z(1)=1.8751;
z(2)=4.6941;
z(3)=7.8548;
z(4)=10.996;
z(5)=14.14;
ft=2*pi/omea;

x=1;
t=1;
ht=0.001;

nt=80;
nx=11;
hx=l/nx;
for i=1:5
  lm(i)=a*(z(i)/l)^2;
  b(i)=z(i)/l;
  sig(i)=(sinh(b(i)*l)-sin(b(i)*l))/(cosh(b(i)*l)+cos(b(i)*l));

den=(4*b(i)*l+2*sig(i)*cos(2*b(i)*l)-2*sig(i)*cosh(2*b(i)*l)...
  -4*cosh(b(i)*l)*sin(b(i)*l)-4*sig(i)^2*cosh(b(i)*l)*sin(b(i)*l)+sin(2*b(i)*l)...
-sig(i)^2*sin(2*b(i)*l)-4*cos(b(i)*l)*sinh(b(i)*l)+4*sig(i)^2*cos(b(i)*l)...
*sinh(b(i)*l)+8*sig(i)*sin(b(i)*l)*sinh(b(i)*l)+sinh(2*b(i)*l)...
+sig(i)^2*sinh(2*b(i)*l));

  A(i)=sqrt(4*b(i)/den);

Xls(i)=A(i)*(cosh(b(i)*ls)-cos(b(i)*ls)-sig(i)*(sinh(b(i)*ls)...
      -sin(b(i)*ls)));

Xlp(i)=A(i)*(cosh(b(i)*lp)-cos(b(i)*lp)-sig(i)*(sinh(b(i)*lp)...
      -sin(b(i)*lp)));
end
u=zeros(nt,nx);
for j=1:nt
    for k=1:nx
          for i=1:5
```

```
            x=k*hx;
            t=j*ht;
            XX(i)=A(i)*(cosh(b(i)*x)-cos(b(i)*x)-sig(i)*(sinh(b(i)*x)-sin(b(i)*x)));
            if t>ft
               u(j,k)=u(j,k)+2*(alpha*XX(i)*Xlp(i))/(omea^2-lm(i)^2)...
               *omea*cos(lm(i)*t-lm(i)*pi/omea)...
               *sin(lm(i)*pi/omea)/lm(i);
            end
            if t<=ft
               u(j,k)=u(j,k)+(alpha*XX(i)*Xlp(i))/(lm(i)^2-omea^2)...
               *(sin(omea*t)-omea*sin(lm(i)*t)/lm(i));
            end
         end
   end
end
%-------------------------------------------------
% Calculate the value of response
% for j=1:nt
%   for k=1:nx
%      u(j,k);
%   end
% end
j=1;

%-------------------------------------------------
% plotting 3-D graph

% figure(1)
% surfl(u)
% title(['Cantilever with full sin pulse (Theoretical Sol)'])
% xlabel('position along beam');
% ylabel('time');
% zlabel('Vertical displacement');
%-------------------------------------------------------
% Plotting Vertical displacement vs Position along beam
%  for j=1:nt
%     for k=1:nx
%        x(k)=[k];
%        y(k)=[u(j,k)];
%     end
%     figure(j+1)
%     plot(x,y)
%     title(['Vertical displacement vs Position',' j= ', num2str(j)])
%     ylabel('Vertical displacemtnt')
%     xlabel('Positon')
%     grid
%  end
%-------------------------------------------------------
% Plotting displacement vs position with a specific time

% time =0.03;
% t= time;
%   for k=1:nx

%        ysum=0;
```

```
%         for i=1:5
%            x=k*hx;
%            XX(i)=A(i)*(cosh(b(i)*x)-cos(b(i)*x)-sig(i)*(sinh(b(i)*x)-sin(b(i)*x)));
%            if time>ft
%               ysum=ysum+2*(alpha*XX(i)*Xlp(i))/(omea^2-lm(i)^2)...
%               *omea*cos(lm(i)*t-lm(i)*pi/omea)...
%               *sin(lm(i)*pi/omea)/lm(i);
%            end
%            if time<=ft
%               ysum=ysum+(alpha*XX(i)*Xlp(i))/(lm(i)^2-omea^2)...
%               *(sin(omea*t)-omea*sin(lm(i)*t)/lm(i));
%            end
%         end
%         yy(k)=ysum;
%   end
% for k=1:nx
%       x(k)=[k];
%       y(k)=[yy(k)];
% end
%    figure(j+1)
%    plot(x,y)
%    title(['Vertical displacement vs Position with specific',' time = ', num2str(time)])
%    ylabel('Vertical displacemtnt (m)')
%    xlabel('Positon')
%    grid
% ------------------------------------------------------
% Plotting displacement vs time at the sensor location

% steptime=0.001;
% for n=1 : 5000
%   t=n*steptime;

%         ysum=0;
%         for i=1:5

%            if t>ft
%               ysum=ysum+2*(alpha*Xls(i)*Xlp(i))/(omea^2-lm(i)^2)...
%               *omea*cos(lm(i)*t-lm(i)*pi/omea)...
%               *sin(lm(i)*pi/omea)/lm(i);
%            end
%            if t<=ft
%               ysum=ysum+(alpha*Xls(i)*Xlp(i))/(lm(i)^2-omea^2)...
%               *(sin(omea*t)-omea*sin(lm(i)*t)/lm(i));
%            end
%         end
%         yy(n)=ysum;
% end
% for n=1:5000
%       x(n)=[n];
%       y2(n)=[yy(n)];
% end
%    figure(j+1)
%    plot(x,y2)
%    title(['Vertical displacement vs time at the sensor',' freq = ', num2str(freq),' Hz'])
%    ylabel('Vertical displacement')
```

```
%     xlabel('Time')
%     grid
%-------------------------------------------------------------
```

```
%-- This program (Excclams.m) has been written to simulate the
%-- solution for clamped-clamped beam with 1 complete sin pulse excitation.
format long;
a=1.38;
l=0.55*2;
lp=0.1315;
 ls=lp; % collocated
% ls=0.1936;
%--Where input frequency is in Hz, Variable name Freq--

freq=4000;
omea=2*pi*freq;

rho=2.7*10^3;
A=23.8*10^(-6);
F0=10;
alpha=F0/(rho*A);
z(1)=4.730;
z(2)=7.853;
z(3)=10.996;
z(4)=14.137;
z(5)=17.279;
ft=2*pi/omea;

x=1;
t=1;
ht=0.001;

nt=80;
nx=11;
hx=l/nx;
for i=1:5
  lm(i)=a*(z(i)/l)^2;
  b(i)=z(i)/l;
  sig(i)=(cosh(b(i)*l)-cos(b(i)*l))/(sinh(b(i)*l)-sin(b(i)*l));

den=(4*b(i)*l+2*sig(i)*cos(2*b(i)*l)-2*sig(i)*cosh(2*b(i)*l)...
  -4*cosh(b(i)*l)*sin(b(i)*l)-4*sig(i)^2*cosh(b(i)*l)*sin(b(i)*l)+sin(2*b(i)*l)...
-sig(i)^2*sin(2*b(i)*l)-4*cos(b(i)*l)*sinh(b(i)*l)+4*sig(i)^2*cos(b(i)*l)...
*sinh(b(i)*l)+8*sig(i)*sin(b(i)*l)*sinh(b(i)*l)+sinh(2*b(i)*l)...
+sig(i)^2*sinh(2*b(i)*l));

  A(i)=sqrt(4*b(i)/den);

Xls(i)=A(i)*(cosh(b(i)*ls)-cos(b(i)*ls)-sig(i)*(sinh(b(i)*ls)...
      -sin(b(i)*ls)));

Xlp(i)=A(i)*(cosh(b(i)*lp)-cos(b(i)*lp)-sig(i)*(sinh(b(i)*lp)...
      -sin(b(i)*lp)));
end
u=zeros(nt,nx);
for j=1:nt
   for k=1:nx
         for i=1:5
            x=k*hx;
```

```
            t=j*ht;
            XX(i)=A(i)*(cosh(b(i)*x)-cos(b(i)*x)-sig(i)*(sinh(b(i)*x)-sin(b(i)*x)));
            if t>ft
               u(j,k)=u(j,k)+2*(alpha*XX(i)*Xlp(i))/(omea^2-lm(i)^2)...
               *omea*cos(lm(i)*t-lm(i)*pi/omea)...
               *sin(lm(i)*pi/omea)/lm(i);
            end
            if t<ft
               u(j,k)=u(j,k)+(alpha*XX(i)*Xlp(i))/(lm(i)^2-omea^2)...
               *(sin(omea*t)-omea*sin(lm(i)*t)/lm(i));
            end
         end
   end
end
%-------------------------------------------------------------
% Calculate the value of response
% for j=1:nt
%   for k=1:nx
%      u(j,k);
%   end
% end
j=1;
%-------------------------------------------------------------
% Plotting 3-D graph
% figure(1)
% surfl(u)
% title(['Clamped-Clamped with full sin pulse (Theoretical Sol)'])
% xlabel('position along beam');
% ylabel('time');
% zlabel('Vertical displacement');
%-------------------------------------------------------------
% Plotting Vertical displacement vs Position along beam
%  for j=1:nt
%    for k=1:nx
%       x(k)=[k];
%       y(k)=[u(j,k)];
%    end
%    figure(j+1)
%    plot(x,y)
%    title(['Vertical displacement vs Position',' j= ', num2str(j)])
%    ylabel('Vertical displacemtnt')
%    xlabel('Positon')
%    grid
%  end
%-------------------------------------------------------------
% Plotting displacement vs position with a specific time

% time =0.035;
% t= time;
%   for k=1:nx

%         ysum=0;
%         for i=1:5
%            x=k*hx;
%
```

```
%            XX(i)=A(i)*(cosh(b(i)*x)-cos(b(i)*x)-sig(i)*(sinh(b(i)*x)-sin(b(i)*x)));
%            if t>ft
%               ysum=ysum+2*(alpha*XX(i)*Xlp(i))/(omea^2-lm(i)^2)...
%               *omea*cos(lm(i)*t-lm(i)*pi/omea)...
%               *sin(lm(i)*pi/omea)/lm(i);
%            end
%            if t<=ft
%               ysum=ysum+(alpha*XX(i)*Xlp(i))/(lm(i)^2-omea^2)...
%               *(sin(omea*t)-omea*sin(lm(i)*t)/lm(i));
%            end
%         end
%         yy(k)=ysum;
%   end
% for k=1:nx
%       x(k)=[k];
%       y(k)=[yy(k)];
% end
%    figure(j+1)
%  plot(x,y)
%    title(['Vertical displacement vs Position with specific',' time = ', num2str(time)])
%    ylabel('Vertical displacement (m)')
%    xlabel('Positon')
%    grid
%-----------------------------------------------------------------
% Plotting displacement vs time at the sensor location

% steptime=0.001;
% for n=1 : 5000
%   t=n*steptime;
%       ysum=0;
%       for i=1:5

%           if t>ft
%              ysum=ysum+2*(alpha*Xls(i)*Xlp(i))/(omea^2-lm(i)^2)...
%              *omea*cos(lm(i)*t-lm(i)*pi/omea)...
%              *sin(lm(i)*pi/omea)/lm(i);
%           end
%           if t<=ft
%              ysum=ysum+(alpha*Xls(i)*Xlp(i))/(lm(i)^2-omea^2)...
%              *(sin(omea*t)-omea*sin(lm(i)*t)/lm(i));
%           end
%        end
%        yy(n)=ysum;
% end
% for n=1:5000
%       x(n)=[n];
%       y1(n)=[yy(n)];
% end
%    figure(j+1)
%    plot(x,y1)
%    title(['Vertical displacement vs time at the sensor',' freq = ', num2str(freq),' Hz'])
%    ylabel('Vertical displacement')
%    xlabel('Time')
%    grid
%-----------------------------------------------------------------
```

```
%-- This program (Tensinca.m) has been written to simulate the
%-- solution for Cantilever beam with 10 complete sin pulse excitation.
format long;
a=1.38;
l=0.55;
lp=0.1315;
ls=lp;  % Collocated
% ls=0.1936;
%--Where input frequency is in Hz, Variable name Freq--

freq=4000;
omea=2*pi*freq;

rho=2.7*10^3;
A=23.8*10^(-6);
F0=10;
alpha=F0/(rho*A);
z(1)=1.8751;
z(2)=4.6941;
z(3)=7.8548;
z(4)=10.996;
z(5)=14.14;

ft=20*pi/omea;

x=1;
t=1;
ht=0.005;

nt=80;
nx=11;
hx=l/nx;
for i=1:5
 lm(i)=a*(z(i)/l)^2;
 b(i)=z(i)/l;

  sig(i)=(sinh(b(i)*l)-sin(b(i)*l))/(cosh(b(i)*l)+cos(b(i)*l));

den=(4*b(i)*l+2*sig(i)*cos(2*b(i)*l)-2*sig(i)*cosh(2*b(i)*l)...
 -4*cosh(b(i)*l)*sin(b(i)*l)-4*sig(i)^2*cosh(b(i)*l)*sin(b(i)*l)+sin(2*b(i)*l)...
-sig(i)^2*sin(2*b(i)*l)-4*cos(b(i)*l)*sinh(b(i)*l)+4*sig(i)^2*cos(b(i)*l)...
*sinh(b(i)*l)+8*sig(i)*sin(b(i)*l)*sinh(b(i)*l)+sinh(2*b(i)*l)...
+sig(i)^2*sinh(2*b(i)*l));

 A(i)=sqrt(4*b(i)/den);

Xls(i)=A(i)*(cosh(b(i)*ls)-cos(b(i)*ls)-sig(i)*(sinh(b(i)*ls)...
     -sin(b(i)*ls)));


Xlp(i)=A(i)*(cosh(b(i)*lp)-cos(b(i)*lp)-sig(i)*(sinh(b(i)*lp)...
     -sin(b(i)*lp)));
end
u=zeros(nt,nx);
for j=1:nt
```

```
    for k=1:nx
        for i=1:5
          x=k*hx;
          t=j*ht;
          XX(i)=A(i)*(cosh(b(i)*x)-cos(b(i)*x)-sig(i)*(sinh(b(i)*x)-sin(b(i)*x)));
          if t>ft
             u(j,k)=u(j,k)+(alpha*XX(i)*Xlp(i))/(lm(i)^2-omea^2)...
             *[sin(omea*t)-omea/lm(i)*sin(lm(i)*t)-sin(omea*(t-20*pi/omea))+omea/lm(i)*sin(lm(i)*(t-
20*pi/omea))];

          end
          if t<=ft
             u(j,k)=u(j,k)+(alpha*XX(i)*Xlp(i))/(lm(i)^2-omea^2)...
             *(sin(omea*t)-omea*sin(lm(i)*t)/lm(i));
          end
        end
    end
end
%-------------------------------------------------------------
% Calculate the value of response
% for j=1:nt
%    for k=1:nx
%       u(j,k);
%    end
% end
j=1;
%-------------------------------------------------------------
% Plotting 3-D graph
% figure(1)
% surfl(u)
% title(['Cantilever with 10 full sin pulse (Exact Sol)'])
% xlabel('position along beam');
% ylabel('time');
% zlabel('Vertical displacement');
%-------------------------------------------------------------
% Plotting Vertical displacement vs Position along beam
%  for j=1:nt
%     for k=1:nx
%        x(k)=[k];
%        y(k)=[u(j,k)];
%     end
%     figure(j+1)
%     plot(x,y)
%    title(['Vertical displacement vs Position',' j= ', num2str(j)])
%     ylabel('Vertical displacemtnt')
%     xlabel('Positon')
%     grid

%  end
%-------------------------------------------------------------
% Plotting displacement vs position with a specific time

% time =0.000011;

% t= time;
```

```
%   for k=1:nx

%         ysum=0;
%         for i=1:5
%             x=k*hx;

%              XX(i)=A(i)*(cosh(b(i)*x)-cos(b(i)*x)-sig(i)*(sinh(b(i)*x)-sin(b(i)*x)));
%              if time>ft
%                 ysum=ysum+(alpha*XX(i)*Xlp(i))/(lm(i)^2-omea^2)...
%                 *[sin(omea*t)-omea/lm(i)*sin(lm(i)*t)-sin(omea*(t-20*pi/omea))+omea/lm(i)*sin(lm(i)*(t-
20*pi/omea))];

%              end
%              if time<=ft
%                 ysum=ysum+(alpha*XX(i)*Xlp(i))/(lm(i)^2-omea^2)...
%                 *(sin(omea*t)-omea*sin(lm(i)*t)/lm(i));
%              end
%          end
%          yy(k)=ysum;
%    end
% for k=1:nx
%         x(k)=[k];
%         y2(k)=[yy(k)];
% end
%     figure(j+1)
%     plot(x,y2)
%     title(['Vertical displacement vs Position with specific',' time = ', num2str(time)])
%     ylabel('Vertical displacement')
%     xlabel('Position')
%     grid
%-------------------------------------------------------------
% Plotting displacement vs time at the sensor location

% steptime=0.001;
% for n=1 : 200
%    t=n*steptime;

%         ysum=0;
%         for i=1:5
%             if t>ft
%                 ysum=ysum+(alpha*Xls(i)*Xlp(i))/(lm(i)^2-omea^2)...
%                 *[sin(omea*t)-omea/lm(i)*sin(lm(i)*t)-sin(omea*(t-20*pi/omea))+omea/lm(i)*sin(lm(i)*(t-
20*pi/omea))];

%             end
%             if t<=ft
%                 ysum=ysum+(alpha*Xls(i)*Xlp(i))/(lm(i)^2-omea^2)...
%                 *(sin(omea*t)-omea*sin(lm(i)*t)/lm(i));
%             end

% end
%          yy(n)=ysum;
% end
% for n=1:200
%         x(n)=[n];
```

```
%         y2(n)=[yy(n)];
% end
%     figure(j+1)
%     plot(x,y2)
%     title(['Vertical displacement vs time at the sensor',' freq = ', num2str(freq),' Hz'])
%     ylabel('Vertical displacement')
%     xlabel('Time')
%     grid
%-----------------------------------------------------------
```

```
%-- This program (Tensin.m) has been written to simulate the
%-- solution for clamped-clamped beam with 10 complete sin pulse excitation.
format long;
a=1.38;
l=0.55*2;
lp=0.1315;
ls=lp;  % Collocated
% ls=0.1936;
%--Where input frequency is in Hz, Variable name Freq--

freq=4000;
omea=2*pi*freq;

rho=2.7*10^3;
A=23.8*10^(-6);
F0=10;
alpha=F0/(rho*A);
z(1)=4.730;
z(2)=7.853;
z(3)=10.996;
z(4)=14.137;
z(5)=17.279;
ft=20*pi/omea;

x=1;
t=1;
ht=0.005;

nt=80;
nx=11;
hx=l/nx;
for i=1:5
  lm(i)=a*(z(i)/l)^2;
  b(i)=z(i)/l;
  sig(i)=(cosh(b(i)*l)-cos(b(i)*l))/(sinh(b(i)*l)-sin(b(i)*l));

den=(4*b(i)*l+2*sig(i)*cos(2*b(i)*l)-2*sig(i)*cosh(2*b(i)*l)...
  -4*cosh(b(i)*l)*sin(b(i)*l)-4*sig(i)^2*cosh(b(i)*l)*sin(b(i)*l)+sin(2*b(i)*l)...
-sig(i)^2*sin(2*b(i)*l)-4*cos(b(i)*l)*sinh(b(i)*l)+4*sig(i)^2*cos(b(i)*l)...
*sinh(b(i)*l)+8*sig(i)*sin(b(i)*l)*sinh(b(i)*l)+sinh(2*b(i)*l)...
+sig(i)^2*sinh(2*b(i)*l));

  A(i)=sqrt(4*b(i)/den);

Xls(i)=A(i)*(cosh(b(i)*ls)-cos(b(i)*ls)-sig(i)*(sinh(b(i)*ls)...
      -sin(b(i)*ls)));

Xlp(i)=A(i)*(cosh(b(i)*lp)-cos(b(i)*lp)-sig(i)*(sinh(b(i)*lp)...
      -sin(b(i)*lp)));
end
u=zeros(nt,nx);
for j=1:nt
   for k=1:nx
         for i=1:5
            x=k*hx;
```

```
            t=j*ht;
            XX(i)=A(i)*(cosh(b(i)*x)-cos(b(i)*x)-sig(i)*(sinh(b(i)*x)-sin(b(i)*x)));
            if t>ft
               u(j,k)=u(j,k)+(alpha*XX(i)*Xlp(i))/(lm(i)^2-omea^2)...
               *[sin(omea*t)-omea/lm(i)*sin(lm(i)*t)-sin(omea*(t-20*pi/omea))+omea/lm(i)*sin(lm(i)*(t-
20*pi/omea))];

            end
            if t<=ft
               u(j,k)=u(j,k)+(alpha*XX(i)*Xlp(i))/(lm(i)^2-omea^2)...
               *(sin(omea*t)-omea*sin(lm(i)*t)/lm(i));
            end
         end
   end
end
%-------------------------------------------------------
% Calculate the value of response
% for j=1:nt
%   for k=1:nx
%      u(j,k);
%   end
% end
j=1;
%-------------------------------------------------------
% Plotting 3-D graph
% figure(1)
% surfl(u)
% title(['Clamped-Clamped with full sin pulse (Exact Sol)'])
% xlabel('position along beam');
% ylabel('time');
% zlabel('Vertical displacement');
%-------------------------------------------------------
% Plotting Vertical displacement vs Position along beam
%  for j=1:nt
%     for k=1:nx
%        x(k)=[k];
%        y(k)=[u(j,k)];
%     end
%     figure(j+1)
%     plot(x,y)
%    title(['Vertical displacement vs Position',' j= ', num2str(j)])
%     ylabel('Vertical displacemtnt')
%     xlabel('Positon')
%     grid

%  end
%-------------------------------------------------------
% Plotting displacement vs position with a specific time

% time =0.000011;
% t= time;
%   for k=1:nx

%        ysum=0;
%        for i=1:5
```

```
%            x=k*hx;

%             XX(i)=A(i)*(cosh(b(i)*x)-cos(b(i)*x)-sig(i)*(sinh(b(i)*x)-sin(b(i)*x)));
%             if time>ft
%                ysum=ysum+(alpha*XX(i)*Xlp(i))/(lm(i)^2-omea^2)...
%                *[sin(omea*t)-omea/lm(i)*sin(lm(i)*t)-sin(omea*(t-20*pi/omea))+omea/lm(i)*sin(lm(i)*(t-
20*pi/omea))];

%             end
%             if time<ft
%                ysum=ysum+(alpha*XX(i)*Xlp(i))/(lm(i)^2-omea^2)...
%                *(sin(omea*t)-omea*sin(lm(i)*t)/lm(i));
%             end
%          end
%          yy(k)=ysum;
%    end
%  for k=1:nx
%         x(k)=[k];
%         y(k)=[yy(k)];
% end
%     figure(j+1)
%     plot(x,y)
%     title(['Vertical displacement vs Position with specific',' time = ', num2str(time)])
%     ylabel('Vertical displacemtnt')
%     xlabel('Positon')
%     grid
%-----------------------------------------------------------------
% Plotting displacement vs time at the sensor location

% steptime=0.001;
% for n=1 : 200
%    t=n*steptime;

%          ysum=0;
%          for i=1:5
%             if t>ft
%                ysum=ysum+(alpha*Xls(i)*Xlp(i))/(lm(i)^2-omea^2)...
%                *[sin(omea*t)-omea/lm(i)*sin(lm(i)*t)-sin(omea*(t-20*pi/omea))+omea/lm(i)*sin(lm(i)*(t-
20*pi/omea))];

%             end
%             if t<=ft
%                ysum=ysum+(alpha*Xls(i)*Xlp(i))/(lm(i)^2-omea^2)...
%                *(sin(omea*t)-omea*sin(lm(i)*t)/lm(i));
%             end

%          end
%          yy(n)=ysum;
% end
% for n=1:200
%         x(n)=[n];
%         y1(n)=[yy(n)];
% end
%     figure(j+1)
%     plot(x,y1)
```

```
%     title(['Vertical displacement vs time at the sensor',' freq = ', num2str(freq),' Hz'])
%     ylabel('Vertical displacement')
%     xlabel('Time')
%     grid
%-------------------------------------------------------------
```

```
%-- This program (Hunsinca.m) has been written to simulate the
%-- solution for Cantilever beam with 100 complete sin pulse excitation.
format long;
a=1.38;
l=0.55;
lp=0.1315;
ls=0.1315; % Collocated
%ls=0.1936;
%--Where input frequency is in Hz, Variable name Freq--

freq=4000;
omea=2*pi*freq;

rho=2.7*10^3;
A=23.8*10^(-6);
F0=10;
alpha=F0/(rho*A);
z(1)=1.8751;
z(2)=4.6941;
z(3)=7.8548;
z(4)=10.996;
z(5)=14.14;

ft=200*pi/omea;

x=1;
t=1;
ht=0.005;

nt=80;
nx=11;
hx=l/nx;
for i=1:5
  lm(i)=a*(z(i)/l)^2;
  b(i)=z(i)/l;

   sig(i)=(sinh(b(i)*l)-sin(b(i)*l))/(cosh(b(i)*l)+cos(b(i)*l));

den=(4*b(i)*l+2*sig(i)*cos(2*b(i)*l)-2*sig(i)*cosh(2*b(i)*l)...
  -4*cosh(b(i)*l)*sin(b(i)*l)-4*sig(i)^2*cosh(b(i)*l)*sin(b(i)*l)+sin(2*b(i)*l)...
-sig(i)^2*sin(2*b(i)*l)-4*cos(b(i)*l)*sinh(b(i)*l)+4*sig(i)^2*cos(b(i)*l)...
*sinh(b(i)*l)+8*sig(i)*sin(b(i)*l)*sinh(b(i)*l)+sinh(2*b(i)*l)...
+sig(i)^2*sinh(2*b(i)*l));

  A(i)=sqrt(4*b(i)/den);

Xls(i)=A(i)*(cosh(b(i)*ls)-cos(b(i)*ls)-sig(i)*(sinh(b(i)*ls)...
      -sin(b(i)*ls)));

Xlp(i)=A(i)*(cosh(b(i)*lp)-cos(b(i)*lp)-sig(i)*(sinh(b(i)*lp)...
      -sin(b(i)*lp)));
end
u=zeros(nt,nx);
for j=1:nt
    for k=1:nx
```

```
        for i=1:5
          x=k*hx;
          t=j*ht;
          XX(i)=A(i)*(cosh(b(i)*x)-cos(b(i)*x)-sig(i)*(sinh(b(i)*x)-sin(b(i)*x)));
          if t>ft
             u(j,k)=u(j,k)+(alpha*XX(i)*Xlp(i))/(lm(i)^2-omea^2)...
             *[sin(omea*t)-omea/lm(i)*sin(lm(i)*t)-sin(omea*(t-200*pi/omea))+omea/lm(i)*sin(lm(i)*(t-
200*pi/omea))];

          end
          if t<=ft
             u(j,k)=u(j,k)+(alpha*XX(i)*Xlp(i))/(lm(i)^2-omea^2)...
             *(sin(omea*t)-omea*sin(lm(i)*t)/lm(i));
          end
        end
   end
end
%-------------------------------------------------------------
% Calculate the value of response
% for j=1:nt
%   for k=1:nx
%      u(j,k);
%   end
% end
j=1;
%-------------------------------------------------------------
% Plotting 3-D graph
% figure(1)
% surfl(u)
% title(['Cantilever with 100 full sin pulse (Exact Sol)'])
% xlabel('position along beam');
% ylabel('time');
% zlabel('Vertical displacement');
%-------------------------------------------------------------
% Plotting Vertical displacement vs Position along beam
% for j=1:nt
%    for k=1:nx
%       x(k)=[k];
%       y(k)=[u(j,k)];
%    end
%    figure(j+1)
%    plot(x,y)
%   title(['Vertical displacement vs Position',' j= ', num2str(j)])
%    ylabel('Vertical displacemtnt')
%    xlabel('Positon')
%    grid

% end
%-------------------------------------------------------------
% Plotting displacement vs position with a specific time

% time =0.000011;

% t= time;
%   for k=1:nx
```

```
%        ysum=0;
%        for i=1:5
%            x=k*hx;

%             XX(i)=A(i)*(cosh(b(i)*x)-cos(b(i)*x)-sig(i)*(sinh(b(i)*x)-sin(b(i)*x)));
%             if time>ft
%                ysum=ysum+(alpha*XX(i)*Xlp(i))/(lm(i)^2-omea^2)...
%                *[sin(omea*t)-omea/lm(i)*sin(lm(i)*t)-sin(omea*(t-
200*pi/omea))+omea/lm(i)*sin(lm(i)*(t-200*pi/omea))];

%            end
%            if time<=ft
%                ysum=ysum+(alpha*XX(i)*Xlp(i))/(lm(i)^2-omea^2)...
%                *(sin(omea*t)-omea*sin(lm(i)*t)/lm(i));
%            end


%         end
%         yy(k)=ysum;
%    end
% for k=1:nx
%        x(k)=[k];
%        y2(k)=[yy(k)];
% end
%    figure(j+1)
%    x=[0,x];
%    y2=[0,y2];
%    plot(x,y2)
%    title(['Vertical displacement vs Position with specific',' time = ', num2str(time)])
%    ylabel('Vertical displacemtnt')
%    xlabel('Positon')
%    grid
%-------------------------------------------------------------

% Plotting displacement vs time at the sensor location

% steptime=0.001;
% for n=1 : 5000
%   t=n*steptime;

%        ysum=0;
%        for i=1:5
%            if t>ft
%                ysum=ysum+(alpha*Xls(i)*Xlp(i))/(lm(i)^2-omea^2)...
%                *[sin(omea*t)-omea/lm(i)*sin(lm(i)*t)-sin(omea*(t-
200*pi/omea))+omea/lm(i)*sin(lm(i)*(t-200*pi/omea))];

%            end
%            if t<=ft
%                ysum=ysum+(alpha*Xls(i)*Xlp(i))/(lm(i)^2-omea^2)...
%                *(sin(omea*t)-omea*sin(lm(i)*t)/lm(i));
%            end
% end
%        yy(n)=ysum;
```

```
% end
% for n=1:5000
%       x(n)=[n];
%       y2(n)=[yy(n)];
% end
%    figure(j+1)
%    plot(x,y2)
%    title(['Cantilever beam with length l at the excitation ',' freq = ', num2str(freq),' Hz'])
%    ylabel('Vertical displacement (m)')
%    xlabel('(*0.001 sec) Time')
%    grid
%-------------------------------------------------------------
```

```
%-- This program (Hunsin.m) has been written to simulate the
%-- solution for clamped-clamped beam with 100 complete sin pulse excitation.
format long;
a=1.38;
l=0.55*2;
lp=0.1315;
ls=0.1315;  %Collocated
%ls=0.1936;
%--Where input frequency is in Hz, Variable name Freq--

freq=4000;
omea=2*pi*freq;

rho=2.7*10^3;
A=23.8*10^(-6);
F0=10;
alpha=F0/(rho*A);
z(1)=4.730;
z(2)=7.853;
z(3)=10.996;
z(4)=14.137;
z(5)=17.279;
ft=200*pi/omea;

x=1;
t=1;
ht=0.005;

nt=80;
nx=11;
hx=l/nx;
for i=1:5
 lm(i)=a*(z(i)/l)^2;
 b(i)=z(i)/l;
 sig(i)=(cosh(b(i)*l)-cos(b(i)*l))/(sinh(b(i)*l)-sin(b(i)*l));

den=(4*b(i)*l+2*sig(i)*cos(2*b(i)*l)-2*sig(i)*cosh(2*b(i)*l)...
 -4*cosh(b(i)*l)*sin(b(i)*l)-4*sig(i)^2*cosh(b(i)*l)*sin(b(i)*l)+sin(2*b(i)*l)...
-sig(i)^2*sin(2*b(i)*l)-4*cos(b(i)*l)*sinh(b(i)*l)+4*sig(i)^2*cos(b(i)*l)...
*sinh(b(i)*l)+8*sig(i)*sin(b(i)*l)*sinh(b(i)*l)+sinh(2*b(i)*l)...
+sig(i)^2*sinh(2*b(i)*l));

 A(i)=sqrt(4*b(i)/den);
Xls(i)=A(i)*(cosh(b(i)*ls)-cos(b(i)*ls)-sig(i)*(sinh(b(i)*ls)...
     -sin(b(i)*ls)));
Xlp(i)=A(i)*(cosh(b(i)*lp)-cos(b(i)*lp)-sig(i)*(sinh(b(i)*lp)...
     -sin(b(i)*lp)));
end
u=zeros(nt,nx);
for j=1:nt
   for k=1:nx
        for i=1:5
           x=k*hx;
           t=j*ht;
           XX(i)=A(i)*(cosh(b(i)*x)-cos(b(i)*x)-sig(i)*(sinh(b(i)*x)-sin(b(i)*x)));
```

```
            if t>ft
               u(j,k)=u(j,k)+(alpha*XX(i)*Xlp(i))/(lm(i)^2-omea^2)...
               *[sin(omea*t)-omea/lm(i)*sin(lm(i)*t)-sin(omea*(t-200*pi/omea))+omea/lm(i)*sin(lm(i)*(t-
200*pi/omea))];

            end
            if t<=ft
               u(j,k)=u(j,k)+(alpha*XX(i)*Xlp(i))/(lm(i)^2-omea^2)...
               *(sin(omea*t)-omea*sin(lm(i)*t)/lm(i));
            end
         end
   end
end
%-------------------------------------------------------
% Calculate the value of response
% for j=1:nt
%   for k=1:nx
%      u(j,k);
%   end
% end
j=1;
%-------------------------------------------------------
% Plotting 3-D graph
% figure(1)
% surfl(u)
% title(['Clamped-Clamped with 100 full sin pulse (Exact Sol)'])
% xlabel('position along beam');
% ylabel('time');
% zlabel('Vertical displacement');
%-------------------------------------------------------
% Plotting Vertical displacement vs Position along beam
%  for j=1:nt
%     for k=1:nx
%        x(k)=[k];
%        y(k)=[u(j,k)];
%     end
%     figure(j+1)
%     plot(x,y)
%    title(['Vertical displacement vs Position',' j= ', num2str(j)])
%     ylabel('Vertical displacemtnt')
%     xlabel('Positon')
%     grid

%  end
%-------------------------------------------------------
% Plotting displacement vs position with a specific time

% time =0.000011;
% t= time;
%   for k=1:nx

%        ysum=0;
%        for i=1:5
%           x=k*hx;
```

```
%             XX(i)=A(i)*(cosh(b(i)*x)-cos(b(i)*x)-sig(i)*(sinh(b(i)*x)-sin(b(i)*x)));
%             if time>ft
%                ysum=ysum+(alpha*XX(i)*Xlp(i))/(lm(i)^2-omea^2)...
%                *[sin(omea*t)-omea/lm(i)*sin(lm(i)*t)-sin(omea*(t-
200*pi/omea))+omea/lm(i)*sin(lm(i)*(t-200*pi/omea))];

%             end
%             if time<=ft
%                ysum=ysum+(alpha*XX(i)*Xlp(i))/(lm(i)^2-omea^2)...
%                *(sin(omea*t)-omea*sin(lm(i)*t)/lm(i));
%             end
%          end
%          yy(k)=ysum;
%    end
% for k=1:nx
%         x(k)=[k];
%         y(k)=[yy(k)];
% end
%    figure(j+1)
%    x=[0,x];
%    y=[0,y];
%    plot(x,y)
%    title(['Vertical displacement vs Position with specific',' time = ', num2str(time)])
%    ylabel('Vertical displacemtnt')
%    xlabel('Positon')
%    grid
%-------------------------------------------------------------
% Plotting displacement vs time at the sensor location

% steptime=0.001;
% for n=1 : 5000
%   t=n*steptime;

%         ysum=0;
%         for i=1:5
%            if t>ft
%               ysum=ysum+(alpha*Xls(i)*Xlp(i))/(lm(i)^2-omea^2)...
%               *[sin(omea*t)-omea/lm(i)*sin(lm(i)*t)-sin(omea*(t-
200*pi/omea))+omea/lm(i)*sin(lm(i)*(t-200*pi/omea))];

%            end
%            if t<=ft
%               ysum=ysum+(alpha*Xls(i)*Xlp(i))/(lm(i)^2-omea^2)...
%               *(sin(omea*t)-omea*sin(lm(i)*t)/lm(i));
%            end



%         end
%         yy(n)=ysum;
% end
% for n=1:5000
%         x(n)=[n];
%         y1(n)=[yy(n)];
% end
```

```
%     figure(j+1)
%     plot(x,y1)
%     title(['Cl-Cl beam with length 2l at the excitation ',' freq = ', num2str(freq),' Hz'])
%     ylabel('Vertical displacement (m)')
%     xlabel('(*0.001 sec) Time')
%     grid
%-------------------------------------------------------------
```

```
%-----This program (differen.m) has been written to execute and
%-----plot the difference between clamped-clamped beam and cantilever beam.
%-----Select any of the two conditions for comparision.
% exatcsin  % Cantilever 1 cycle
% excclams  % cl-cl 1 cycle
% exathsin   % Cantilever 1/2 cycle
% exhclams   % cl-cl ½ cycle
% tensinca   % Cantilever  10 cycle
% tensin     % cl-cl 10 cycle
% hunsinca   % Cantilever  100 cycle
% hunsin     % cl-cl 100 cycle
figure(3)
zssum=0;
for n=1:5000
  x(n)=[n];
  z(n)=[y1(n)-y2(n)];
  zssum=zssum+z(n)^2;
end
plot(x,z)
title(['Difference between cl-cl and Cantilever at freq =  ', num2str(freq) , ' Hz'])
ylabel('Vertical displacement (m)')
xlabel('(*0.001 sec) Time ')
grid
zssum
```

```
/* The following C program is specially used for the dSPACE digital signal processer in Experiment */
/* Piezo Sensor*/
/* Date:1,July, 1997 */
/* Input frequency is 4000 Hz, number of cycle is 100 */
/* declaration of input / output functions */


float ds2002(long base, long channel);
void  ds2101(long base,long channel,float value);

#include <c:\c30tools\math.h>
#include <c:\c30tools\stdio.h>

/*********************************/
/* declaration of variables      */
/*********************************/
int count1=10, count2=1;
float ht=0.000025;  /* Sampling time to the actuator */
float f=4000;     /* Input frequency */
int j=0;
int i=0;
float y1;        /* Forcing function */
/*Sampling time*/
float st = 0.000025;

/* measured variables from A/D converter (DS2002) */
float mes_sgn_nf=0;
/* measured variables from A/D converter (DS2002)*/
float unvar=0;

/*** filter parameters ***/
float af1,af2,af3,bf1,bf2,bf3;

/*** initialization parameters **/
float mes_sgn_nf_1=0,mes_sgn_nf_2=0.;
float mes_sgn_f=0.,mes_sgn_f_1=0,mes_sgn_f_2=0.;




/*********************************/
/* interrupt loop                */
/*********************************/

c_int10()

{



/*  Using Trace program to read desired program variables*/
  if (j<401001)
          {
                  asm("       trapu   27"); /* call TRACE30 */
```

```
        }
  else
        {
                if (count1 == 1200)

                        {       {
                                        asm("       trapu   27"); /* call TRACE30 */
                                       }
                         count1=1;
                        }

                 count1++;
        }
/*************************************************************************/
/**       Input signal to Actuator   (delay for 10 sec)                 **/
/*************************************************************************/
if (j>400000)     /* delay for 10 sec for each sampling time =0.000025s */
        {

   y1=10.*sin(2*3.1416*f*ht*i);
                if(j>=401001) y1=0;
                ds2101(0x00000090,0x00000004,y1/10.);
                i=i+1;



 /*************************************/
 /**       sensor reading            **/
 /*************************************/

                mes_sgn_nf=10*ds2002(0x00000020, 0x00000020);  /* y axis */
                unvar=10*ds2002(0x00000020,0x0000001b);
 /*************************************************************************/
 /*butterworth filter (March 1,1997)*/
/*second order              wn=10                wn15hz          wn=25hz*/
bf1=0.00024135904904199; /*0.24135904904199*10^(-3)  0.00053716977481   0.00146031630553*/
bf2=0.00048271809808420; /*0.48271809808420*10^(-3)  0.00107433954962   0.00292063261106*/
bf3=0.00024135904904177; /*0.24135904904177*10^(-3)  0.00053716977481   0.00146031630553*/
af2=-1.95557824031504;       /*-1.95557824031504        -1.93338022587993  -1.88903307939452*/
af3=0.95654367651120;        /*0.95654367651120         0.93552890497918   0.89487434461664*/

 /*joint acceleration after filtering*/

 mes_sgn_f=bf1*mes_sgn_nf+bf2*mes_sgn_nf_1+bf3*mes_sgn_nf_2-af2*mes_sgn_f_1-
af3*mes_sgn_f_2;


 mes_sgn_f_2=mes_sgn_f_1;
 mes_sgn_f_1=mes_sgn_f;

 mes_sgn_nf_2=mes_sgn_nf_1;
 mes_sgn_nf_1=mes_sgn_nf;

 if (count2 < 3) mes_sgn_f = mes_sgn_nf;
```

```
  count2=count2+1;

   }
   j=j+1;
  }


/*****************************************************/
/* the main part of program (loop)                   */
/*****************************************************/


void init();
void timer1(float time);

main()


{
 init();
 timer1(0.000025);

 for (;;)
   ;
}
```

TEST TARGET (QA-3)

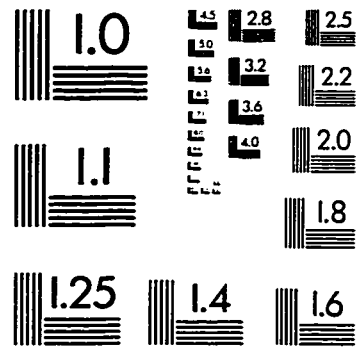

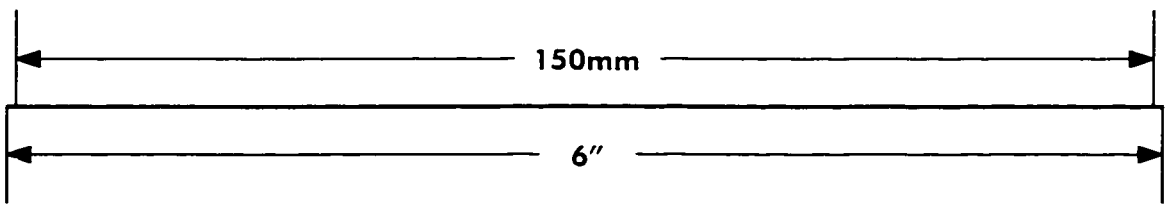

APPLIED IMAGE, Inc
1653 East Main Street
Rochester, NY 14609 USA
Phone: 716/482-0300
Fax: 716/288-5989